universität wien

MASTERARBEIT / MASTER'S THESIS

Titel der Masterarbeit / Title of the Master's Thesis

„Exploring response plasticity induced by shear stress in ovarian cancer cells in vitro“

verfasst von / submitted by

Denise Framke, BSc

angestrebter akademischer Grad / in partial fulfilment of the requirements for the degree of

Master of Science (MSc)

Wien, 2023 / Vienna, 2023

Studienkennzahl lt. Studienblatt / degree programme code as it appears on the student record sheet:	UA 066 659
Studienrichtung lt. Studienblatt / degree programme as it appears on the student record sheet:	Masterstudium Lebensmittelchemie UG 2002
Betreut von / Supervisor:	Ass.-Prof. Dott. Ric. Giorgia Del Favero, Privat Doz.
Mitbetreut von / Co-Supervisor:	Mgr. Martina Karasová, Bc. Ph.D.

Abstract

Ovarian cancer is the number one cause of death within the group of gynecological cancers. Due to a wide variety of molecular characteristics ovarian cancer is a very heterogenous disease whit a lot of challenges in treatment. Even tough cisplatin is one of the most potential drugs used in ovarian cancer treatment, the late onset of therapy and evolving resistance within the tumor often results in poor prognosis for the patient. Since the ovary is surrounded by a very motile environment within the abdomen, physical forces play a central role in the tumor microenvironment. Extracellular mechanical stimulation is translated through the mechanotransducing apparatus (cytoskeleton, mechanical gated ion channels, mechanosensitive proteins) to appropriate cellular responses via altering protein localization and/or affecting multiple intracellular signaling pathways. The main goal of this thesis was to investigate the effects of physical stressors, especially shear stress, on ovarian cancer cells. Experiments were carried out using the epithelial non-serous SKOV3 and high-grade serous OVCAR3 ovarian cancer cell lines. First, the effect of shear stress on cytotoxicity of cisplatin was evaluated. The results of cisplatin treatment showed some significant differences between static and shear stress-exposed cells in the SKOV3 cell line, but not in OVCAR3 cell line. Secondly, to explore the intracellular pathways activated through shear stress, immunofluorescence was performed. As first, morphological features like nuclear area and actin cytoskeleton were assessed. Furthermore, the analysis was deepened on structural proteins like Caveolin-1, the mechano-gated ion channel Piezo1, as well as on mechano-sensitive transcription factors and related proteins (YAP1, Ajuba, Nrf2). Lastly, a variety of post-translational modifications like farnesylation, acetylation and phosphorylation was evaluated in order to identify possible regulatory events. Taken together, our data showed significant differences between the two cell lines with regard to shear stress-induced cellular responses. Generally, OVCAR3 cells responded faster than SKOV3 cells, with morphometric rearrangement of the nucleus after 3h of incubation and YAP1 translocation. However, no effect could be seen in the cisplatin treatment. SKOV3 on the other hand sustained Nrf2 nuclear translocation after shear stress, which could be the main factor in modulated cytotoxicity of cisplatin in SKOV3 after shear stress exposure. Summarizing the results, multiple responses to shear stress might be involved in the pathophysiology of ovarian cancer and more experiments are needed to elucidate the pathways to further understand the heterogeneity of this lethal disease.

Zusammenfassung

Eierstockkrebs ist die häufigste Todesursache in der Gruppe der gynäkologischen Krebserkrankungen. Aufgrund einer Vielzahl von molekularen Merkmalen ist Eierstockkrebs eine äußerst heterogene Erkrankung, die eine Vielzahl von Herausforderungen bei der Behandlung mit sich bringt. Obwohl Cisplatin eines der am besten geeigneten Medikamente zur Behandlung von Eierstockkrebs ist, führen der späte Therapiebeginn und die sich entwickelnde Resistenz des Tumors häufig zu einer schlechten Prognose für die Patientin. Die Eierstöcke liegen umgeben von einer Vielzahl an sehr agilen Organen und Strukturen, weshalb physikalische Kräfte als Teil der Mikroumgebung des Tumors nicht außer Acht gelassen werden dürfen. Die extrazelluläre mechanische Stimulation wird durch den mechanotransduzierenden Apparat (Zytoskelett, mechanisch gesteuerte Ionenkanäle, mechanosensitive Proteine) in die entsprechende zelluläre Antwort umgesetzt, zum Beispiel indem die Proteinlokalisierung verändert und/oder mehrere intrazelluläre Signalwege beeinflusst werden. Das Hauptziel dieser Arbeit war es, die Auswirkungen von physikalischen Stressoren, insbesondere von Scherspannung, auf Eierstockkrebszellen zu untersuchen. Die Experimente wurden mit den epithelialen nicht-serösen SKOV3- und hochgradig serösen OVCAR3-Eierstockkrebs-Zelllinien durchgeführt. Zunächst wurde der Einfluss von Scherspannung auf die Zytotoxizität von Cisplatin untersucht, dessen Ergebnisse signifikanten Unterschiede in der SKOV3-Zelllinie zwischen statischen und den der Scherspannung ausgesetzten Zellen zeigten, nicht jedoch in der OVCAR3-Zellinie. Des Weiteren wurde eine Immunmarkierung durchgeführt, um die durch Scherspannung aktivierten Signalwege zu untersuchen. Zunächst wurden morphologische Merkmale wie die Fläche des Zellkerns und das Aussehen des Aktin-Zytoskeletts bewertet. Außerdem wurden Strukturproteine wie Caveolin-1, der mechanisch gesteuerte Ionenkanal Piezo1 sowie mechanosensitive Transkriptionsfaktoren und Proteine (YAP1, Ajuba, Nrf2) untersucht. Darüber hinaus wurde eine Reihe von posttranslationalen Modifikationen wie Farnesylierung, Acetylierung und Phosphorylierung evaluiert, um mögliche regulatorische Vorgänge zu identifizieren. Insgesamt zeigten unsere Daten signifikante Unterschiede zwischen den beiden Zelllinien im Hinblick auf die durch Scherspannung ausgelösten zellulären Reaktionen. Im Allgemeinen reagierten die OVCAR3-Zellen schneller als die SKOV3-Zellen, allerdings ohne Auswirkungen auf die Effizienz der Cisplatin-Behandlung. Nach Scherspannung konnte eine Translokalisation von Nrf2 in den Zellkern bei SKOV3 beobachtet werden, was der Hauptgrund für die modulierte Zytotoxizität von Cisplatin in SKOV3 nach Exposition gegenüber

Scherspannung sein könnte. Zusammenfassend lässt sich sagen, dass verschiedene Reaktionen durch die Scherspannung ausgelöst werden, an der Pathophysiologie des Ovarialkarzinoms beteiligt sein könnten. Jedoch sind weitere Experimente erforderlich, um Signalwege aufzuklären und die Heterogenität dieser tödlichen Krankheit besser zu verstehen.

Acknowledgements

I would like to thank to my supervisor Ass.-Prof. Giorgia Del Favero for the valuable knowledge I was able to receive and her always uplifting and enthusiastic nature making my Master project an unforgettable amazing time. I am very grateful to Mgr. Martina Karasová, Bc. Ph.D. for guiding me through the experiments and teaching me various approaches and hacks. I would like to thank Endre Kiss MSc. Ph.D. for teaching me cell culture and imaging techniques. I am grateful to Maximilian Jobst MSc. for introducing me to Origin Pro and together with Janice Bergen MSc. for making the days in the lab feel like home. Last but not least, I want to express my deep gratitude for my loved ones supporting me through this journey.

This work was supported by the Austrian science fund FWF with the project number P35822-B.

Abbreviations

ARID1A	AT-rich interaction domain 1A
BK	big potassium
BRCA1/2	breast cancer gene
CA 19.9	carbohydrate antigen
CA125	cancer antigen
Cav	caveolin
CDX2	caudal type homebox protein
CK7, CK20	cytokeratin
cPt	cisplatin
ECM	extracellular matric
ENac	epithelial sodium channel
ER	estrogen receptor
FAK	focal adhesion kinase
FLN-A	filamin A
FTase	farnesyltransferase
gDNA	genomic DNA
GGTase	geranylgeranyltransferase
GPCR	G-protein coupled receptor
HER2	human epidermal growth factor receptor
KRAS	K-Ras protein
LATS1/2	large tumor suppressor kinase
mDNA	mitochondrial DNA
MST1/2	mammalian STE20-like protein kinase
Nrf2	nuclear factor erythroid 2-related factor 2
OGCT	ovarian germ cell tumor
p53/TP53	cancer anti-oncogene
PARP	poly (ADP-ribose) polymerase
PAX8	paired-box protein
PFI	platinum-free interval
PI3KCA	phosphatidylinositol-4,5-biphosphate 3-kinase
PIEZO	mechanosensitive ion channel protein
PR	progesterone receptor
PTEN	phosphatase and tension homolog
PTM	post-translational modification
TAZ	WW-domain-containing transcription regulator
TEAD	transcriptional enhancer factor domain
TREK	mechano-gated potassium channel
TRP	transient receptor potential
VEGF	vascular endothelial growth factor
WT1	wilms-tumor protein
YAP	Yes-associated protein

Table of Contents

List of Figures

1 Introduction

The ovary lies within the peritoneum surrounded by abdominal organs and fluids. This particular location makes it very difficult to be examined, favoring a dysregulated cell into a tumor without noticing until disease symptoms appear. Additionally, cells of different origin can develop into ovarian cancer creating an aggressive disease with a wide heterogenicity in morphology, as well as immunophenotypes and molecular signatures. Moreover, the abdominal cavity is exposed to various physical stimuli from blood flow and the progression of ascites impacting tumorigenesis, metabolism and chemoresistance which contributes to shape the disease [1].

1.1 Ovarian cancer

1.1.1 Epidemiology and etiology

Ovarian cancer only accounts for 1,5 % of all cancer cases in Europe but is the most lethal of female cancers, with a 5-year survival up to 45,6 % [2, 3]. In 2020, out of globally 6,6 ovarian cancer incidences per 100 000 inhabitants, mortality occurred in 4,2 cases per 100 000 inhabitants. Occurrence is highest in Europe with 8,8 ovarian cancer incidences per 100 000 inhabitants and a mortality of 4,7 incidences per 100 000 inhabitants [4]. Ovarian cancer is diagnosed primarily in postmenopausal women aged 55-74 years, with case fatality increasing with age [5]. The total number of mortality decreased over the last decades, where the use of oral contraceptives have been found to influence the occurrence of ovarian cancer and especially for middle-aged and elderly women, the long-term use led to a reduction of 30-50 % [6, 7]. The decrease in number is also caused by an improvement of early detection and treatment, even though the treatment methods not necessarily prevent mortality but extend the survival rate [8].

1.1.2 Characteristics

Ovarian cancer is less a single disease rather than a multitude of different types of cell abnormality affecting the ovaries, the fallopian tube und the primary peritoneal cavity. The origin can further be differentiated into epithelial, germinal cells and stroma [9, 10]. However, tumorigenesis is mainly induced by non-ovarian tissue, such as the endometrium, endocervical glands or gastrointestinal epithelium metastasizing into the ovary [11]. In addition to morphological changes, ascites is associated with most stages of ovarian cancer and is characterized as the accumulation of intraperitoneal fluid. Within the peritoneal cavity, fluid levels average 2,3 mL in healthy women and pathologically rise more than ten-fold to 25

mL to ascites [12]. Metastasis within the abdomen is related to ascites with the omentum being the most common site [13]. *Figure 1* represents the female anatomy with the most common ovarian cancer sites through metastasis.

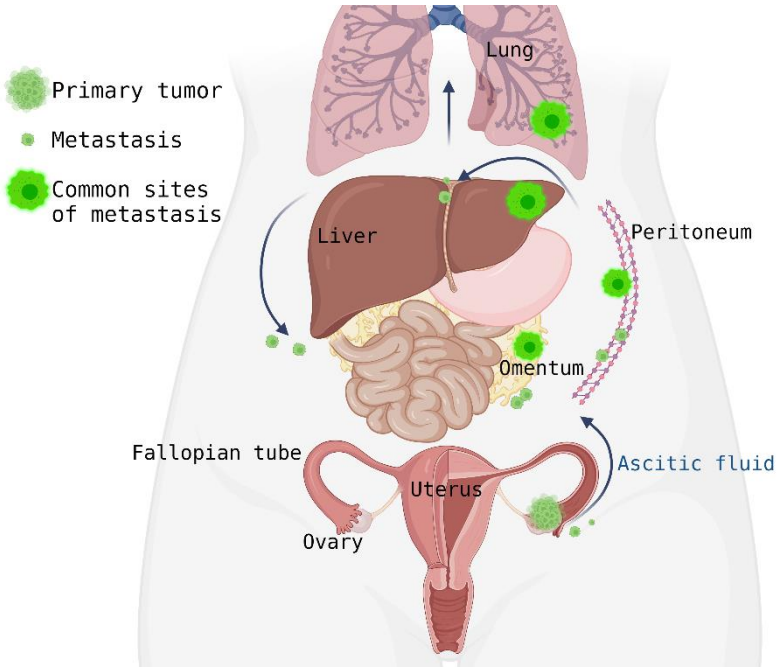

Figure 1: Female anatomy and ovarian cancer metastasis illustrated with BioRender.com.

For ***epithelial ovarian carcinomas*** (EOC) there is a wide morphologic variety separated by their cell types, such as serous carcinomas (SC), mucinous carcinomas (MC), endometrioid carcinomas (EC) and clear-cell carcinomas (CCC). Additionally, exist also less prevalent types like malignant transitional cell (Brenner) tumors, mixed and undifferentiated types. Furthermore, the EOC are divided into two types which arise from distant pathways, namely type I and II. Type I represents EOC with low-grade, including low-grade (LG) SC, low-grade EC, MC and CCC. Type II are high-grade EOC, including high-grade (HG) SC, undifferentiated carcinoma and carcinosarcoma [10].

Serous carcinomas (SC) occur in the majority of EOC-cases and as mentioned before, can be subdivided into two groups: *High-Grade SC* (HGSC) is the dominant type of SC with an occurrence of 70 % of EOC, characterized by an aggressive and fast cancerogenic development, which results in poor prognosis for patients. The majority originated from the distal end of the fallopian tube developing a serous tubal intraepithelial carcinoma (STIC) as precursor for OC [9, 11]. HGSC is positive for CK7, PAX8 and WT1, but usually negative for CK20 [10]. In 80 % of cases the estrogen receptor (ER) and in 30 % the progesterone receptors (PR) are positive [11]. Additionally, p53 is mutated - overexpressed or negative. One of the most prevalent genomic

mutations in HGSC is in the TP53 tumor suppressor gene, as well as in BRCA1 and BRCA2 [9, 10]. On the other hand, *Low-Grade SC* (LGSC) have been shown to develop from serous cystadenoma and adenofibroma in a stepwise progression represented and account for 5 % of EOC. These tumors grow slowly with a better survival rate than HGSC [10, 11]. LGSC is positive for CK7, WT1 and ER. Activation has been shown for KRAS and BRAF in 50 % of cases and p53 remains wildtype [10].

Mucinous Carcinomas are evolved in 2-3 % of EOC with a heterogenous pattern and good prognosis. MC are positive for CK7, CK20 and PAX8 in 80 % of cases, but negative for the hormone receptors ER and PR, and WT1. In 75 % of cases mutations in KRAS are detected and HER2 amplification is present in 20 % [10, 14].

The ***Endometrial Carcinomas*** are positive for CK7, PAX8 and hormone receptors expression, but are negative for WT1 and CK20. In high-grade cases, p53 can be overexpressed. For EC, PTEN and ARID1A show mutations, which can also be found in endometriosis cysts, leading to the possibility of endometriosis being a precursor. EC make up 10 % of EOC [10].

Clear Cell Carcinomas (CCC) represent 5-10 % of EOC and are clearly associated with endometriosis, occurring to have a rather mal prognosis. The tumors are positive for napsin A and negative for WT1, p53 and ER which is contrary to other EOC. In 50 % of cases ARID1A is mutated and some cases also show mutations in PI3KCA [10].

Seromucinous Carcinomas are rare and exhibit a variety of cell types, such as serous, endocervical-type, mucinous, endometrioid and squamous cells with different pattern, which differs between the stages of tumorigenesis. CK7, hormone receptors, CA125, CA 19.9 and PAX8 are positive, and additionally WT1 in some cases. CK20 and CDX2 are negative. Endometriosis seems to be a precursor since endometrioid neoplasms are often found in the same ovary as seromucinous carcinomas. The same mutation in ARID1A is to be found in both cell types [10, 14].

Ovarian germ cell tumors (OGCT) are a rare type with a malignancy of 2-3 % of all OC and develop from normal embryotic and extra-embryotic cells. OGCT arises predominantly in girls and young women with mean diagnosis age of 16-20 years [15]. Cellular characteristics are mostly nonspecific, except for some teratoma which show fat within the solid mass. Markers

for OGCT are secretion of chorionic gonadotrophin (β-hCG), α-fetoprotein and occasionally an increase in serum lactic dehydrogenases isoenzyme-1 [16].

OC arising from ***stroma cells*** are very rare and develops from the stroma, which is the connective tissue. The exact cause of this kind of OC is barely researched, but some indications lead to genetic mutations [17, 18].

1.1.3 Therapy

The therapy of OC consists of multiple steps including surgery and chemotherapy. Firstly, a primary cytoreduction is advised, including not only the adnexal masses but depending on grade also the gastrointestinal tract and uterus. Furthermore, chemotherapy follows as second step [1]. Due to the wide heterogeneity in OC cancer biology, the treatment had to be tailored to the specific type and origin of the tumor [19]. Ovarian cancer initially shows a high sensitivity to platinum-based chemotherapeutic drugs, such as carboplatin and cisplatin, but due to emerging resistance, options have been expanded to more sophisticated approaches including an antibody against vascular endothelial growth factor (VEGF), namely bevacizumab, and oral inhibitors of poly (ADP-ribose) polymerase (PARP) [20].

Currently, the most effective platinum-based drug is cisplatin (cPt). Up-taken cPt binds to plasma proteins and enters the cell mainly via passive diffusion through copper transporter Ctr1 and Ctr2. cPt is positively charged leading to high affinity for the negatively charged DNA, RNA and proteins [21]. cPt binds to genomic (gDNA) or mitochondrial DNA (mDNA) [22], precisely to the N_7 atoms of purine bases in the DNA, causing monoadducts which further lead to inter- and intra-molecular crosslinks of DNA-suppressing DNA replication and RNA transcription leading to strand-breaks and further mutations [21]. The damaging of DNA is followed by an inhibition of DNA, mRNA and protein synthesis, as well as regulatory arrest of DNA resulting in the activation of signal transduction pathways which further lead to necrosis or apoptosis [22, 23]. *Figure 2* provides a schematic representation of the intracellular effects of cPt. Even though the main target is DNA, also other targets like mitochondria, zinc finger motifs of proteins and other organelles have been shown to be targeted by cPt [24].

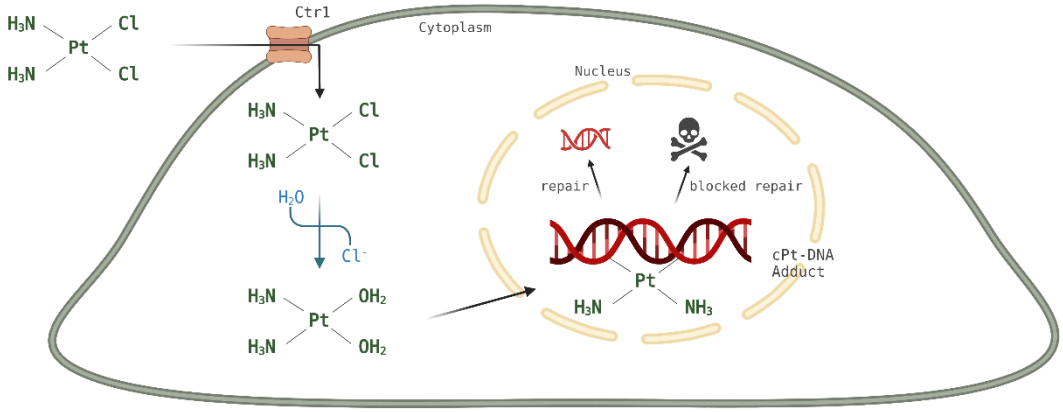

Figure 2: Mechanism of cPt in ovarian cancer cells illustrated with BioRender.com.

Even though initial sensitivity of OC to cPt is very high, chances of recurrence are likely, which results in a significant resistance [23]. Platinum-sensitive OC are defined with a platinum-free interval (PFI) of more than six months, which is the time between the last treatment dose and the relapse evidence of cancer progression. In contrast to platinum-resistant OC with a PFI of less than six months [1]. Resistance mechanisms have been classified into four groups to pre-target (before cPt binds to cellular targets), on-target (alterations of DNA-cPt-adducts), post-target (mutation or expression changes in downstream signaling pathways inducing apoptosis) and off-target (activation of not directly to cPt linked signaling pathways) [25]. Especially OC cPt-resistance is induced by on- and post-target mechanisms involving enhanced DNA-repair and decreased induction of apoptosis [21, 26]. To increase results of cPt treatment in OC, strategies like molecular target therapy and immunotherapy, platinum-complexes and non-platinum metal-complexes, phytochemicals as sensitizers and nanoparticle drug delivery systems are focus of research [26].

1.2 Mechanotransduction

The cells are surrounded by a microenvironment, which is essential for their survival, function and homeostasis of the whole tissue. The communication on cellular level is triggered by chemical (e.g. hormones) or mechanical cues. Mechanical cues can be sensed by the mechanosensitive apparatus including plasma membrane, cytoskeleton, and associated proteins, which further translate the cues into biochemical signals generating biological responses [27, 28]. Those occur within milliseconds and control further, long-term responses (within seconds to days) [29]. The physical stimuli include shear stress, pressure and stiffness [30]. Every cell has a different response to the mechanical stimulation, depending on the type

of mechanical cue, activated signaling pathways and cell cycle phase. The structures responsible, for example stretch receptors in muscle cells [31], baroreceptors in the arteries [32] or mechanosensitive ion channels in the cell membranes of various cells [33], are called mechanosensors. Those include for instance mechano-gated ion channels [34], adhesion molecules (e.g. integrins) [35] and cytoskeletal elements [36]. Upon activation, mechanosensors undergo force-dependent conformational changes leading to biochemical alteration of proteins and cellular pathways [37]. Overall, the communication goes in both ways: firstly, the mechanical cues lead to intracellular biochemical responses and further alteration in signaling pathways and changes in gene expression. Secondly, intracellular biochemical signals alter the extracellular matrix (ECM), cytoskeleton and cell membrane proteins, which further generate force and result in mechanical signals [28]. Furthermore, there are two kinds of transduction, focal adhesion for communication between the cell and their surrounding tissue, and adherents junctions for cell-cell communication [37]. In *figure 3* the cell with surrounding microenvironment responsible for mechanotransduction is illustrated.

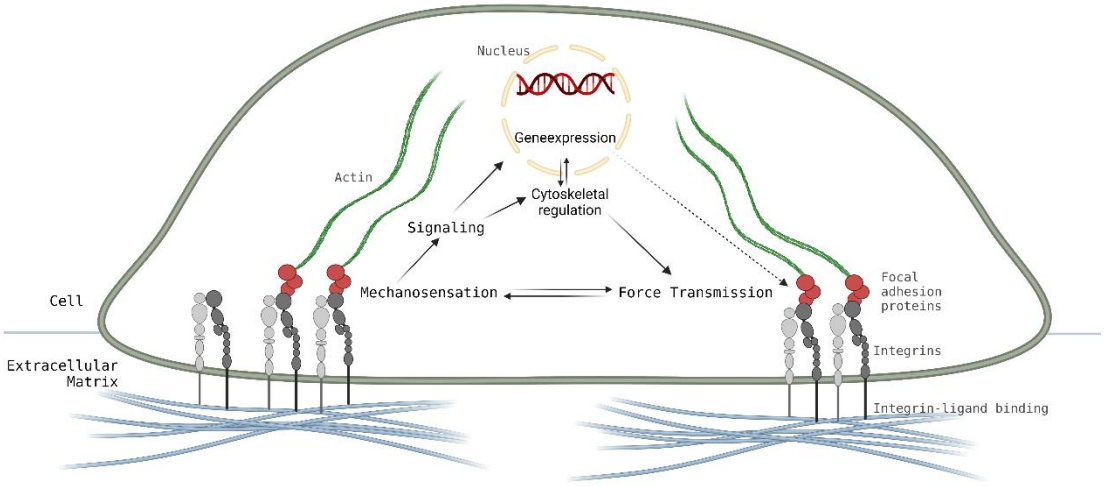

Figure 3: Cell with extracellular matrix and structures involved in mechanotransduction illustrated with BioRender.com.

1.2.1 Mechanosensation

Mechanoreceptors are responsible for the conversion of an internal or external mechanical signal into a chemical and/or electrical signal. In mammals, there is a wide range of receptors: The G-protein coupled receptors (GPCRs) are known for their mechanosensation of sight, smell and taste [34]. Amongst the multitude of GPCRs, some also respond to mechanical forces even

though the responses are slower than for mechanosensitive ion channels [29]. Furthermore, mechanical signals from cationic currents from Na^+, K^+ and Ca^{2+} are processed through non-selective ion channels. Physical stimuli are also associated with mechanistic alterations like a conformational change, loss of function or change in expression pattern through stretch, pressure, or channel kinetics [34]. The mostly well-known mechanosensitive ion channels are Epithelial sodium channel (ENaC), Piezo, TREK, transient receptor potential (TRP) and big potassium (BK) [28]. Especially Piezo1 is of great interest due to mechanosensitive properties resulting in activation of downstream signaling pathways, including regulation of gene transcription, proliferation, adhesion and migration [38]. In addition, the transmembrane protein family of integrins play an important role in mechanosensation, particularly in the context of cell adhesion and migration. Integrins are important for linking the extracellular matrix to the intracellular cytoskeleton, allowing cells to sense and respond to mechanical forces [39]. Integrins form heterodimeric complexes consisting of an α and a β subunit, with different combinations of subunits giving rise to different integrin types with distinct functions. When integrins bind to extracellular matrix proteins, they can transmit mechanical forces to the cytoskeleton through a process known as outside-in signaling involving the activation of intracellular signaling pathways, as Rho family GTPases and focal adhesion kinase (FAK), which can regulate cytoskeletal dynamics, gene expression, and cell behavior [35].

1.2.2 Cell membrane

The lipid membrane is a thin, flexible layer that surrounds the cell and separates its internal from the external environment. It is composed of a double layer of phospholipid molecules which creates a barrier that is impermeable to most molecules and ions, allowing the cell to maintain a distinct internal environment. In addition to phospholipids, the lipid membrane also contains other molecules such as cholesterol and glycolipids which are the major structural lipids, influencing its physical properties such as fluidity and thickness. Another special region of the cell membrane are lipid rafts, which are enriched in certain types of lipids, such as cholesterol and sphingolipids. Lipid rafts can be important for a variety of cellular processes, including signal transduction, trafficking and membrane organization, as well as membrane fluidity and the importance for interaction between membrane proteins [40]. The mechanical stimuli has effects on the shape and tension of the plasma membrane, which further sustains mechanotransduction [41]. Regarding the transmission from force to signal there are two possible models described in literature. On the one hand, the force-from-lipids

describes the conversion of tension from hydrostatic and steric forces from the lipid-bilayer into conformational changes of the ion channels, which then produces movement of the gates [42]. The mechanosensitivity of the ion channel therefore depends on the protein-lipid interaction [29]. The membrane proteins have multiple internal states leading to different conformational changes as response to the membrane tensions [43]. These interactions are postulated to happen without the need for additional elements of the cellular environment. On the other hand, the model tethering to ECM or cytoskeleton describes the contact of mechanosensitive proteins to the ECM, the cytoskeleton or both, where the mechanical stimulation is sensed and then further transmitted to ion channels via connecting structures. Especially Piezo1 and TREK-1 are known to be modulated by cytoskeletal elements [42].

Another important feature of the cell surface is the **Caveolae**, which are flask-shaped non-coated structures and play an important role in signal transduction. The proteins cavins and caveolins (Cav) are enriched in those structures, especially Cav1 is involved in various signaling cascades [44, 45] and an important player in the control of focal adhesion stability, actin organization, lipid and cholesterol homeostasis, actomyosin contraction, and contributes to mechanosensing and adaptation to mechanical stimulation [45, 46].

1.2.2.1 Piezo1

The family of Piezo channels are non-selective cation channels, which are mechanically activated, resulting in influx of Na^+ and Ca^{2+}. Apart from physical cues, Piezo1 can be activated by the compound YODA1 (2-[5-[[(2,6-dichlorophenyl)methyl]thio]-1,3,4-thiadiazol-2-yl]pyrazine), which is the only known activator so far [47]. In endothelial cells Piezo1 can be activated through shear stress, which further causes Ca^{2+} influx meditating Piezo1-specific downstream signaling events [48]. As a mechanosensitive ion channel, Piezo1 activity is also affected by the alteration of cytoskeletal structure and lipid modulation [49] and high stress can lead to a loss of channel inactivation [50].

1.2.2.2 Caveolin-1

As briefly mentioned above, the small integral membrane protein Cav1 is part of the family of caveolins as mechanosensitive structures. In this regard, mechanical stimulation can promote phosphorylation leading to increased expression of caveolar genes [45]. Furthermore, the reversible phosphorylation of Cav1 as response to physical cues has significant effects on signaling events and cell-EMC interactions. However, the caveolae dynamics are coupled to

the actin cytoskeleton and Cav1 interacts with the protein filamin A (FLN-A), which links integrins to the cytoskeleton. This leads to a mutual regulation of Cav1 and actin cytoskeleton [51]. Furthermore, YAP and TAZ can be modulated by Cav1 resulting in modulated downstream gene expression [52].

1.2.3 Actin cytoskeleton and extracellular matrix

Enclosed by the lipid bilayer is the **cytoskeleton** which surrounds the nucleus and integrates the activity of various cytoplasmatic proteins and organs. This results in a dynamic and adaptive structure, mainly consisting of actin filaments, microtubules and intermediate filaments, providing cell shape and mechanics. Those compartments can interact with each other through nonspecific (e.g. steric interactions and enlargement) or specific (e.g. proteins) signals [53]. The cytoskeleton provides viscoelastic properties, which not only sustains and responses to forces from the outside, but also can change through polymerization of actin filaments through cues from inside [28]. The forces generated through polymerization and depolymerization lead to changes in cell shape and organization of cellular compartments, as an example for intercellular mechanical stimuli. Shear stress, as an example for an extracellular mechanical force, through e.g. blood flow, can lead to a stiffening of the actin cytoskeleton [53].

However, the **ECM** surrounds the whole network, which composition varies between the tissues, but mainly consists of water, proteoglycans and several fibrous proteins. Due to the ECM structural support and stability, cell adhesion, survival etc., are provided. The attachment is ensured by surface receptors like integrins, syndecans and selectins. Integrin-based adhesive structures play the main role in sensing the properties and conditions of the substrate. Especially important for cell-matrix interactions are integrin-dependent structures like focal adhesion, podosomes and hemidesmosomes. Except for hemidesmosomes, integrin-based structures connect the actin cytoskeleton with the ECM, while hemidesmosomes serve as attachment of epithelial cells to the intermediate filaments [54].

1.2.4 Mechanosensitive transcription factors

Mechanosensitive transcription factors, like YAP1 and Nrf2, are a class of proteins that play a crucial role in translating mechanical cues into gene expression changes. They act as molecular switches that respond to extracellular mechanical forces by binding to specific DNA sequences and modulating the transcription of target genes [55, 56].

1.2.4.1 YAP/TAZ and Hippo pathway

Two of the most important and well researched proteins involved in mechanotransduction are Yes-associated protein 1 (YAP) and WW-domain-containing transcription regulator 1 (WWTR1 or TAZ). Both proteins share 46% of amino acid identity and are responsible for the same functions, leading to a signal amplification [57]. YAP and TAZ are transcriptional regulators which are activated and controlled by a variety of factors like cell shape, polarity, cell-cell adhesion, extracellular forces, cellular growth factors, metabolic pathways and the Hippo pathway [58, 59]. This leads to an interplay between mechanics, metabolism and developmental signal cascades in tuning the YAP/TAZ activity. This balance can be disrupted in pathological conditions and can lead to several diseases including cancer [60]. As mentioned above, the cytoskeleton controls several factors of the cell which further means that YAP/TAZ are regulated and activated by F-actin and integrin-dependent focal adhesions. For F-actin, not the total amount but the subcellular organization, fine structure and tension, has found to be the key player [56].

Furthermore, the Hippo signaling pathway is one of the main regulators of YAP/TAZ and controls their cellular localization (cytoplasmic vs. nuclear) through the phosphorylation status. When the Hippo pathway is active, YAP/TAZ are phosphorylated by the Hippo kinases, MST1/2 and LATS1/2 at specific serine residues and are sequestered in the cytoplasm by binding to 14-3-3 proteins, leading to their inactivation and degradation by the proteasome. On the other hand, when YAP/TAZ are not phosphorylated, they can translocate to the nucleus and act as transcriptional coactivators. Once YAP/TAZ are translocated to the nucleus, they interact with transcriptional enhancer factor (TEA)-domain (TEAD) family of DNA-binding factors to activate gene expression. In addition to the Hippo pathway, YAP/TAZ phosphorylation can be regulated by other signaling pathways, such as the Wnt and GPCR pathways. For example, GPCR signaling can activate YAP/TAZ by inhibiting LATS1/2, leading to decreased phosphorylation and nuclear localization of YAP/TAZ. [60-63]. The YAP/TAZ target genes are predominantly genes involved in proliferation and differentiation. YAP/TAZ overactivation triggers hyperproliferation, organ overgrowth, anchorage-independent growth and cancer [58, 59]. Ajuba is a protein involved in Hippo signaling as a binding partner of LATS2 and has been shown to negatively regulate YAP activity trough LATS family [64]. Overexpression of Ajuba is associated with an increase in YAP1 phosphorylation and a decrease in YAP1 nuclear localization [65, 66]. In this regard, the Hippo signaling pathway and

its key players YAP and TAZ could be an interesting target in cancer research, since its activity is activated by oncogenes or by inactivation of tumor-suppressor genes [61]. *Figure 4* shows the previous described signaling pathways with special focus on the Hippo signaling with YAP/TAZ activity.

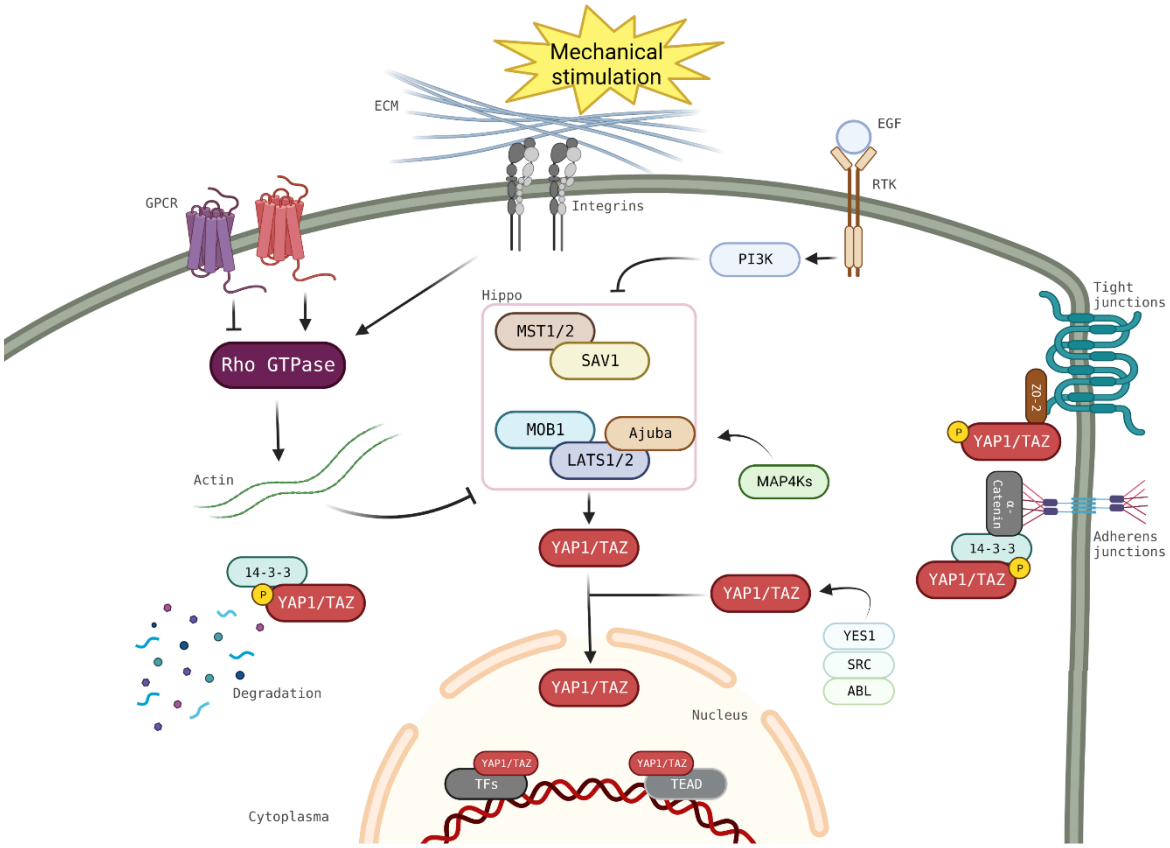

Figure 4: Intracellular signaling pathways with special focus on Hippo signaling and YAP/TAZ activity illustrated with BioRender.com.

1.2.4.2 Nrf2

The Nuclear factor erythroid 2-related factor 2 (Nrf2) is a transcription factor that plays an important role in the regulation and expression of genes involved in antioxidant defense [67]. Nrf2 belongs to the subfamily of basic leucine zippers and is regulated by a complex network of transcriptional and post-translational factors [68]. Nrf2 is known to be the master transcriptional regulator of cellular redox homeostasis and therefore is activated through oxidative stress. In addition, mechanosensitive activation through various pathways (e.g. Ca^{2+}, NO, PI3K and Rho) meditated by ion channels, G-protein coupled receptors, growth factor-receptors and integrins are involved in the nuclear translocation of Nrf2 [69]. In unstressed conditions Nrf2 interacts with Kelch-like-ECH-associated protein 1 (KEAP1) resulting in ubiquitination and degradation of Nrf2 resulting in low cellular concentrations [55, 70]. As

response to oxidative and mechanical stimuli Nrf2 stabilizes, accumulates and translocates to the nucleus, activating the transcription of downstream targets through binding to the anti-oxidative response element (ARE) on their promotors [71]. Nrf2 is highly sensitive to shear stress in vitro and nuclear translocation can be meditated through the PI3K-signaling pathway via depolarization of the actin cytoskeleton [70]. Additionally, activation of Piezo1 has been shown to activate Nrf2 through Ca^{2+}/CamKII signaling under stress conditions [67]. Target genes play a crucial role in the antioxidative stress response and drug detoxification, as well as in autophagy, metabolism and carcinogenic protein responses [55, 72]. Nrf2 has been shown to induce the expression of detoxification and antioxidant enzyme and inhibits gene transcription of pro-inflammatory cytokines [73]. But prolonged high shear stress seemed to induce pro-inflammatory effects elucidating negative impacts of activated Nrf2 in cancer cells [74]. The activation and response of Nrf2 is briefly illustrated in *figure 5*.

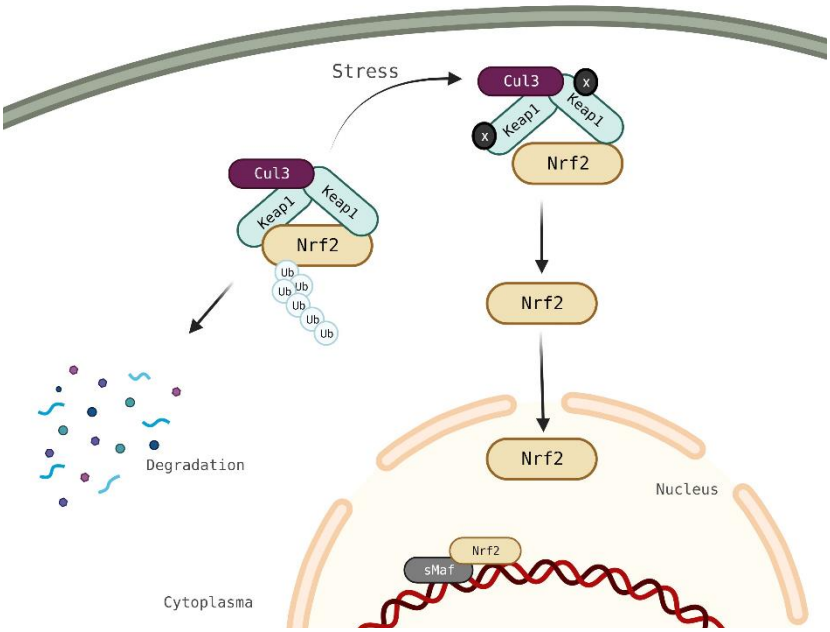

Figure 5: Intracellular signaling pathways of Nrf2 illustrated with BioRender.com.

1.2.5 Post-translational modification

However, the surrounding microenvironment can undergo structural changes through protein post-translational modification (PTM), which is an important factor for maturation and cellular processing of proteins. PTM is characterized as the enzyme-catalyzed covalent conjunction of various chemical groups to protein side chains. Those changes can result in activation, inhibition or degradation of downstream signaling pathways. More than 300 PTMs have been characterized and can be divided into phosphorylation, acetylation, lipid-related modification,

metabolite-related modification and ubiquitin-like small-molecule modification [75]. The most abundant PTM is **phosphorylation** with over 250 000 phosphorylation sites, most frequently serine, threonine and tyrosine sites [76]. The reversible reaction of adding a phosphor group has a strong impact on the function of the protein and on various cellular functions such as cell growth, differentiation and apoptosis. Consequently, phosphorylation is essential for normal cellular processes, abnormal phosphorylation is the prime cause for alterations of structural, functional and regulatory proteins [77]. Furthermore, signal transduction is controlled by the activity of kinases and phosphases. Even though a wide variety of phosphorylated proteins are known, the direct function of phosphorylation sites and phosphoforms must be explored [76]. Another modification is the **N-acetylation**, defined as the transfer of an acetyl group e.g. from acetyl-coenzym A to the α- or ε-amino group of a protein [78]. Acetylation is catalyzed by the lysine acetyltransferase (KATs) and acetylated proteins are involved in a variation of processes such as metabolism, translocation, protein degradation and cytoskeleton organization [79]. On the other hand, **lipid modifications** describe the cleavage of lipid-based residues to the protein, causing the conversion from hydrophilic proteins into hydrophobic membrane proteins resulting in a high affinity for the membrane lipid bilayer. This modification is necessary for the meditation of protein-protein as well as membrane-protein interactions, the regulation of localization and function of proteins [80-82]. Lipids used for PTM are prenyl groups which are intermediates in the cholesterol biosynthesis, namely farnesyl with 15 carbon chains and geranylgeranyl with 20 carbon chains. Farnesyltransferase (FTase) and geranyl-geranyltransferase (GGTase) catalyze the covalent binding of farnesyl or geranylgeranyl to the thiol group of cysteine in C-terminus in approximately 300 proteins [83]. For instance, farnesylated proteins include the pro-oncogenes of Ras superfamily (H-, K-, N-Ras GDP/GTP binding GTPase), which are involved in the regulation of proliferation, differentiation, cell adhesion and apoptosis, as well as the tumor-suppressor proteins of Rho GDP/GTP binding GTPases controlling many cellular processes. As well as the PRL family of tyrosine phosphatases taking part in the regulation of cell growth and mitosis, and nuclear lamins, which are constitutes of the nuclear lamina playing a role in DNA replication, cell division, protein trafficking and gene transcription, are another groups of proteins regulated by farnesylation. [81]. As elucidated, PTMs are involved in a variety of signal transduction pathways whose dysfunction can cause cancer and other diseases. It leads to attempts in treatment trials to target the inhibition of FTase and GGTase

in order to decrease proliferation and induce apoptosis [83]. Inhibition of farnesylation and geranylgeranylation through statins has been shown to suppress YAP/TAZ nuclear translocation, especially the inhibition of RhoA geranylgeranylation leads to inhibition of YAP and TAZ [84, 85].

1.3 Mechanotransduction in ovarian cancer

Mechanical stimulation is especially important for the ovary since it is a dynamic structure both intrinsic due to the reproductive cycle and extrinsic because of the physical forces within the abdomen. For instance, ascites buildup and fluid movement, intestinal fluid flow and blood flow provoke shear stress in ovarian cancer [86]. Physiological relevant shear stress rates in gastrointestinal models range from 0,14-11 dyn/cm^2 and have been used to estimate rates in the ovaries [12]. The shear stress due to the constant fluid flow leads to a suppression of E-cadherin expression, as well as structural changes like stress fiber formation and cell elongation. In this regard, the metastatic cascade is linked to the detachment of the cancer cells from the surface, migration to secondary sites followed by tumor growth [86]. Aside from advantages in metastasis, shear stress has shown to increase chemoresistance, underpinning the lethality of ovarian cancer [87].

Nevertheless, mechanical cues lead to activation of several signaling pathways, including the Hippo pathway. In the ovary, the Hippo signaling has a functional variety and is involved in diverse molecular mechanisms. It triggers the translation and generation of cellular responses to external stimulation in order to maintain the ovarian tissue growth and homeostasis. [88].

1.4 Aim of the thesis

With the thesis we aim to investigate the effects that mechanical cues (i.e. shear stress) has on *i)* cell proliferation, *ii)* cytotoxicity of cisplatin treatment and *iii)* intracellular signaling pathways through mechanotransduction. The two ovarian cancer cell lines SKOV3 and OVCAR3 are used to elucidate the heterogenous behavior of ovarian cancer and show the various responses of shear stress through the mechanotransducing apparatus. Initial experiments with different biomechanical stimulation protocols of 3 and 24 hours support the identification of the optimal response of the cell in regard of proliferation pattern and are further used to explore cytotoxicity and mechanosensitive signaling pathways. Special focus is laid on how shear stress can impact the cytotoxic potential of cisplatin since both cell lines show initial resistance to several drugs. Secondly, mechanosensitive intracellular signaling pathways are investigated by microscopy and image analysis. Main targets are the keystones nucleus and actin cytoskeleton, and further Caveolin-1 and Piezo1 as part of the cell membrane, YAP1 and Ajuba mechanically modulated within the Hippo pathway, post-translational modulation with farnesylation, acetylation and phosphorylation and finally Nrf2 as a mechanosensitive transcription factor.

The results should provide a basic overview on how shear stress might be involved in the pathophysiology of ovarian cancer leaving space to connect the different responses and pathways involved to dive deeper into the disease.

2 Materials and Methods

2.1 Materials

Table 1: Lists of reagents and material used.

Name	*Supplier*	*Reference ID*	*Additional Information*
Solutions			
McCoy's 5A Medium	Gibco	22330-021	
RPMI 1640 Medium	Gibco	21875-034	
Fetal calf serum	Gibco	10270-106	
Penicillin/Streptomycin	Gibco	15140-122	
Insulin-Transferrin-Selenium	Gibco	41400-045	
Trypsin	Gibco	-	
DPBS	Gibco	14190-094	
PBS-A	Self-prepared	ROTH 3904.1 VMR 26764.298 ROTH 0962.2 ROTH 4984.1	0,4 g KH_2PO_4 0,4 g KCl 16 g NaCl 4,4 g Na_2HPO_4 dissolved in 1 L autoclaved H_2O pH adjusted to 7,2
Washing Buffer	Self-prepared		0,05 % Triton-X in PBS-A
Permeabilization Buffer	Self-prepared		0,2 % Triton-X in PBS-A
Donkey Serum	Sigma Aldrich	D9663-10ML	Diluted from 35 % stock solution
Mounting Medium with DAPI	Abcam	AB104139	
Phalloidin-488 Oregon Green	Invitrogen	07466	Dissolved in MeOH
Crystal Violet			0,1 % dissolved in EtOH
WST-1	Roche	11644807001	
CASYton	Omni Life Science	-	
Antibodies			
Mouse mAb to Ajuba	Santa Cruz Biotechnology	sc-374610	
Mouse mAb to Acetylated Lysine	Invitrogen	MA1-2021	
Alexa Fluor 647 donkey anti-mouse igG	Invitrogen	A31571	
Rabbit mAb to YAP1	Abcam	AB52771	
Rabbit pAb to Farnesylation	Invitrogen	PA-12554	
Rabbit pAb to Phosphoserine/ threonine/tyrosine	Invitrogen	61-8300	
Rabbit mAb to Nrf2	Abcam	Ab62352	
Rabbit to pAb Piezo1	Invitrogen	PA5-106296	

Alexa Fluor 647 donkey anti-rabbit igG	Invitrogen	A31573	
Goat pAb to Caveolin-1	Abcam	AB211503	
Alexa Fluor 647 donkey anti-goat igG	Invitrogen	A21447	
Treatments			
YODA	SIGMA	SML1558	1 mM stock solution

The materials used for the experiments are listed in *Table 1*. Cisplatin was a generous gift from the collaboration partners from the department of analytical chemistry. The cell lines were acquired from the American Type Culture Collection (ATCC) and cultivated according to their specification.

2.1.1 SKOV3

The non-serous SKOV3 cell line (HTB-77) is of epithelial morphology, isolated from ovarian adenocarcinoma. SKOV3 are a more robust and resistant cell line, especially to tumor necrosis factor and cytotoxic drugs including cisplatin [89]. SKOV3 are classified as CCC and carry mutations of PIK3CA, ARID1A and TP53 [90]. Morphologically the cells are oval and elongated as shown in *figure 6*.

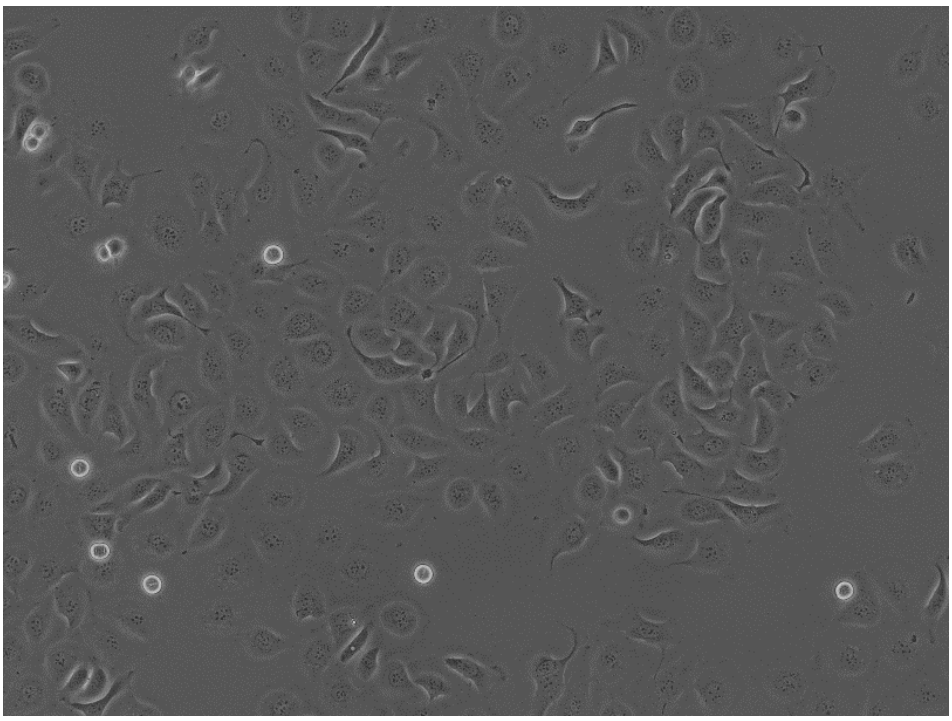

Figure 6: SKOV3 cells

Image taken with Olympus SC50, 10x magnification

2.1.2 OVCAR3

The serous OCVAR3 cell line (HTB-161) is of epithelial morphology and were isolated from malignant ascites of a patient with progressive adenocarcinoma. The cell line grows in colonies and displays resistance to clinically relevant concentrations of drugs including cisplatin [91]. OVCAR3 is one of the most extensively used OC cell line and serves as model for HGSC. OVCAR3 show a loss of p53 and a very high frequency of copy number alterations [92]. The cells are small and rather round in morphology as seen in *figure 7*.

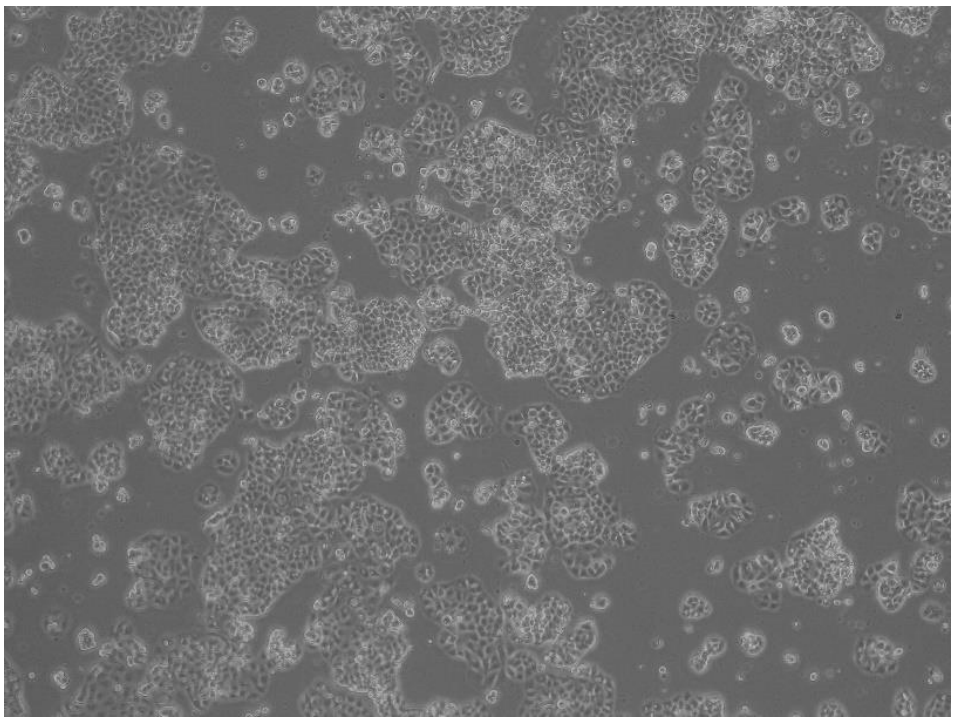

Figure 7: OVCAR3 cells

Image taken with Olympus SC50, 10x magnification

2.2 Methods

Following the methods implemented in this work will be presented, including cell cultivation and experimental layouts.

2.2.1 Cell Cultivation

Cell maintaining

The cells are cultivated in flasks in an incubator at 37°C and 5% CO_2. SKOV3 are passaged 2-3 times a week after reaching a confluency of over 90 %. OVCAR3 are passaged 1-2 times a week after reaching a confluency of approximately 85 %.

Media composition

The composition of cell culture medium for SKOV3 cells is shown in *table 2*, and for OVCAR3 cells in *table 3*.

Table 2: Composition of SKOV3 cultivation medium

Agent	*Quantity*
McCoy's 5A Medium	89 %
Fetal Calf Serum	10 %
Penicillin/Streptomycin Solution	1 %

Table 3: composition of OVCAR3 cultivation medium

Agent	*Quantity*
RPMI-1640 Medium	78 %
Fetal Calf Serum	20 %
Insulin-Transferrin-Selenium [100 µg/mL]	1 %
Penicillin/Streptomycin Solution	1 %

Cell Counting

In the beginning, the number of cells per mL Trypan blue solution was counted manually diluting the cell suspension 1:5 with Trypan blue. After cell death permeabilization of the cell membrane is increased and cells are dyed blue but living cells with intact cell membrane remain transparent. 10 µL of the solution was added to a Neubauer counting chamber and counted under the use of Olympus SC50 *(Olympus, Tokyo, Japan)* microscope with 10x magnification. For the calculation living-cell concentration *equation 1* was used.

$$\frac{cells}{mL} = \frac{mean\ living\ cells * dilution\ factor}{camber\ depth * counted\ area} \quad (1)$$

Furthermore, automated cell counter and analyzer CASY *(OMNI Life Science, Bremen, Germany)* was used for determination of the number of cells per mL cell suspension. 20 µL of cell suspension were diluted in 10 mL of CASYton and then measured. For further calculations the amount of viable cells/mL is used.

2.2.2 Experiments

Shear Stress

The following experiments include mechanical stimulation of the cells with shear stress. For application, cells were exposed to shaking on the orbital shaker IKA MS 3 control *(IKA, Staufen,*

Germany) at 250 – 500 rpm dependent on experiment and plate used for times ranging from one to 24 hours. The shear stress was applied and assessed to the other plate-layouts according to Warboys et al [93]. Pursuant to this equation 250 rpm in a 6-well or 300 rpm in a 12-well plate are equivalent to approximately 2,8 dyn/cm^2 [94]. Respectively, for every shear stress plate a static control plate was seeded.

Proliferation

Proliferation rates influenced by application of shear stress was determined in two different experiments with 3 biological replicates:

For first basic analysis cells were seeded into T35-dishes *(Sarstedt, Nümbrecht, Germany)* with a density of 10 k cells/cm^2 for SKOV3 and 50 k cells/cm^2 for OVCAR3. Two layouts were established as seen in *figure 8*. For the first layout, cells were seeded and settled for 24 hours to create a monolayer and then shaken for 3 hours at 250 rpm. For the second layout, cells were seeded right before shaking to stimulate the effects of shear stress in the blood stream. After 24, 48 and 72 hours cells were counted manually using the Neubauer counting camber.

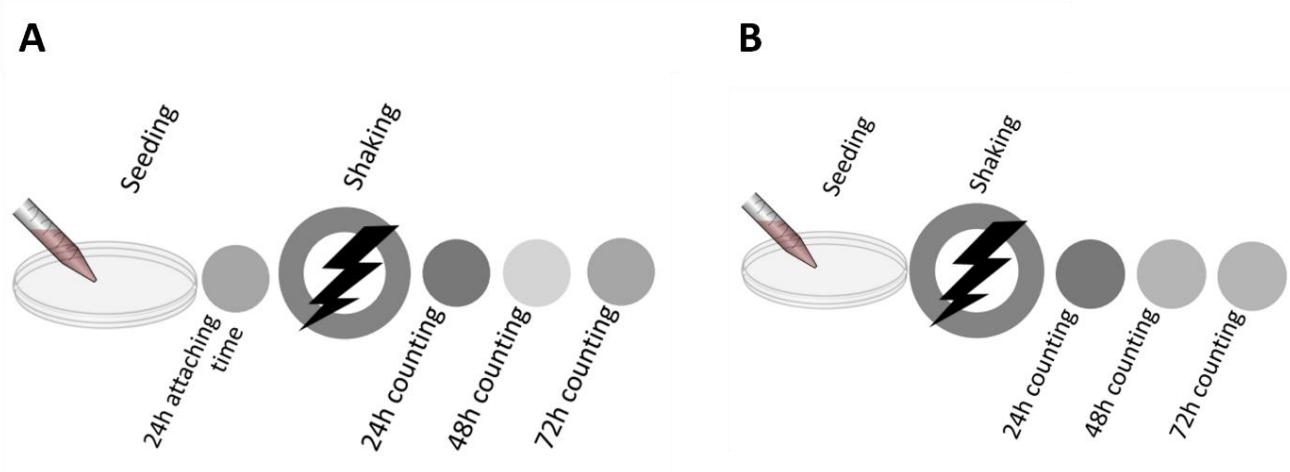

Figure 8: Visualization of proliferation experiment

Layout A: Monolayer, Layout B: Suspension

Cytotoxicity of Cisplatin

In order to determine the effects of Cisplatin on SKOV3 and OVCAR3 cell lines, a titration of the drug was performed. The experiments were performed under shear stress, to elucidate if the application of mechanical stimulus can modify the cell response. For the experiment two different layouts were performed with six cisplatin-concentration ranging from 0,5 to 20 µM respectively for one to five biological replicates:

Firstly, the cells were seeded in a density of 10 k cells/cm^2 for SKOV3 and 50 k cells/cm^2 for OVCAR3 into 6- or 12- well plates *(Sarstedt, Nümbrecht, Germany)* and settled to a monolayer for 24 hours. The plates were shaken with 250 rpm for 6- and 300 rpm for 12-well plate for 3 and 24 hours. Directly after shaking the cells were reseeded into 96-well *(Sarstedt, Nümbrecht, Germany)* plates with the same densities. Treatment was ether applied on the same day as reseeded after 3 hours of recovery time or 24 hours after reseeding as illustrated in *figure 9*. WST-1 assay was used to analyze cell viability after 24 hours of treatment followed by Crystal Violet assay for cell mass.

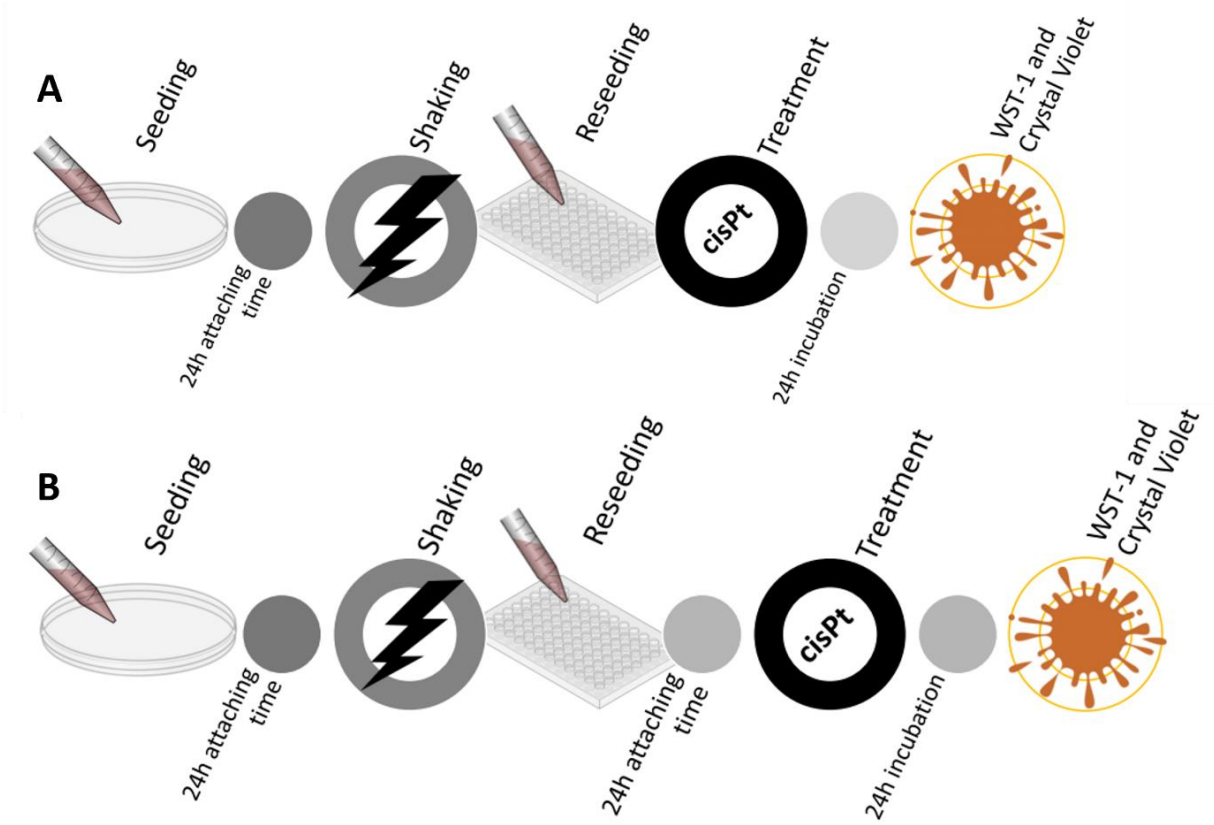

Figure 9: Visualization of cisplatin experiment No. 1.

Layout A: treatment at T0, Layout B: treatment at T24

Secondly cells were treated without the additional step of reseeding as shown in *figure 10*. SKOV3 were seeded with 10 k cells/cm^2 for 3 hours and 7,5 k cells/cm^2 for 24 hours of shear stress into 12-well plates and for OVCAR3 50 k cells/cm^2. The plate was divided into 3 different layouts: For layout A the cells were treated after shaking and incubated for 48 hours, layout B was also treated after shaking but incubated for 24 hours and then medium was changed.

Layout C was treated 24 hours after shaking and incubated for 24 hours. The cell mass was assessed with Crystal Violet assay.

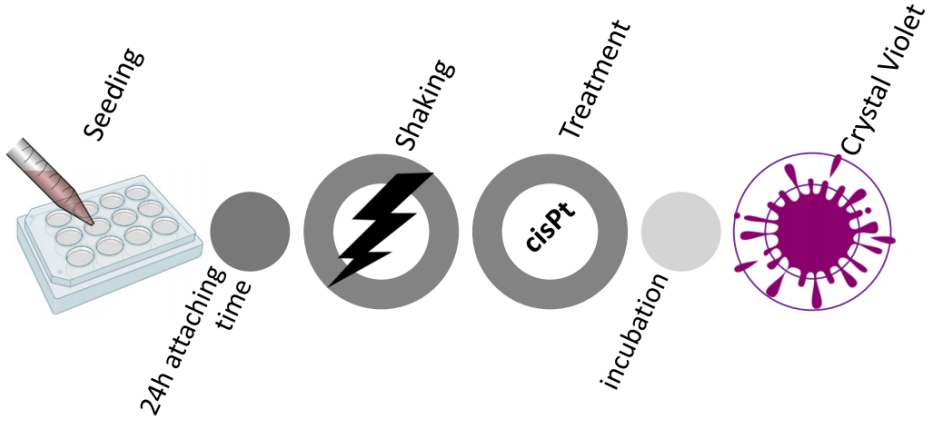

Figure 10: Visualization of cisplatin experiment No. 2

WST-1

Cell viability was assessed using WST-1 assay previously described by Del Favero et al., 2018 adapted to the cell lines used [95]. Briefly, the WST-1 solution was diluted 1:20 with according medium and incubated for one hour. WST-1 is a colorless salt that is cleaved by viable cells through mitochondrial dehydrogenases activity, reacting into the colored formazan dye. The number of viable cells is directly proportional to the intensity of the solution [96]. Absorbance was measured at 440 nm using multi-detector microplate reader Synergy H1 Hybrid *(Biotek, Bad Friedrichshall, Germany)*.

Crystal Violet

Cell mass was measured using Crystal Violet assay. As described by Del Favero et al., 2021 the cells were fixed with 96% ethanol for 10 minutes and 0,1 % crystal violet solution was added [97]. The Crystal Violet assay detects cells that are attached to the surface. The intensity of staining solution is directly proportional to the cell biomass in the plate [98]. A destaining solution 1 % acetic acid solution was used, and absorbance was measured at 595 nm using multi-detector microplate reader Synergy H1 Hybrid *(Biotek, Bad Friedrichshall, Germany)*.

Immunostaining and microscopy

Different mechanosensitive proteins have been quantified using fluorescent staining and microscopic analysis. The staining protocol previously described by Del Favero et al., 2020 was adapted [99]. Plates were seeded and shaken as described above. The cells were fixed with 3,5 % formaldehyde for 10 minutes and stored with PBS-A in the fridge until stained. For staining procedure, the fixed cells were permeabilizated, to remove lipids and allow the antibodies to

pass through the cell membrane, using permeabilization buffer for 15 minutes. Afterwards, the cells were blocked with 2 % donkey serum for one hour aiming to increase sensitivity of the staining. Ajuba, Farnesylation, Phosphorylation and YAP1 antibodies were diluted 1:1000, Cav1-antibody 1:750 and Nrf2-antibody 1:500 in 0,25 % donkey serum and incubated for 24 hours. After washing procedure, the adequate Alexa Fluor 647 secondary antibodies, donkey anti-mouse for Ajuba, donkey anti-rabbit for YAP1, Farnesylation, Phosphorylation and Nrf2 and donkey anti-goat for Cav1 and phalloidin, diluted 1:1000 in 0,25 % donkey serum, were incubated for 3 hours and another washing procedure was performed. For the final steps post-fixation with 3.5 % formaldehyde solution was performed, quenched with glycin/PBS-A solution, followed by washing and finally covered with mountain medium containing DAPI.

For Acetylation staining protocol by Jobst et al., 2023 was adapted [100]. Same steps were applied as described for the other procedures but acetylated lysine antibody (diluted 1:500) was incubated for two hours and following steps preceded the same day. As second antibody donkey anti-mouse in a dilution 1:1000, as well as phalloidin 1:000 was incubated.

Staining procedure for Piezo1 was adapted according to Bergen et al., 2023 [101]. After fixation of the cells with 3,5 % formaldehyde, blocking with 2 % donkey serum for one hour was carried out, followed by incubation of Piezo1 antibody diluted 1:400 in 0,25 % donkey serum for 24 hours in the fridge. The cells were washed with PBS-A only and secondary antibody donkey anti-rabbit diluted 1:1000 in 0,25 % donkey serum was incubated for two hours. Another washing procedure with only PBS-A was performed followed by permeabilization for 15 minutes. Afterwards another blocking step for one hour and two-hour incubation with phalloidin diluted 1:1000 was performed. Subsequent washing and post-fixation steps were same as described above.

2.2.3 Imaging and Statistical Analysis

Image Analysis

Live cell imaging was performed at Lionheart FX automated microscope *(BioTek Instruments, Winooski, VT, USA)* using the channels DAPI (377-447 nm), GFP (469-525 nm), CY5 (628-685 nm) and phase contrast. The software used for capturing images and cellular analysis was Gen5 *(BioTek Instruments, Winooski, VT, USA)*. First analysis of the dataset was performed in an automated fashion, in order to achieve high-throughput data screening. Nuclei area was

detected using DAPI mask and for cytoskeleton area the secondary mask determining size via GFP channel was applied.

Statistical analysis

Analyzed values were calculated with Excel *(Microsoft, Remond, WA, USA)* and statistics were performed in OriginPro 2023 *(OriginLab Corporation, Northampton, MA, USA)* software. For the shear stress experiments the Mann-Whitney-Test, for cytotoxicity experiments the one-way ANOVA with Fisher-LSD and for immunostaining experiments the Student's t-Test was performed. Differences were identified as significant with a threshold value (p) of 0,05.

3 Results

Following the results of experiments performed are shown.

3.1 Proliferation

The results of the proliferation experiment show a strong variety in proliferation pattern between the cell lines as well as between the experimental layouts. *Figure 11* summarizes the proliferation pattern and comparison of growth.

Graph A shows SKOV3 shaken in suspension where shear stress leads to a lower proliferation rate compared to static control. A similar result is seen for OVCAR3, where in graph C, shear stress of the suspension leads to cell death compared to the static control, which is not seen when OVCAR3 are shaken in a monolayer as displayed in graph D. In both cell lines the shear stress proliferation rates in the suspension layout catch up with static control between the time points of 48 and 72 hours after shear stress. A very different pattern is seen for SKOV3 monolayer expressed in graph B, where proliferation rates do not show any differences in the first 48 hours after shear stress.

In contrast to proliferation pattern, the percentual growth of each experiment shows significant differences within the experiments as well as cell lines. Graph E shows the growth within the first 24 hours after shear stress and recapitulate how OVCAR3 and SKOV3 react to the shear stress individually depending on their condition of either suspension or monolayer. The differences in growth diminish within the time range of 24 to 72 hours after shear stress as seen in graph F. Even though some significant differences are seen for SKOV3 suspension and comparison of shear stressed OVCAR3 suspension with monolayer.

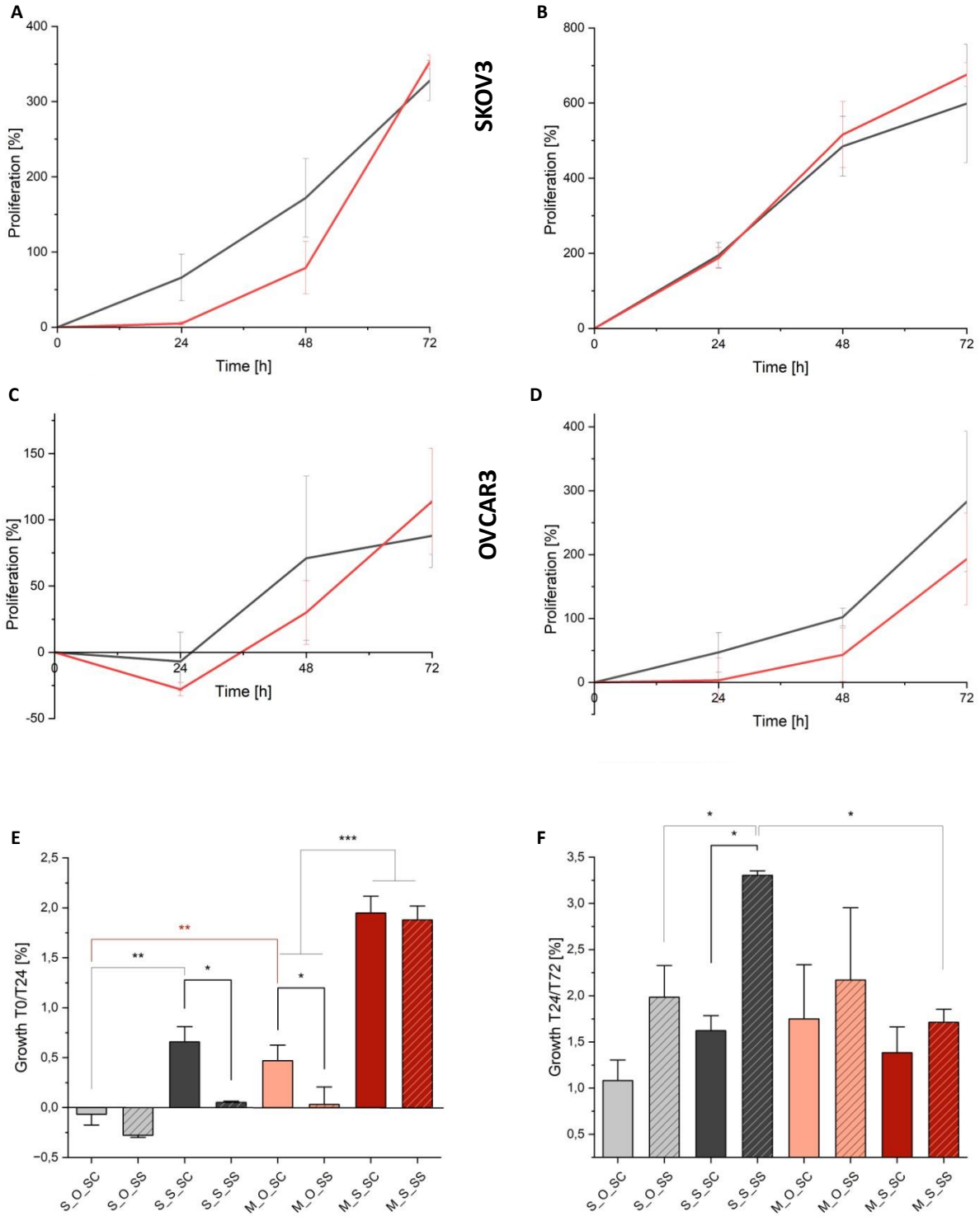

Figure 11: Proliferation rates of SKOV3 and OVCAR3 cell lines and comparison of percentual growth

Displayed are the means plus standard derivation after n = 3 biological experiments.
A: Suspension of SKOV3, B: Monolayer of SKOV3, C: Suspension of OVCAR3, D: Monolayer of OVCAR3, black = static control (SC), red = shear stress (SS).
E: Comparison of growth in the time frame from seeding to 24 hours after shear stress of both cell lines
D: Comparison of growth in the time frame from 24 hours after shear stress to 72 hours of both cell lines
S_O = Suspension OVCAR3, S_S = Suspension SKOV3, M_O = Monolayer OVCAR2, M_S = Monolayer SKOV3
*Significant difference with *p<0,05, **p<0,01, ***p<0,001 (t-Test).*

3.2 Cytotoxicity

The results of the WST-1 assay are expressed as cell viability (Test/Controls in percentage) and Crystal Violet assay as cell mass. Controls were set to 100 % so that cytotoxic effect of cisplatin can be determined for each concentration. As shown in *figure 12*, the treatment with cisplatin either directly after re-seeding (T0) or 24 hours after (T24) in concentrations of 5, 10 and 20 µM has significant effects on both, cell viability and cell mass compared to the solvent control. 3 hours of shear stress did not lead to a significant variation in sensitivity or resistance compared to static control.

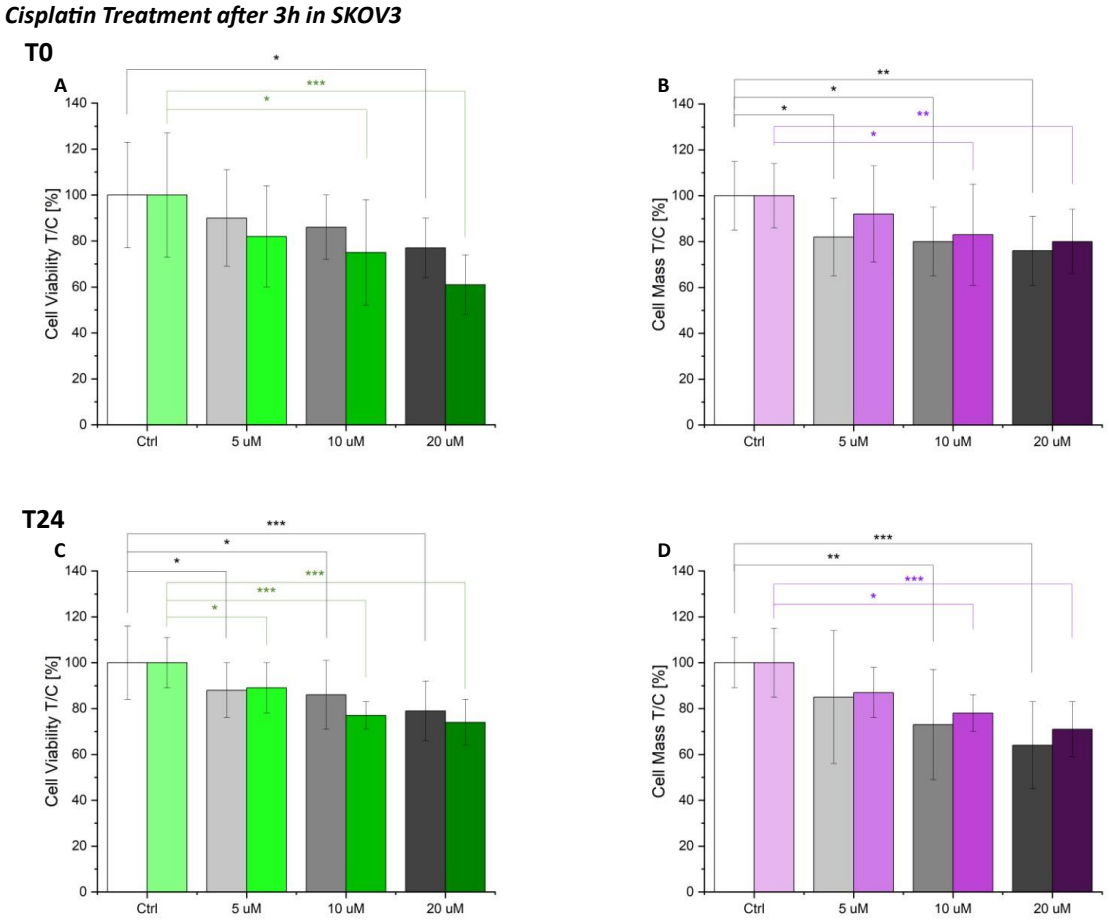

Figure 12: WST-1 and Crystal Violet: Cytotoxicity of Cisplatin in SKOV3 cell line after 3 hours of shear stress

Displayed are the means plus standard derivation for each treatment condition as treatment over control (T/C) for SKOV3 cell line after n = 3 biological experiments. Ctrl = untreated control, white to grey = static control, green = WST-1 of cPt treatment (A+C), purple = Crystal Violet of cPt treatment (B+D).
*Significant difference to control with *p<0,05, **p<0,01, ***p<0,001 (ANOVA).*

Subsequently, in order to verify if shear stress could trigger direct effects additional experiments were performed directly after the performance of the shear stress protocol. The results are depicted in *figure 13* and *14* for SKOV3 after application of 3 and 24 hours of shear stress respectively. The focus of the experiments was to see differences caused by the cisplatin treatment in shear stress and static control groups, hence significances of the treatment efficiency is not shown. As summarized in *figure 13*, for 3 hours of shear stress no significant differences are seen between static control and sheared cells, neither after 48 hours (A) and 24 hours (B) of treatment at T0 nor with treatment at T24 with 24 hours of incubation time (C).

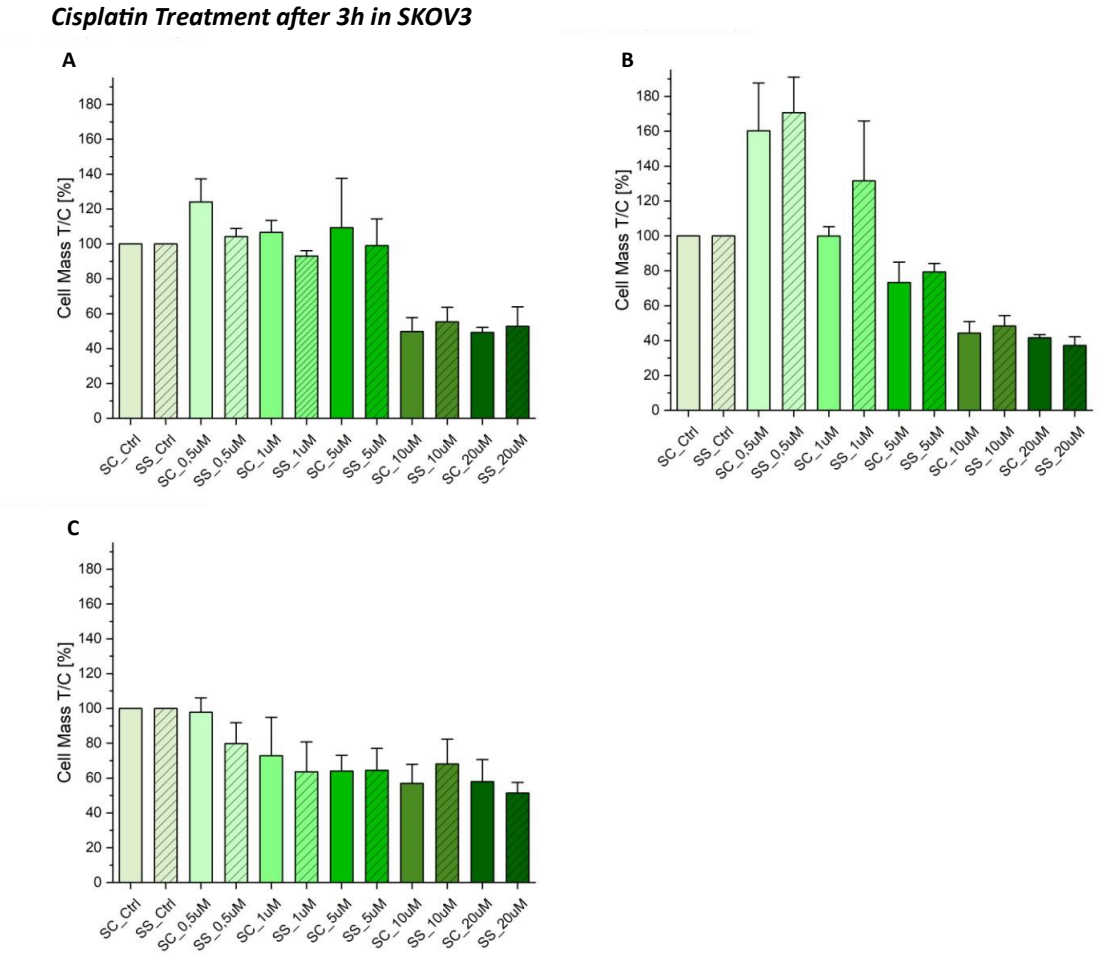

Figure 13: Crystal Violet: Cytotoxicity of Cisplatin in SKOV3 cell line after 3 hours of shear stress

Displayed are the means plus standard derivation for each treatment condition as treatment over control (T/C) for SKOV3 cell line and 3 hours of shears stress after n = 3-4 biological experiments. Ctrl = untreated control, blank = static control (SC), stripes = shear stress (SS). A = 48 hours treatment at T0, B = 24 hours treatment at T0, C = 24 hours treatment at T24.
No significant differences between static control and shear stress to control (ANOVA), treatment efficiency is not shown.

In comparison, after 24 hours of shear stress significant differences are seen between the groups for the treatment of 1 µM and 20 µM cisplatin in 48 (A) and 24 hours (B) of treatment at T0. No such effects are seen for treatment at T24 and 24 hours incubation (C), even though the trend looks similar to the other layouts.

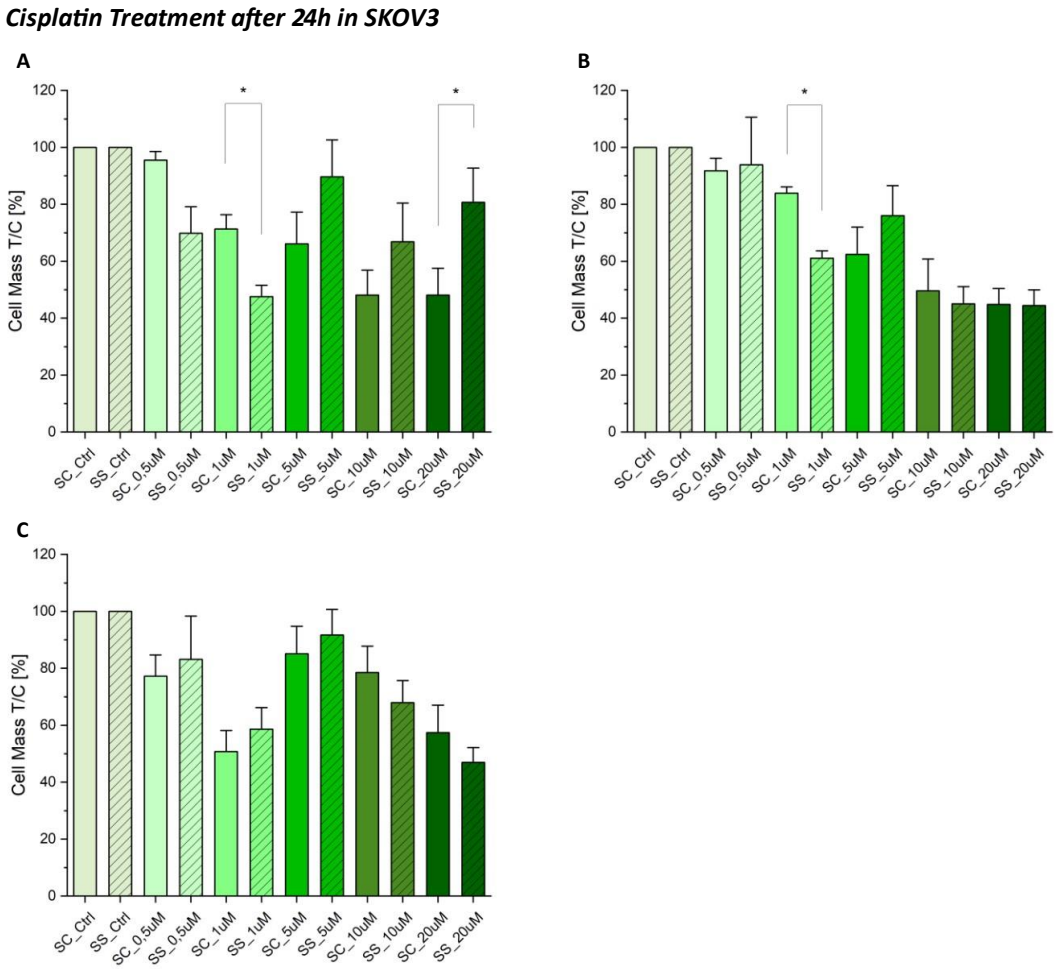

Figure 14: Crystal Violet: Cytotoxicity of Cisplatin in SKOV3 cell line after 24 hours of shear stress

Displayed are the means plus standard derivation for each treatment condition as treatment over control (T/C) for SKOV3 cell line and 24 hours of shears stress after n = 3-4 biological experiments. Ctrl = untreated control, blank = static control (SC), stripes = shear stress (SS). A = 48 hours treatment at T0, B = 24 hours treatment at T0, C = 24 hours treatment at T24.
*Significant difference to control with *p<0,05, **p<0,01, ***p<0,001 (ANOVA), treatment efficiency is not shown.*

The results for OVCAR3 are shown in *figure 15* after 3 and *figure 16* after 24 hours of shear stress. For both shear times and all layouts no significant differences are obtained between static control and shear stress, with similar trends of treatment efficiency. Moreover, after 3 hours of shear stress treatment efficiency is linear for layout A and B with a higher cell viability in mostly static control, contrary to layout C where nothing can be observed.

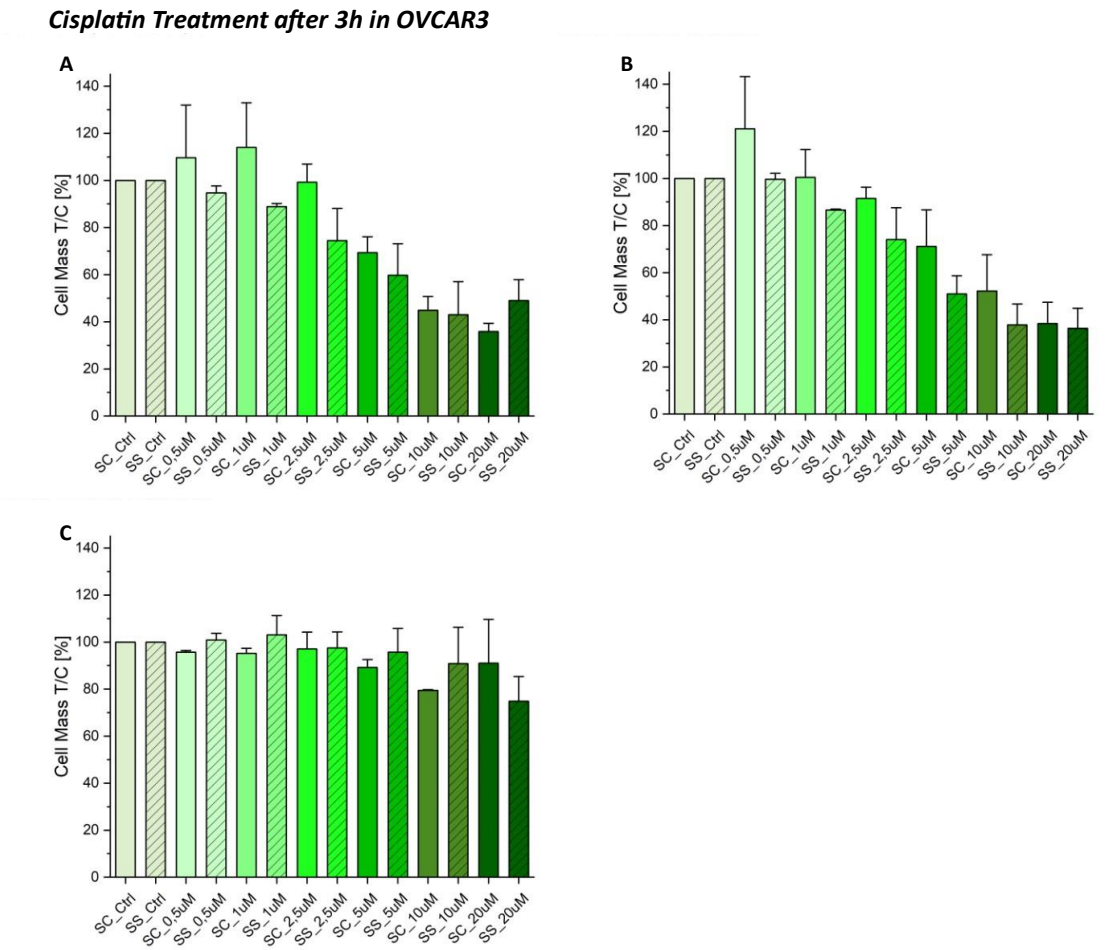

Figure 15: Crystal Violet: Cytotoxicity of Cisplatin in OVCAR3 cell line after 3 hours of shear stress

Displayed are the means plus standard derivation for each treatment condition as treatment over control (T/C) for OVCAR3 cell line and 3 hours of shears stress after n = 3 biological experiments. Ctrl = untreated control, blank = static control (SC), stripes = shear stress (SS). A = 48 hours treatment at T0, B = 24 hours treatment at T0, C = 24 hours treatment at T24.
No significant differences between static control and shear stress to control (ANOVA), treatment efficiency is not shown.

Different results are seen in *figure 16* after 24 hours of shear stress with an overall linear treatment efficiency in all 3 layouts. In layout A and B a higher treatment efficiency can be observed for static control with concentrations of 0,5 – 2,5 µM reversing the trend with concentrations of 5 – 20 µM with higher efficiency for sheared cells. Again, this can not be seen in layout C.

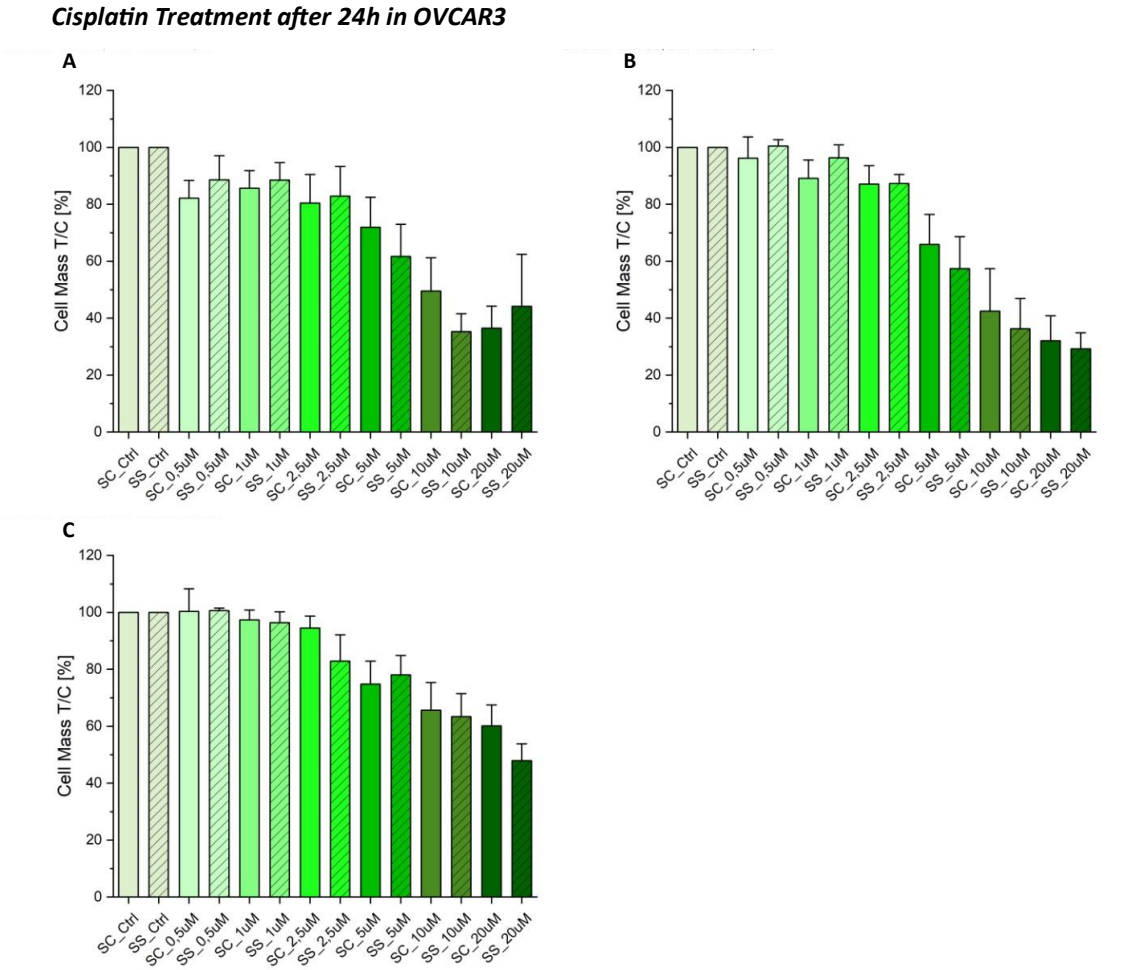

Figure 16: Crystal Violet: Cytotoxicity of Cisplatin in OVCAR3 cell line after 24 hours of shear stress

Displayed are the means plus standard derivation for each treatment condition as treatment over control (T/C) for OVCAR3 cell line and 24 hours of shears stress after n = 3 biological experiments. Ctrl = untreated control, blank = static control (SC), stripes = shear stress (SS). A = 48 hours treatment at T0, B = 24 hours treatment at T0, C = 24 hours treatment at T24.
No significant differences between static control and shear stress to control (ANOVA), treatment efficiency is not shown.

3.3 Immunostaining and microscopy

Once described that shear stress experiments significantly modulated the sensitivity to cisplatin, additional experiments were performed to investigate what pathways could be potentially affected by the application of the physical stimuli. For immunostaining and microscopy, the focus laid on basic morphologic elements like the nucleus and actin cytoskeleton, as well as the mechanosensitive elements involved especially in the YAP1 and Nrf2 signaling pathways. The targets investigated in the present thesis are highlighted in *figure 17*.

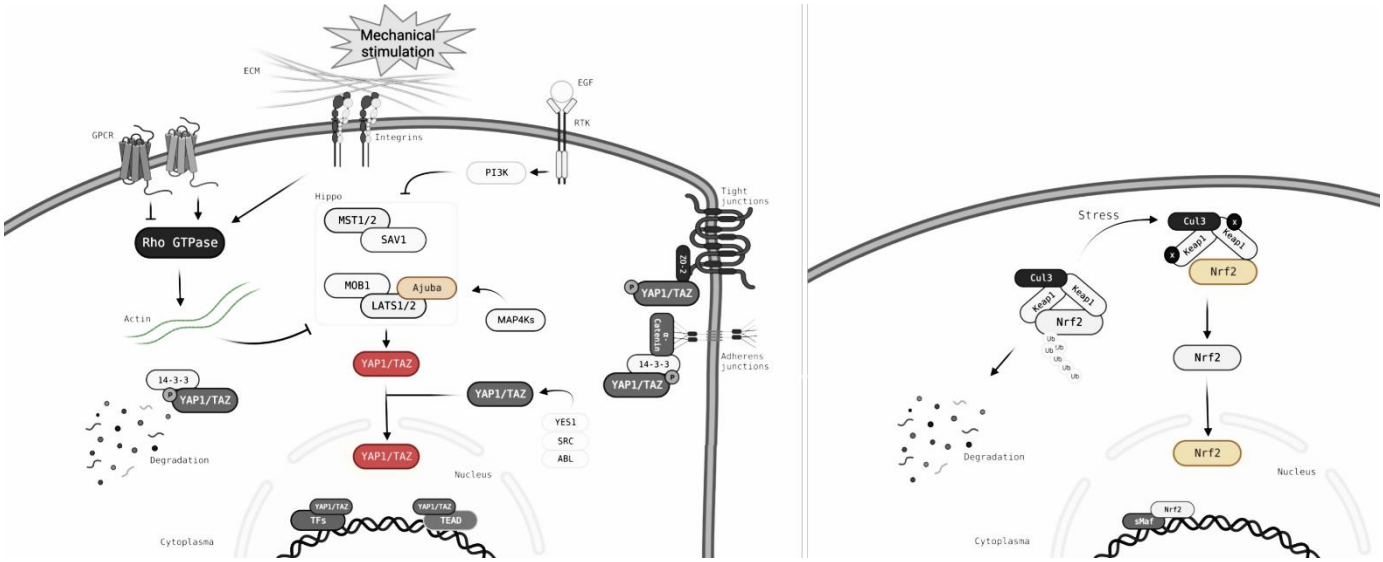

Figure 17: YAP1 and Nrf2 pathways modified from figure 4 and 5.

3.3.1 Nuclei and Cytoskeleton

The microscopic analysis of the nuclear morphology and the actin cytoskeleton was used to assess the morphological changes of the cells after shear stress and give a first impression of cell sensitivity to physical cues. The data shown for nuclei are achieved from the nuclear region and the data of actin from the cytoplasmic area.

Images and cellular analysis of nuclei is seen in *figure 18* for SKOV3 cell line and shows no significant differences in cell area for 3 hours of shear stress compared to control (C). In contrast to 24 hours of shear stress where cell area was increased through shear stress (D).

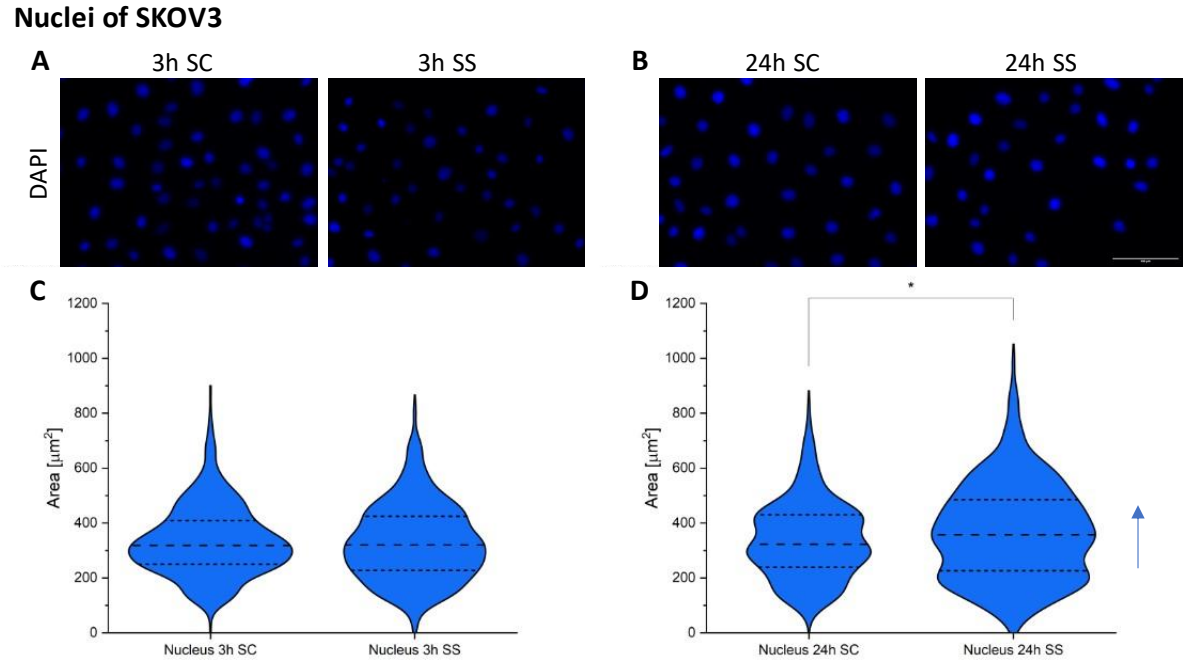

Figure 18: Microscopy: Nuclei of static control and shear stress (SKOV3)

Displayed are images and violin plot with quartiles of SKOV3 cell line after n = 3-5 biological experiments. SC = static control, SS = shear stress. A+C = 3 hours static and shear, B+D = 24 hours static and shear.
*Significant difference with *p<0,05, **p<0,01, ***p<0,001 (t-Test).*
A+B: Images are acquired with Lionheart FX automated microscope, 20x magnification, nuclei in blue, scale bar 100 µm.

Figure 19 shows actin cytoskeleton, which intensity is slightly decreased after 3 hours (C) but increased after 24 hours of shear stress in comparison to the static control (D) for SKOV3 cell line. However, it is worth noticing that actin rather redistributed upon application of shear stress, as visible in panels A and B after shear stress which is observed stronger after 24 hours of shear stress.

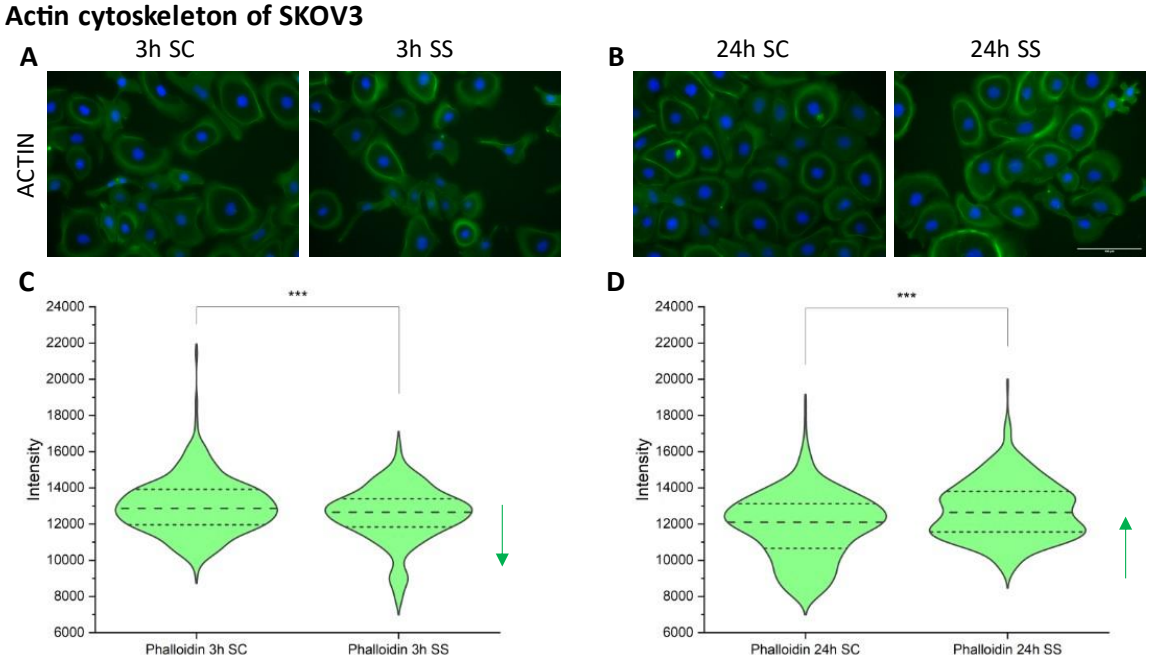

Figure 19: Microscopy: Actin cytoskeleton of static control and shear stress (SKOV3)

Displayed are images and violin plot with quartiles of SKOV3 cell line after n = 3-5 biological experiments. SC = static control, SS = shear stress. A+C = 3 hours static and shear, B+D = 24 hours static and shear.
*Significant difference with *p<0,05, **p<0,01, ***p<0,001 (t-Test).*
A+B: Images are acquired with Lionheart FX automated microscope, 20x magnification, nuclei in blue and actin in green, scale bar 100 µm.

Furthermore, images and graphs of OVCAR3 nuclei are displayed in *figure 20*. After 3 hours of shear stress the nuclei area is increased (C), which is not seen after 24 hours of shear stress in comparison to static control cells (D).

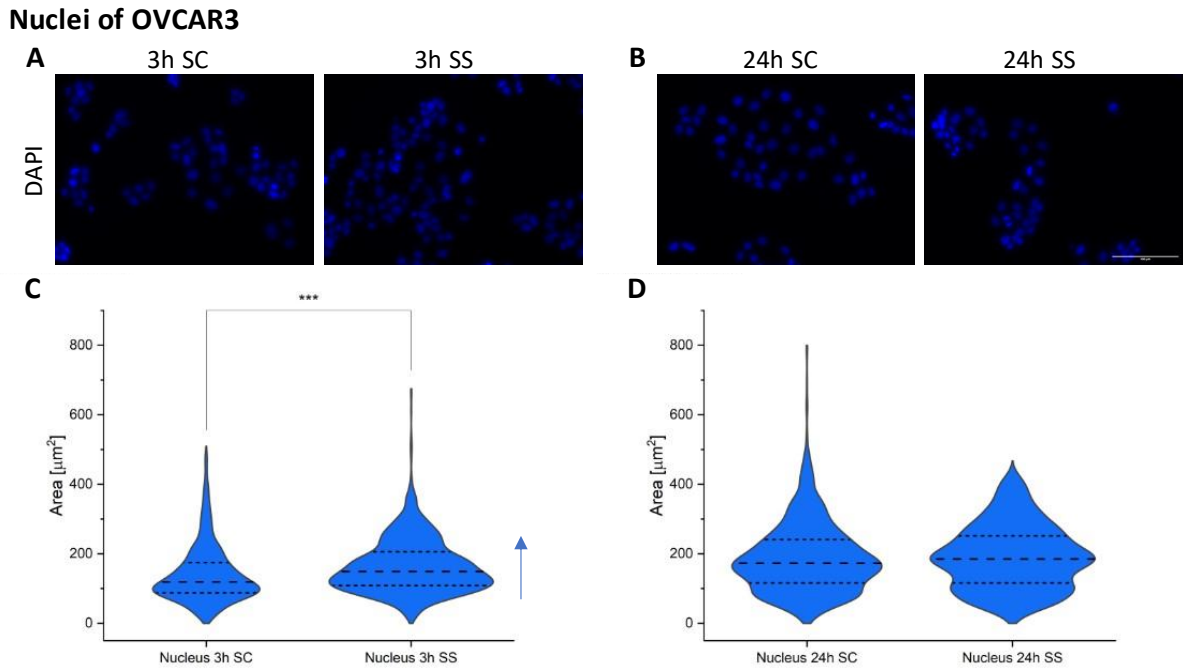

Figure 20: Microscopy: Nuclei of static control and shear stress (OVCAR3)

Displayed are images and violin plot with quartiles of OVCAR3 cell line after n = 3 biological experiments. SC = static control, SS = shear stress. A+C = 3 hours static and shear, B+D = 24 hours static and shear.
*Significant difference with *p<0,05, **p<0,01, ***p<0,001 (t-Test).*
A+B: Images are acquired with Lionheart FX automated microscope, 20x magnification, nuclei in blue, scale bar 100 µm.

The actin cytoskeleton analysis is shown in *figure 21*, with significant rearrangement which resulted in an average decrease in intensity after 3 (C) as well as after 24 hours (D) of shear stress via automated quantification.

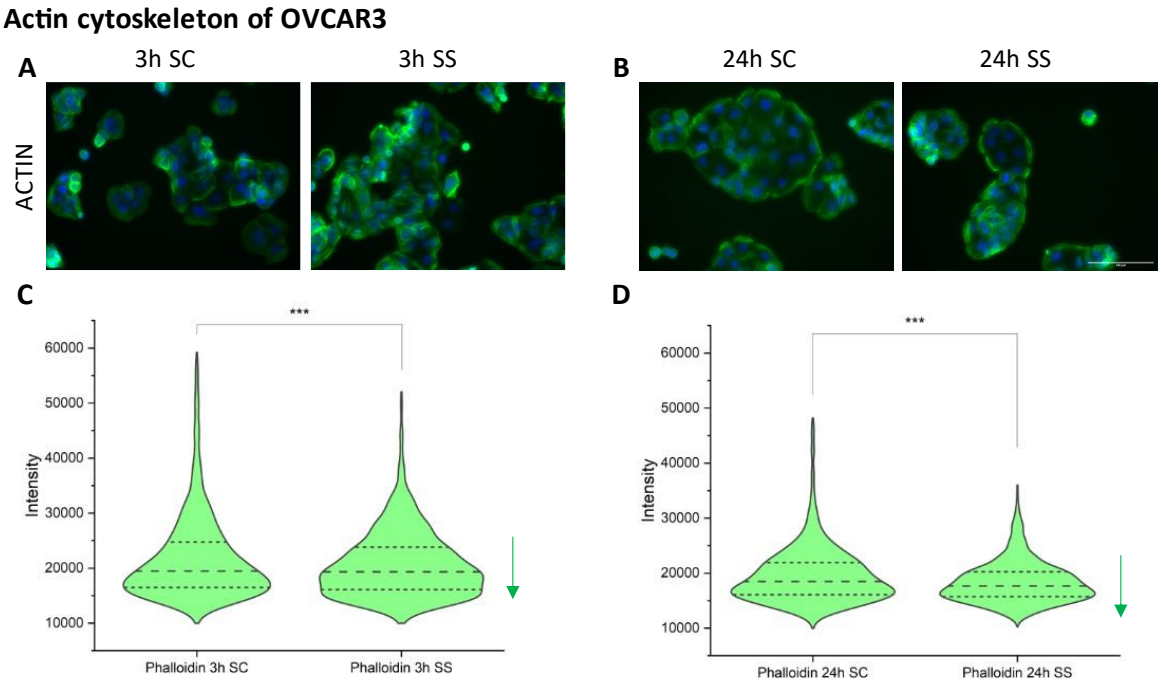

Figure 21: Microscopy: Actin cytoskeleton of static control and shear stress (OVCAR3)

Displayed are images and violin plot with quartiles of OVCAR3 cell line after n = 3 biological experiments. SC = static control, SS = shear stress. A+C = 3 hours static and shear, B+D = 24 hours static and shear.
*Significant difference with *p<0,05, **p<0,01, ***p<0,001 (t-Test).*
A+B: Images are acquired with Lionheart FX automated microscope, 20x magnification, nuclei in blue and actin in green, scale bar 100 µm.

3.3.2 Caveolin-1

As a crucial mechanosensitive protein in the cell membrane, Caveolin-1 was another important target observed under the influence of shear stress [45]. The results reported below refer to the quantification of the signal intensity in correspondence of the nuclear area.

As seen in *figure 22*, Cav1 is significantly increased in SKOV3 cell line after 3 (C) and 24 hours (D) of shear stress compared to static control. The changes in distribution of Cav1 are also noticeable on the images A and B, where intensity signal is stronger in static control within the cytoplasm compared to sheared cells with both durations.

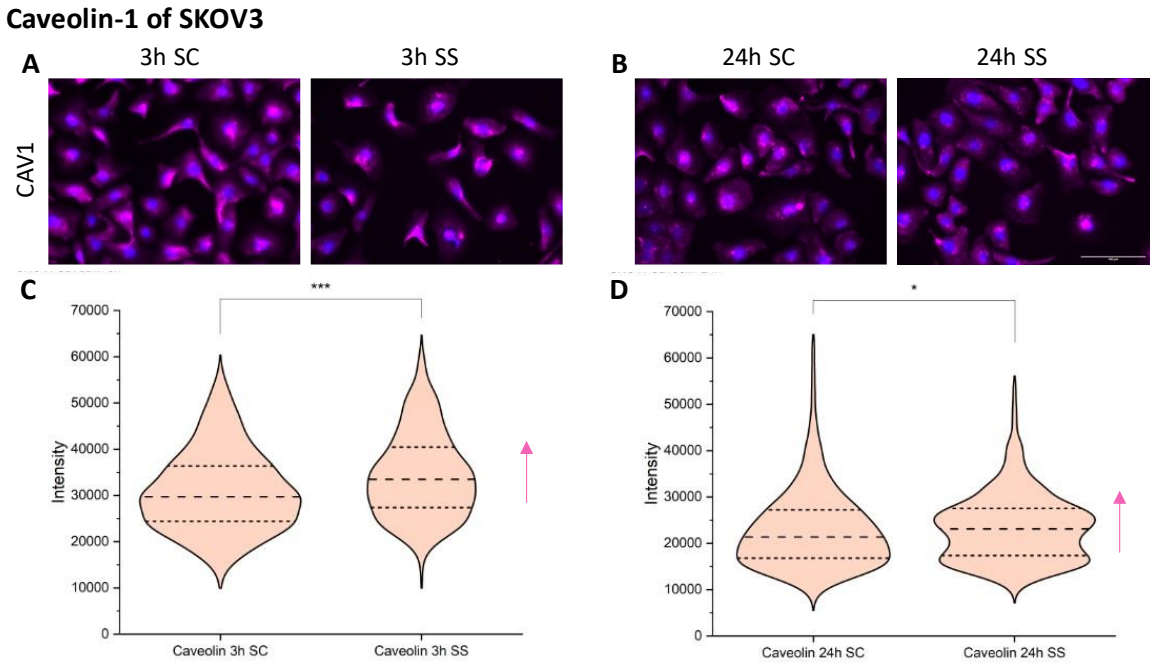

Figure 22: Microscopy: Cav1 of static control and shear stress (SKOV3)

Displayed are images and violin plot with quartiles of SKOV3 cell line after n = 3-5 biological experiments. SC = static control, SS = shear stress. A+C = 3 hours static and shear, B+D = 24 hours static and shear.
*Significant difference with *p<0,05, **p<0,01, ***p<0,001 (t-Test).*
A+B: Images are acquired with Lionheart FX automated microscope, 20x magnification, nuclei in blue and Cav1 in pink, scale bar 100 µm.

In contrast, significant decrease of Cav1 is seen for OVCAR3 after 3 hours of shear stress (C), but not after 24 hours (D) as demonstrated in *figure 23*.

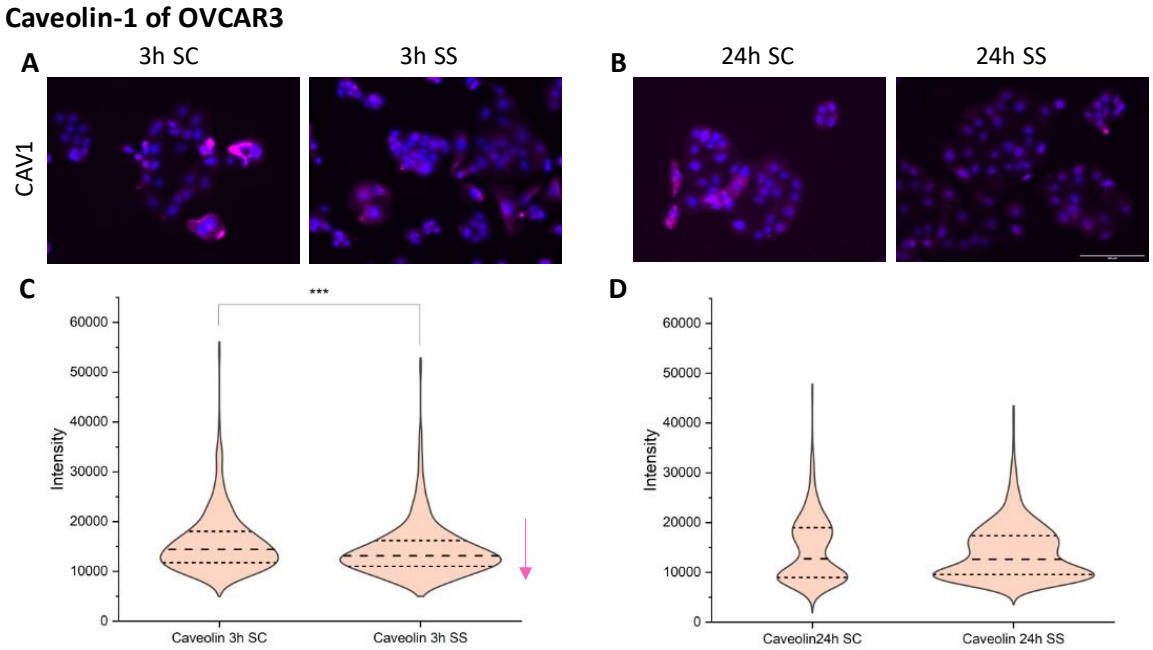

Figure 23: Microscopy: Cav1 of static control and shear stress (OVCAR3)

Displayed are images and violin plot with quartiles of OVCAR3 cell line after n = 3 biological experiments. SC = static control, SS = shear stress. A+C = 3 hours static and shear, B+D = 24 hours static and shear.
*Significant difference with *p<0,05, **p<0,01, ***p<0,001 (t-Test).*
A+B: Images are acquired with Lionheart FX automated microscope, 20x magnification, nuclei in blue and Cav1 in pink, scale bar 100 µm.

3.3.3 Ajuba

Ajuba is a protein involved in the regulations on YAP activity [64], which might give an interesting insight into the signaling events influenced by shear stress. The results reported below refer to the quantification of the signal intensity in correspondence of the nuclear area.

Shear stress leads to an increase in Ajuba intensity after 3 hours (C), but a decrease after 24 hours (D) as shown in *figure 24* in SKOV3 cell line, even though the analysis shows very heterogeneous results for the biological replicates.

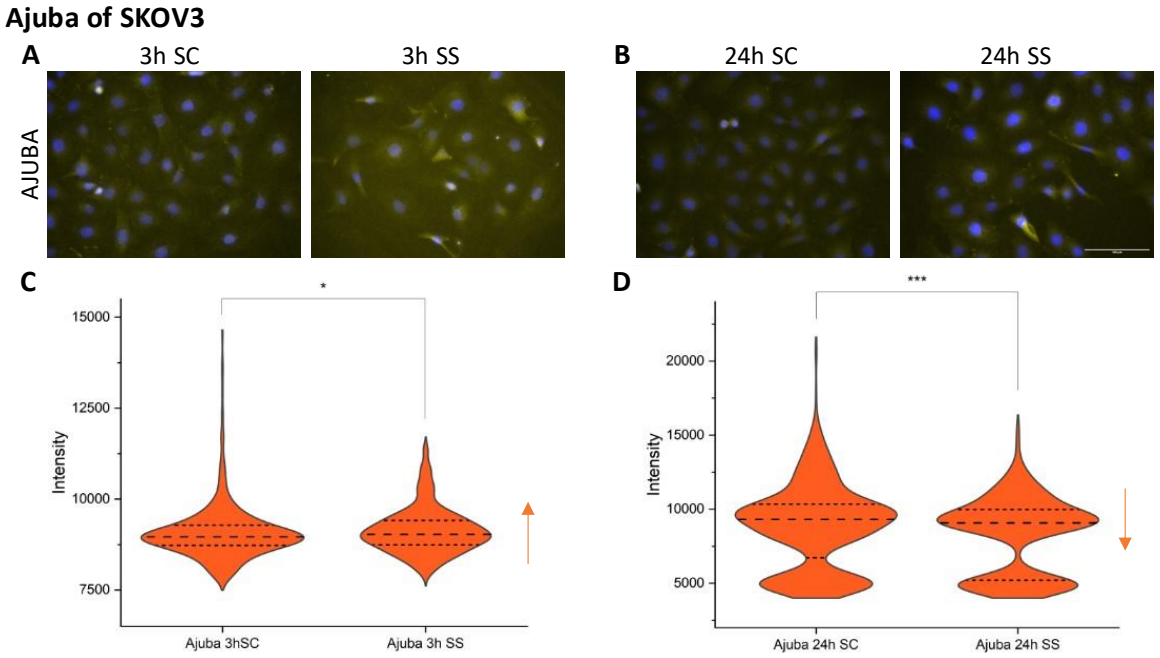

Figure 24: Microscopy: Ajuba of static control and shear stress (SKOV3)

Displayed are images and violin plot with quartiles of SKOV3 cell line after n = 3-5 biological experiments. SC = static control, SS = shear stress. A+C = 3 hours static and shear, B+D = 24 hours static and shear.
*Significant difference with *p<0,05, **p<0,01, ***p<0,001 (t-Test).*
A+B: Images are acquired with Lionheart FX automated microscope, 20x magnification, nuclei in blue and Ajuba in yellow, scale bar 100 µm.

Intensity of Ajuba in OVCAR3 cell line is very low, justifying why the images A and B are demonstrated without nuclei in *figure 25*. Ajuba is significantly decreased after 3 hours of shear stress (C), in contrast to a non-significant decreasing trend after 24 hours (D).

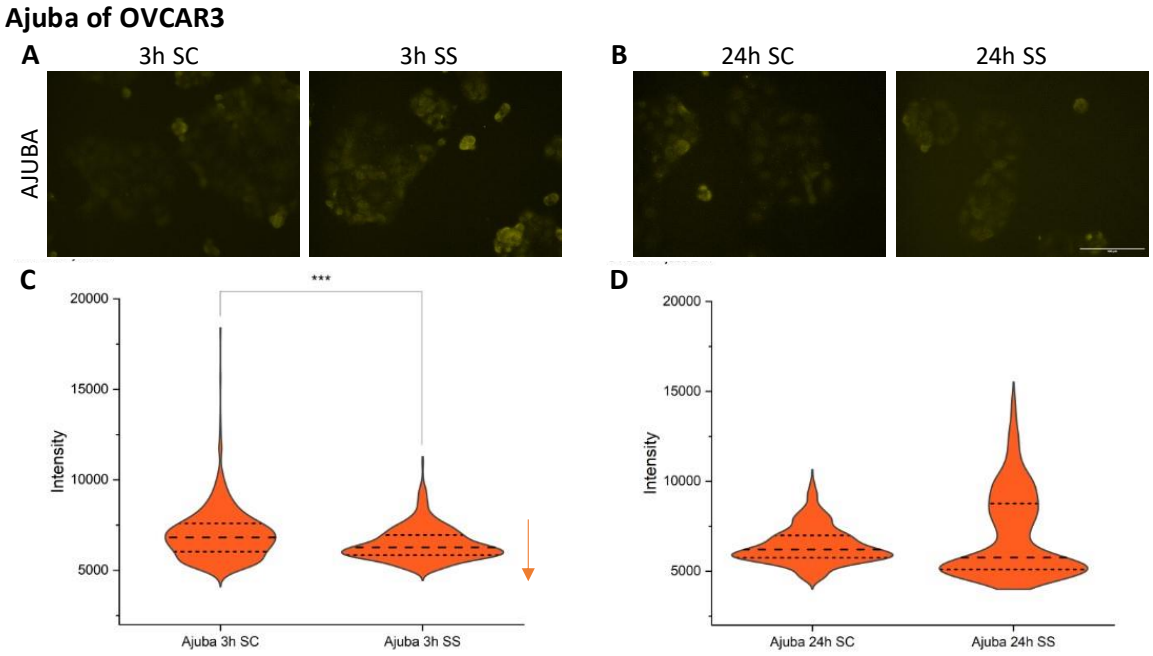

Figure 25: Microscopy: Ajuba of static control and shear stress (OVCAR3)

Displayed are images and violin plot with quartiles of OVCAR3 cell line after n = 3-5 biological experiments. SC = static control, SS = shear stress. A+C = 3 hours static and shear, B+D = 24 hours static and shear.
*Significant difference with *p<0,05, **p<0,01, ***p<0,001 (t-Test).*
A+B: Images are acquired with Lionheart FX automated microscope, 20x magnification, Ajuba in yellow, scale bar 100 µm.

3.3.4 Piezo1

As a mechanosensitive ion channel, Piezo1 is activated through shear stress and further influences signaling cascades, including the Hippo pathway, and could elucidate differences in the cell lines [47]. Image analyzation was performed for nuclear and cytoplasmic area and results for total intensity was received.

SKOV3 cell line shows no differences in total Piezo1 intensity after 3 hours of shear stress (C), but significantly decreases after 24 hours of shear stress compared to static control (D) displayed in *figure 26*.

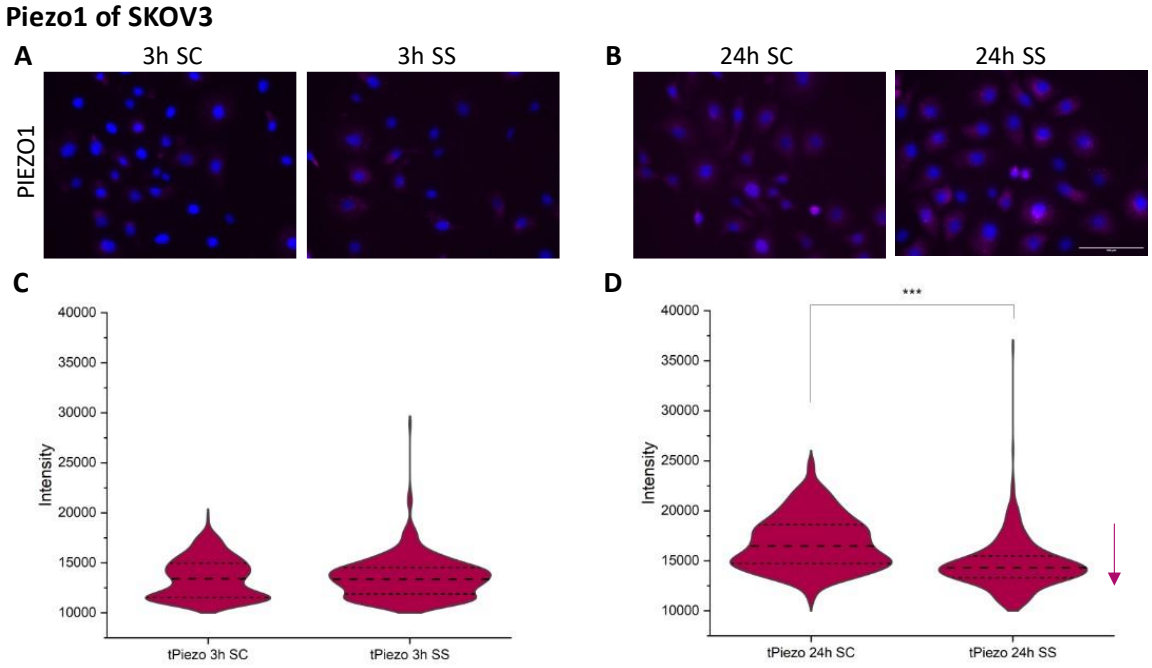

Figure 26: Microscopy: Piezo1 of static control and shear stress (SKOV3)

Displayed are images and violin plot with quartiles of SKOV3 cell line after n = 3 biological experiments. SC = static control, SS = shear stress, tPiezo = total Piezo. A+C = 3 hours static and shear, B+D = 24 hours static and shear.
*Significant difference with *p<0,05, **p<0,01, ***p<0,001 (t-Test).*
A+B: Images are acquired with Lionheart FX automated microscope, 20x magnification, nuclei in blue and Piezo1 in pink, scale bar 100 µm.

As seen in *figure 27*, more pronounced decreases are seen for OVCAR3 cell line. Total intensity of Piezo1 is significantly reduced after 3 and 24 hours of shear stress when compared to their static controls.

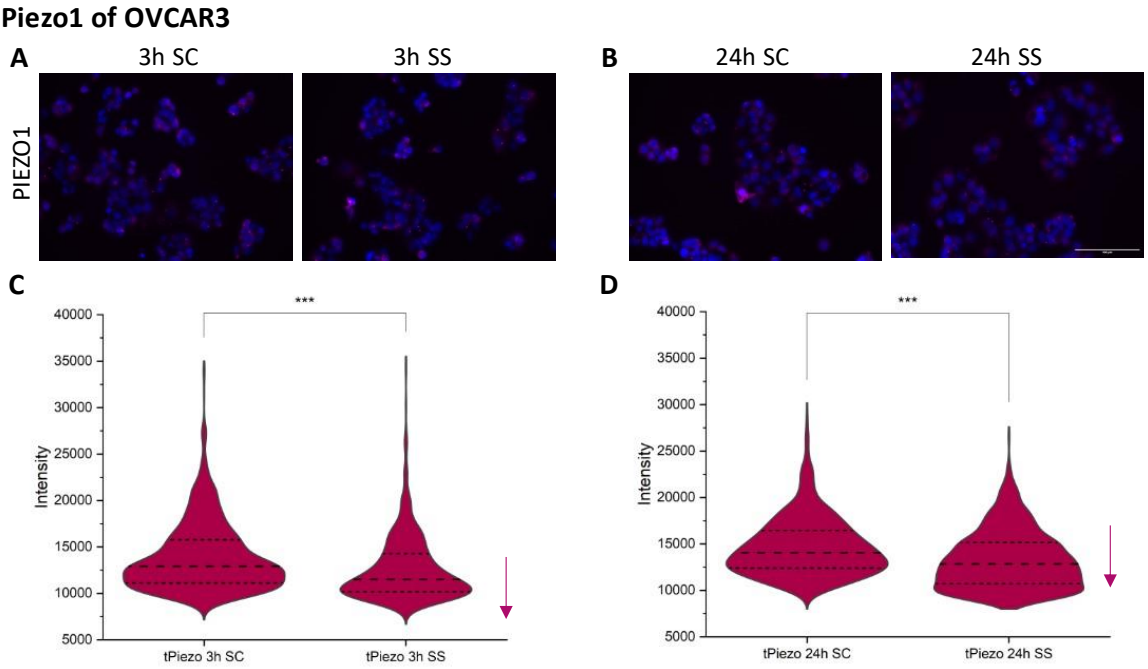

Figure 27: Microscopy: Piezo1 of static control and shear stress (OVCAR3)

Displayed are images and violin plot with quartiles of OVCAR3 cell line after n = 3 biological experiments. SC = static control, SS = shear stress, tPiezo = total Piezo. A+C = 3 hours static and shear, B+D = 24 hours static and shear.
*Significant difference with *p<0,05, **p<0,01, ***p<0,001 (t-Test).*
A+B: Images are acquired with Lionheart FX automated microscope, 20x magnification, nuclei in blue and Piezo1 in pink, scale bar 100 µm.

3.3.5 YAP

The key player of the Hippo pathway YAP1 is a mechanosensitive protein regulating a variety of transcription factors [59]. Therefore, effects of shear stress have been elucidated and to additionally put the information into context, 0,1 µM YODA treatment was performed to chemically activate Piezo1 and mimic effects of shear stress [100]. The results are acquired as total intensity from nuclear and cytosolic area and the quotient of those to show nuclear translocation.

As seen in *figure 28* the intensity of total YAP, as well as translocation of YAP into the nucleus is not induced through shear stress for SKOV3 cell line.

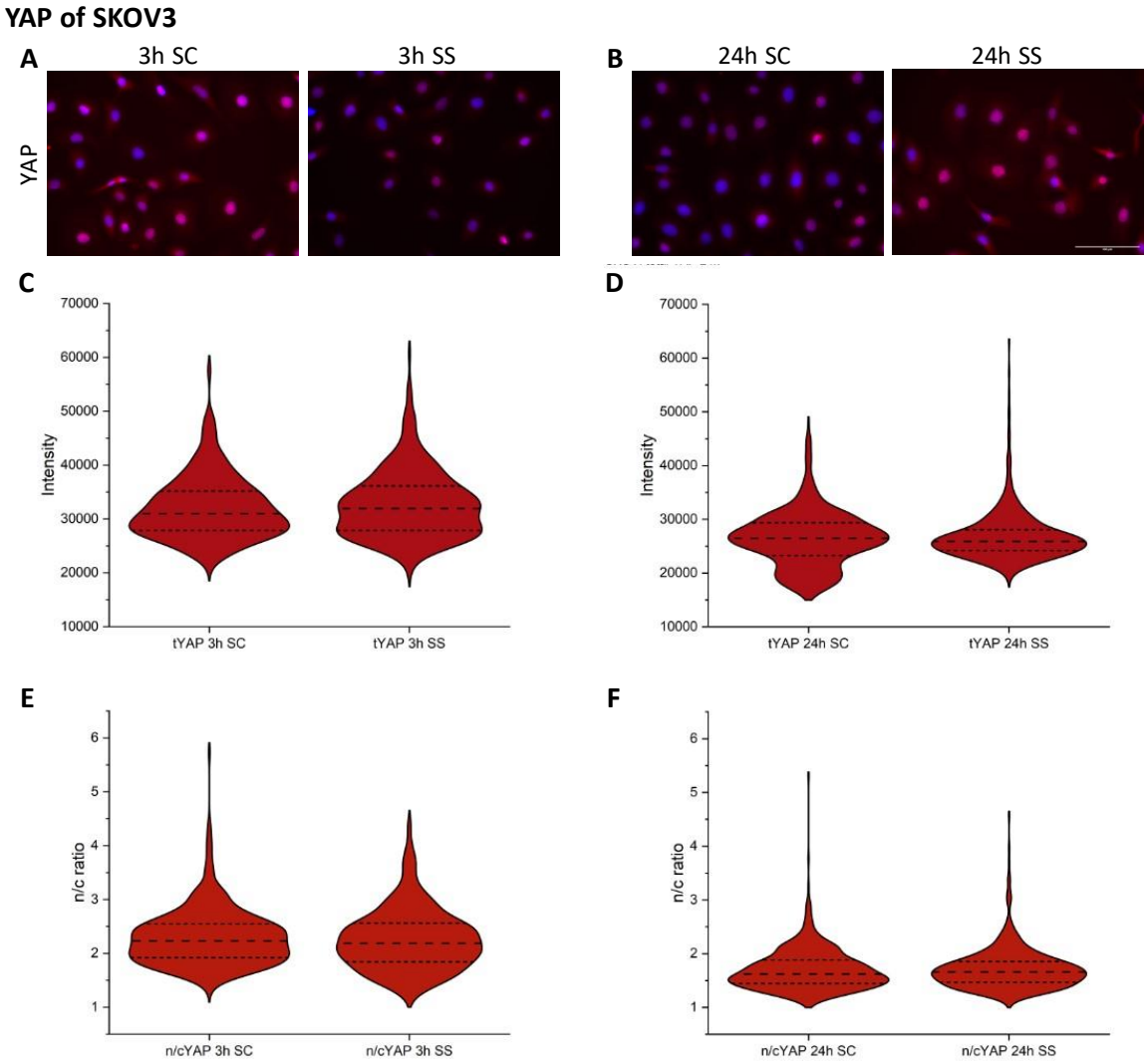

Figure 28: Microscopy: total YAP and YAP translocation of static control and shear stress (SKOV3)

Displayed are images and violin plot with quartiles of SKOV3 cell line after n = 3 biological experiments. SC = static control, SS = shear stress, tYAP = total YAP, n/c = nucleus to cytoplasm. A+C+E = 3 hours static and shear, B+D+F = 24 hours static and shear.
No significant differences between control and shear stress with (t-Test).

A+B: Images are acquired with Lionheart FX automated microscope, 20x magnification, nuclei in blue and YAP1 in red, scale bar 100 µm.

In comparison, *figure 29* shows more pronounced results for SKOV3 cell line after treatment with YODA with significant increases in total YAP after 3 (C) and 24 hours (D) of incubation. After 3 hours of YODA, YAP translocation is significantly increased, but not after 24 hours.

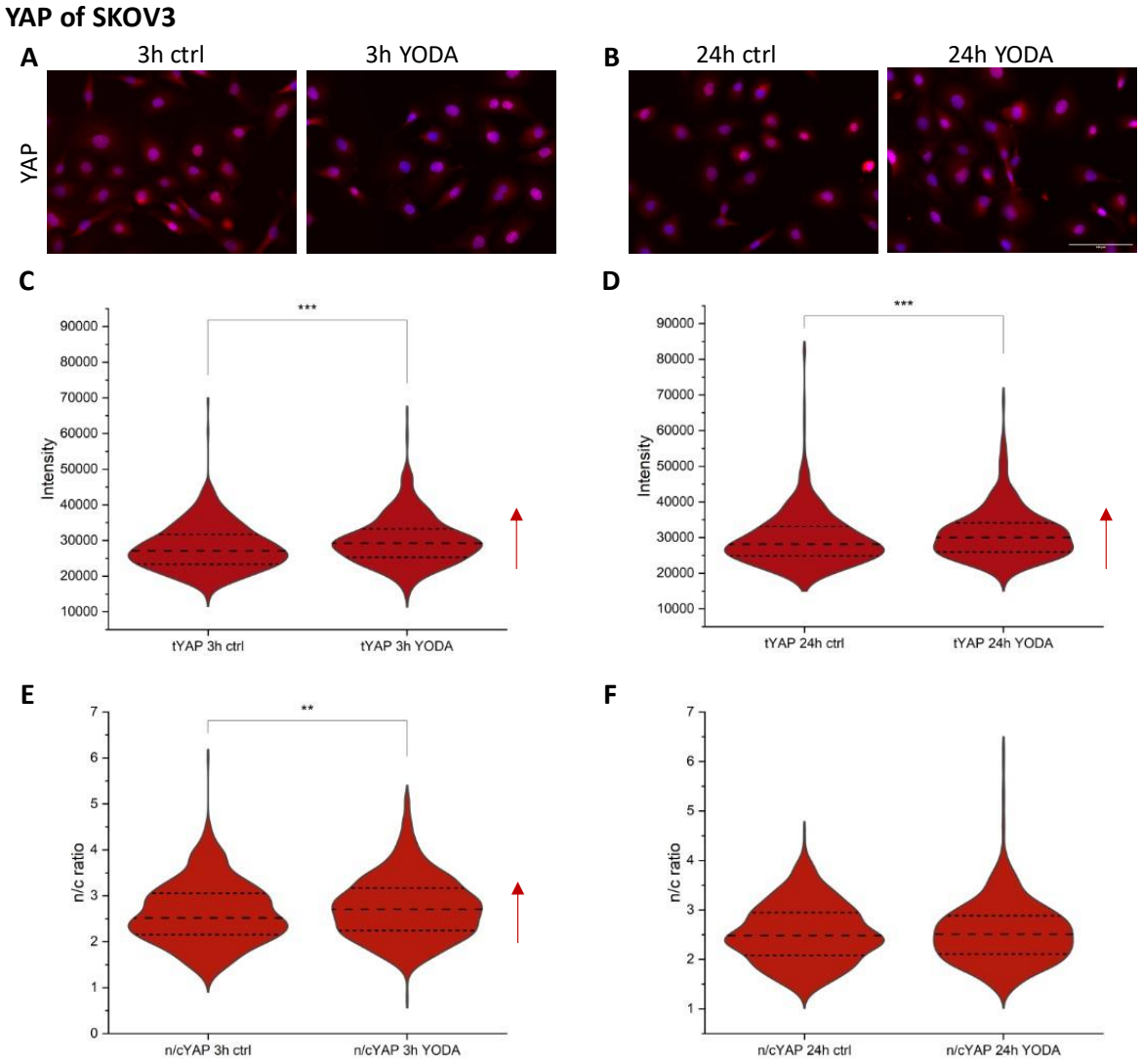

Figure 29: Microscopy: total YAP and YAP translocation after YODA treatment (SKOV3)

Displayed are images and violin plot with quartiles of SKOV3 cell line after n = 4 biological experiments. ctrl = untreated control, YODA = YODA treatment, tYAP = total YAP, n/c = nucleus to cytoplasm. A+C+E = 3 hours treatment incubation, B+D+F = 24 hours treatment incubation.
*Significant difference with *p<0,05, **p<0,01, ***p<0,001 (t-Test).*
A+B: Images are acquired with Lionheart FX automated microscope, 20x magnification, nuclei in blue and YAP1 in red, scale bar 100 µm.

Analysis of YAP1 for OVCAR3 cell line is shown in *figure 30*. Translocation can be obtained for OVCAR3 cell line after 3 (E) and 24 (F) hours of shear stress, but no significant changes in total YAP concentration (C and D).

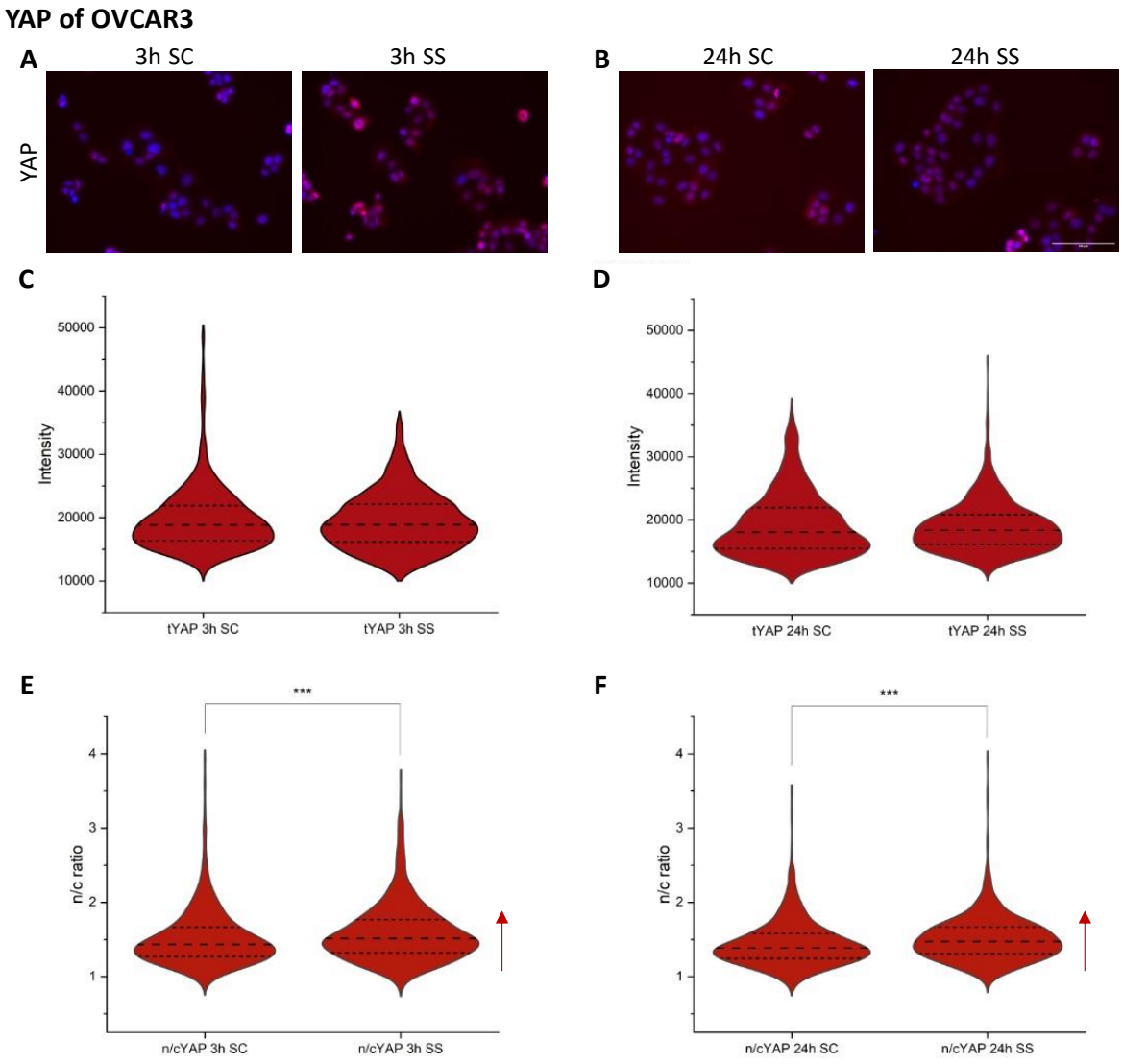

Figure 30: Microscopy: total YAP and YAP translocation of static control and shear stress (OVCAR3)

Displayed are images and violin plot with quartiles of OVCAR3 cell line after n = 3 biological experiments. SC = static control, SS = shear stress, tYAP = total YAP, n/c = nucleus to cytoplasm. A+C+E = 3 hours static and shear, B+D+F = 24 hours static and shear.
*Significant difference with *p<0,05, **p<0,01, ***p<0,001 (t-Test).*
A+B: Images are acquired with Lionheart FX automated microscope, 20x magnification, nuclei in blue and YAP1 in red, scale bar 100 µm.

Differentially to SKOV3, OVCAR3 cell line shows less pronounced results after treatment with YODA as displayed in *figure 31*. Total intensity of YAP is increased after shear stress, which is significant after 24 hours (D) of incubation. A significantly higher translocation of YAP is achieved after 3 hours (E) of treatment incubation, but not after 24 hours.

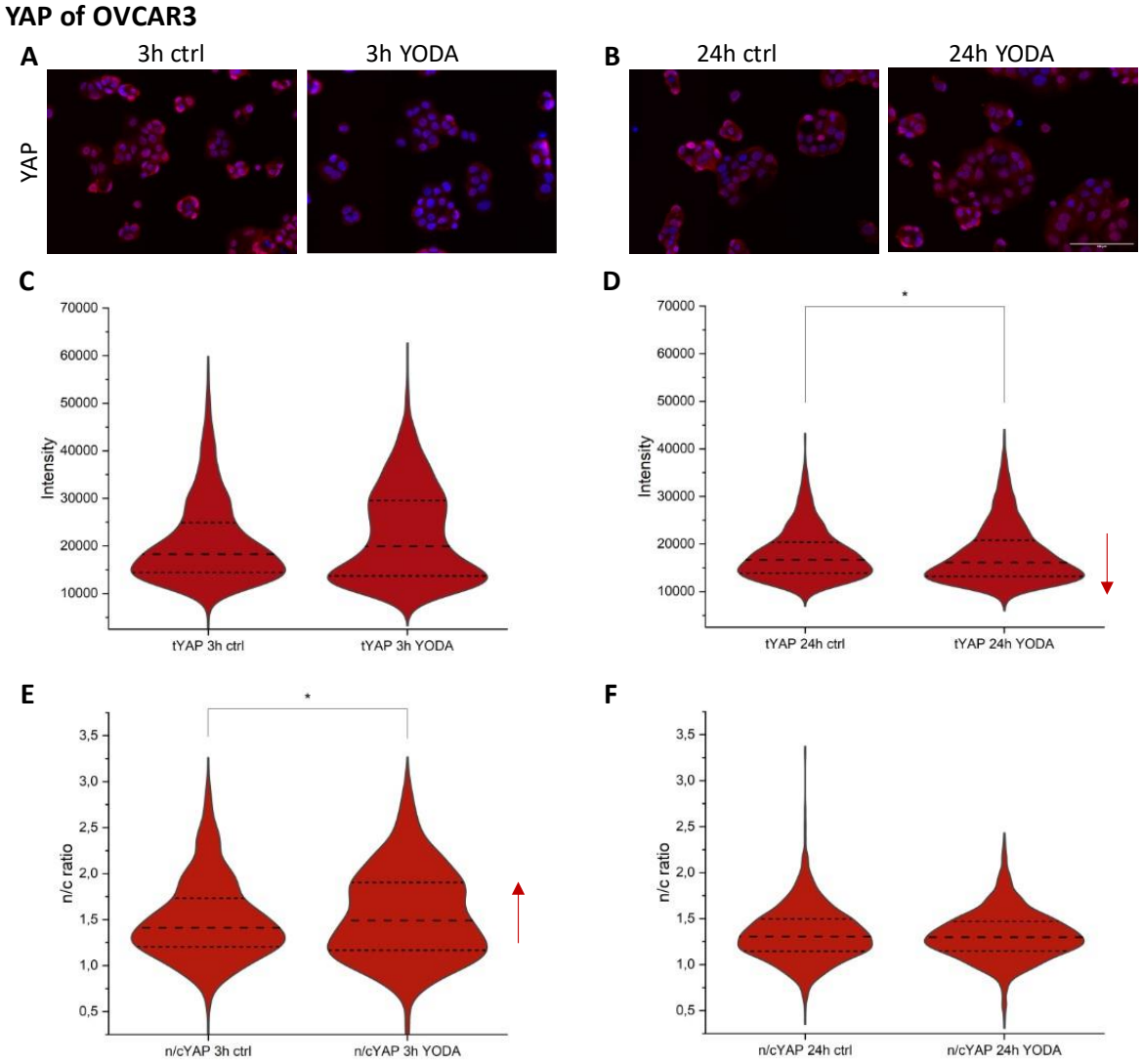

Figure 31: Microscopy: total YAP and YAP translocation after YODA treatment (OVCAR3)

Displayed are images and violin plot with quartiles of OVCAR3 cell line after n = 4 biological experiments. ctrl = untreated control, YODA = YODA treatment, tYAP = total YAP, n/c = nucleus to cytoplasm. A+C+E = 3 hours treatment incubation, B+D+F = 24 hours treatment incubation.
*Significant difference with *p<0,05, **p<0,01, ***p<0,001 (t-Test).*
A+B: Images are acquired with Lionheart FX automated microscope, 20x magnification, nuclei in blue and YAP1 in red, scale bar 100 µm.

3.3.6 Nrf2

Compared to YAP1, Nrf2 follows a different pathway and the transcriptional regulation is important for detoxification events [55]. Nrf2 signaling might be interesting to elucidate the responses of cisplatin treatment. The results are acquired as total intensity from nuclear and cytosolic area and the quotient of those.

Figure 32 represents Nrf2 of SKOV3 cell line, 3 hours of shear stress leads to a significant decrease of total Nrf2 intensity (C) compared to the static control in contrast to a significant increase after 24 hours (D). Similar are the results for Nrf2 translocation which is lowered trough 3 hours of shear stress (E) but increased trough 24 hours (F).

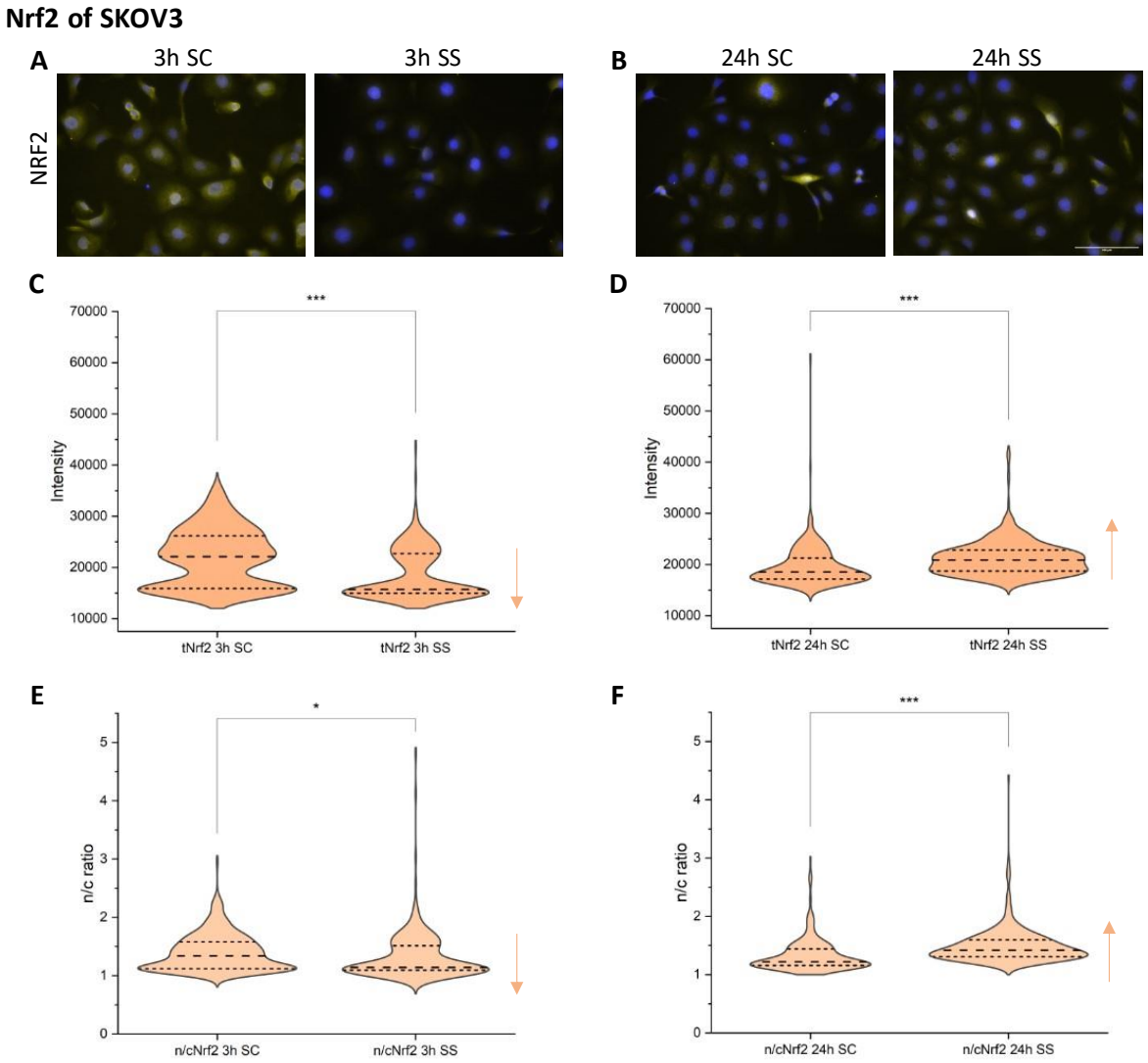

Figure 32: Microscopy: Nrf2 of static control and shear stress (SKOV3)

Displayed are images and violin plot with quartiles of SKOV3 cell line after n = 3 biological experiments. SC = static control, SS = shear stress, tNrf2 = total Nrf2, n/c = nucleus to cytoplasm. A+C+E = 3 hours static and shear, B+D+F = 24 hours static and shear.
*Significant difference with *p<0,05, **p<0,01, ***p<0,001 (t-Test).*

A+B: Images are acquired with Lionheart FX automated microscope, 20x magnification, nuclei in blue and Nrf2 in yellow, scale bar 100 µm.

For OVCAR3 cell line 3 hours of shear stress did not influence the intensity of Nrf2 (C) nor the translocation (E) as shown in *figure 33*. But after 24 hours total intensity of Nrf2 decreases significantly with shear stress (D). Also, a reduction in translocation can be seen after 24 hours of shear stress compared to the static control (F).

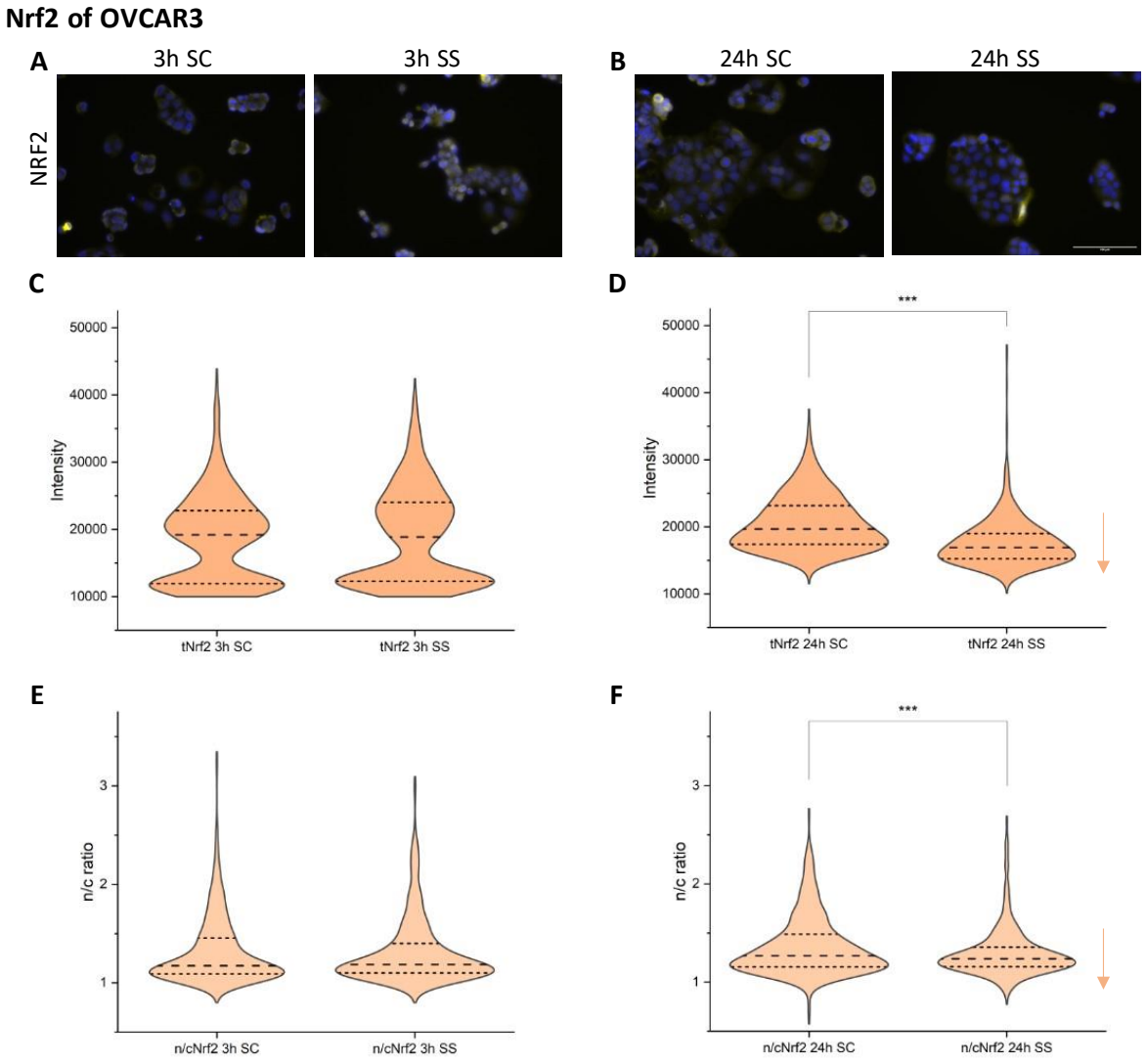

Figure 33: Microscopy: Nrf2 of static control and shear stress (OVCAR3)

Displayed are images and violin plot with quartiles of OVCAR3 cell line after n = 3 biological experiments. SC = static control, SS = shear stress, tNrf2 = total Nrf2, n/c = nucleus to cytoplasm. A+C+E = 3 hours static and shear, B+D+F = 24 hours static and shear.
*Significant difference with *p<0,05, **p<0,01, ***p<0,001 (t-Test).*
A+B: Images are acquired with Lionheart FX automated microscope, 20x magnification, nuclei in blue and Nrf2 in yellow, scale bar 100 µm.

3.3.7 PTMs

Analyzing different post-translational modification might give insights into the differences of SKOV3 and OVCAR3 cell lines. Farnesylation is important for the Hippo pathway [81], acetylation for metabolism [79] and phosphorylation for signal transduction [77]. The results for farnesylation and acetylation were quantified from the nuclear area and for phosphorylation are acquired as total intensity from nuclear and cytosolic area and the quotient of those.

Farnesylation is significantly increased after 3 (C) and 24 hours (D) of shear stress in SKOV3 cell line compared to static control as shown in *figure 34*.

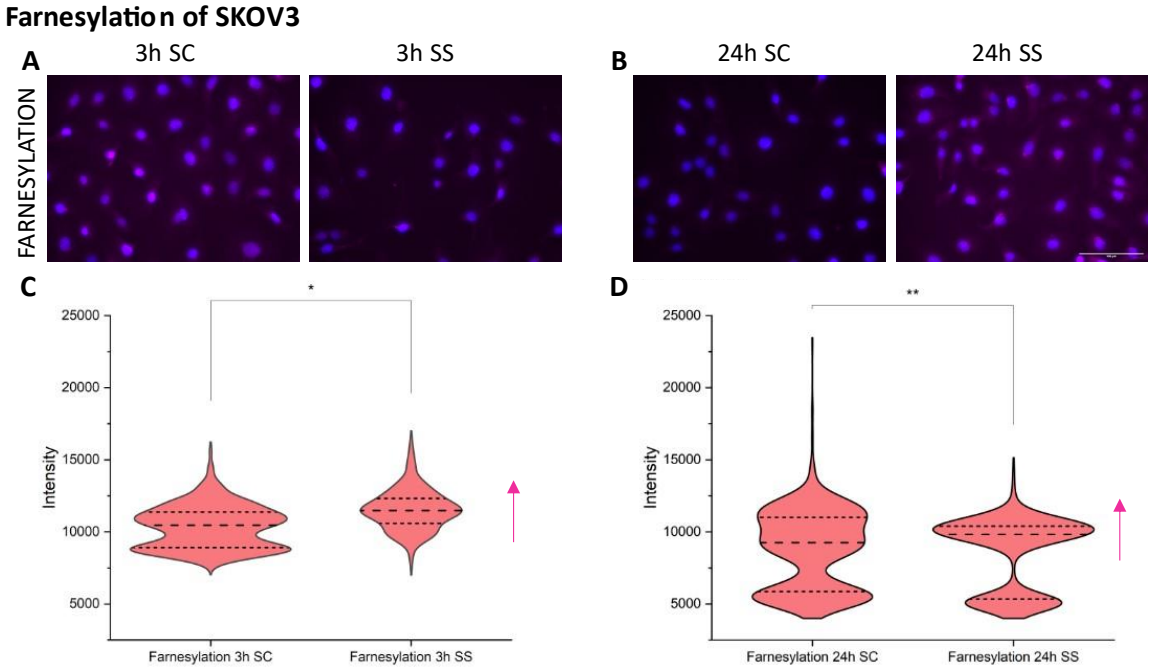

Figure 34: Microscopy: Farnesylation of static control and shear stress (SKOV3)

Displayed are images and violin plot with quartiles of SKOV3 cell line after n = 3-5 biological experiments. SC = static control, SS = shear stress. A+C = 3 hours static and shear, B+D = 24 hours static and shear.
*Significant difference with *p<0,05, **p<0,01, ***p<0,001 (t-Test).*
A+B: Images are acquired with Lionheart FX automated microscope, 20x magnification, nuclei in blue and farnesylation in pink, scale bar 100 µm.

In contrast, a significant decrease in farnesylation intensity is seen for OVCAR3 cell line after 3 (C) and 24 hours (D) of shear stress as displayed in *figure 35*.

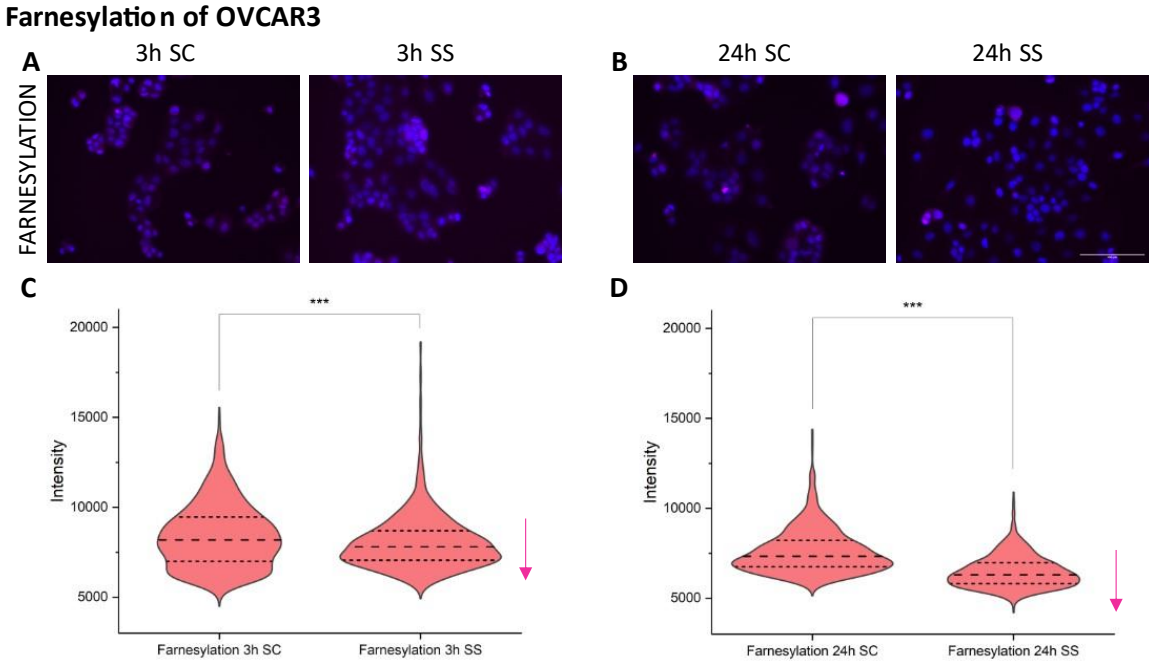

Figure 35: Microscopy: Farnesylation of static control and shear stress (OVCAR3)

Displayed are images and violin plot with quartiles of OVCAR3 cell line after n = 3-5 biological experiments. SC = static control, SS = shear stress. A+C = 3 hours static and shear, B+D = 24 hours static and shear.
*Significant difference with *p<0,05, **p<0,01, ***p<0,001 (t-Test).*
A+B: Images are acquired with Lionheart FX automated microscope, 20x magnification, nuclei in blue and farnesylation in pink, scale bar 100 µm.

As seen in *Figure 36*, acetylation is not significantly increased after 3 hours of shear stress (C), but after 24 hours (D) in SKOV3 cell line. Acetylation seems to decrease over time when comparing overall intensities in graph C and D.

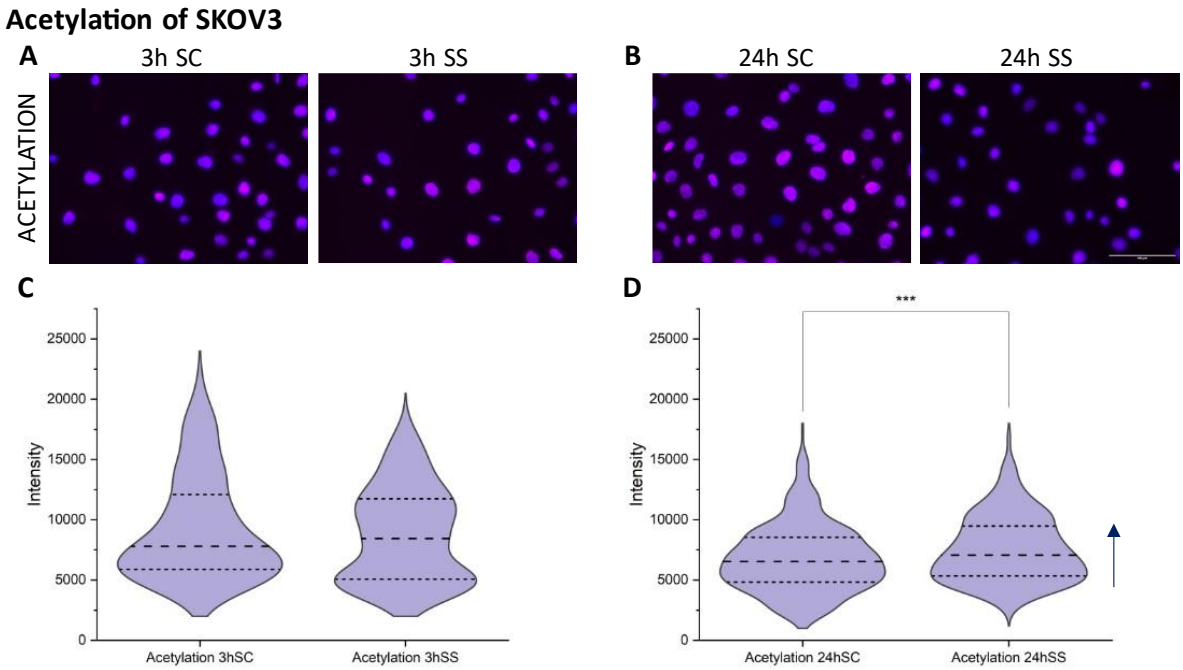

Figure 36: Microscopy: Acetylation of static control and shear stress (SKOV3)

Displayed are images and violin plot with quartiles of SKOV3 cell line after n = 3 biological experiments. SC = static control, SS = shear stress. A+C = 3 hours static and shear, B+D = 24 hours static and shear.
*Significant difference with *p<0,05, **p<0,01, ***p<0,001 (t-Test).*
A+B: Images are acquired with Lionheart FX automated microscope, 20x magnification, nuclei in blue and acetylation in pink, scale bar 100 µm.

In contrast, OVCAR3 cell line shows a slight significant increase in acetylation after 3 hours of shear stress (C) compared to the static control but decreases significantly after 24 hours of shear stress (D) as displayed in *Figure 37*. Also, for OVCAR3 the overall intensity reduction was observed over time seen in graph C and D.

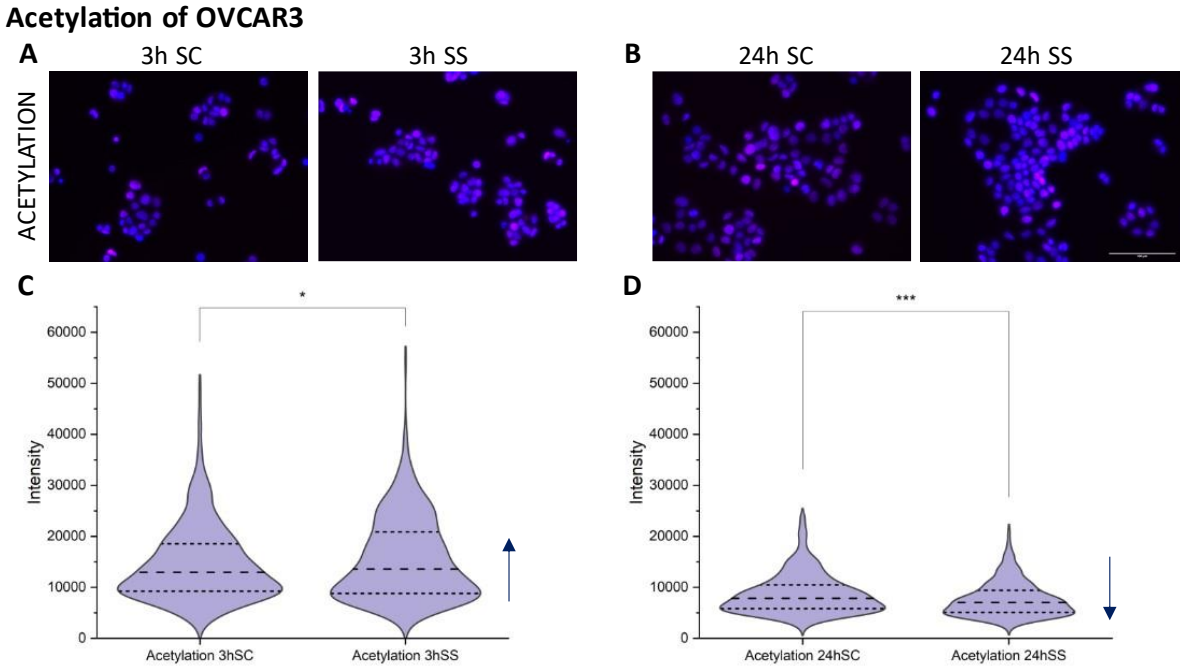

Figure 37: Microscopy: Acetylation of static control and shear stress (OVCAR3)

Displayed are images and violin plot with quartiles of OVCAR3 cell line after n = 3 biological experiments. SC = static control, SS = shear stress. A+C = 3 hours static and shear, B+D = 24 hours static and shear.
*Significant difference with *p<0,05, **p<0,01, ***p<0,001 (t-Test).*
A+B: Images are acquired with Lionheart FX automated microscope, 20x magnification, nuclei in blue and acetylation in pink, scale bar 100 µm.

Phosphorylation for SKOV3 cell line is presented in *figure 38* and shows a significant decrease in total phosphorylation after 3 (C) and 24 hours (D). Similar, the translocation of phosphorylation significantly reduces after 3 (E) and 24 hours (F) of shear stress compared to the static control.

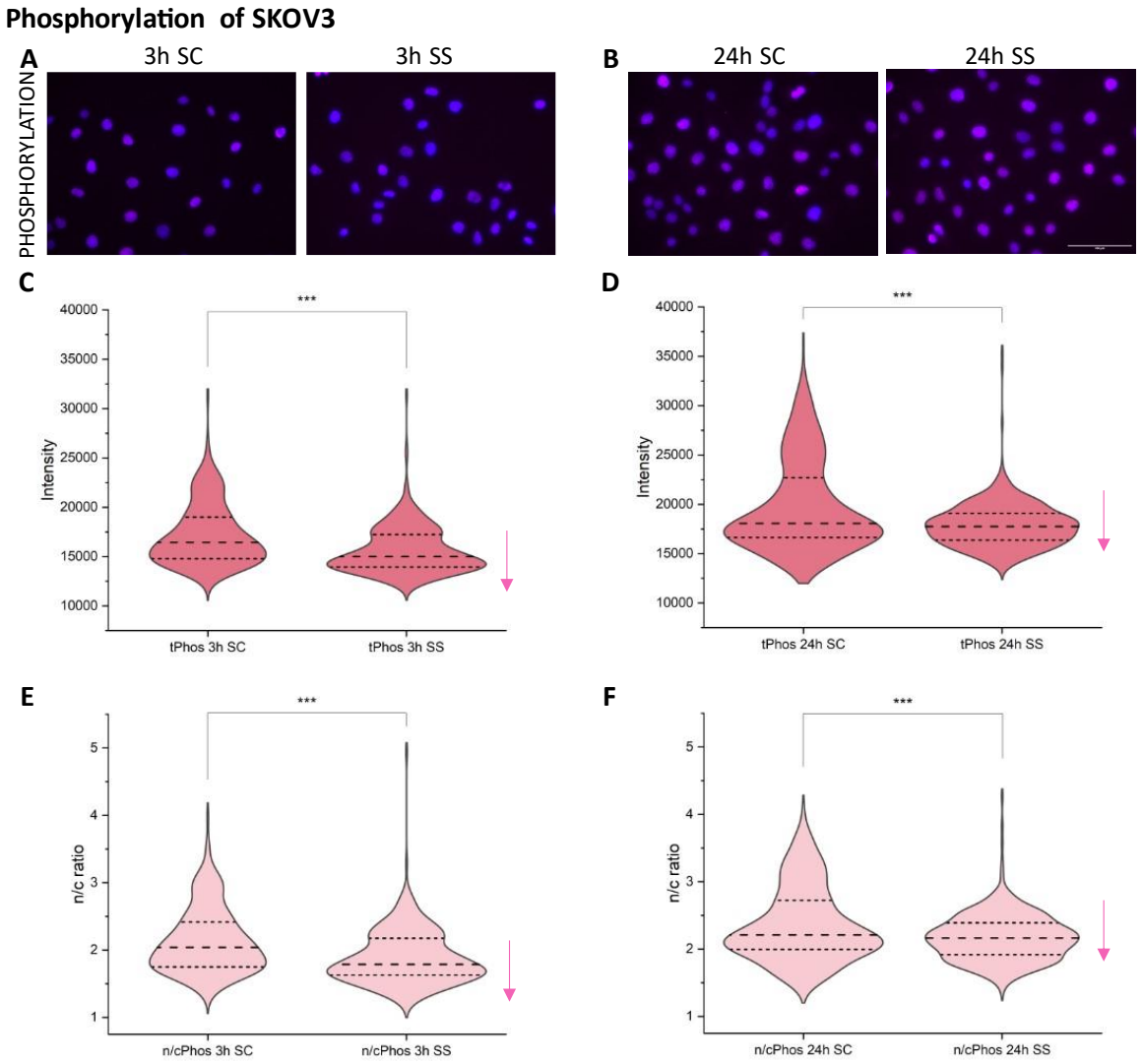

Figure 38: Microscopy: Phosphorylation of static control and shear stress (SKOV3)

Displayed are images and violin plot with quartiles of SKOV3 cell line after n = 3 biological experiments. SC = static control, SS = shear stress, tPhos = total Phosphorylation, n/c = nucleus to cytoplasm. A+C+E = 3 hours static and shear, B+D+F = 24 hours static and shear.
*Significant difference with *p<0,05, **p<0,01, ***p<0,001 (t-Test).*
A+B: Images are acquired with Lionheart FX automated microscope, 20x magnification, nuclei in blue and phosphorylation in pink, scale bar 100 µm.

On the other hand, OVCAR3 shows a significant increase in total phosphorylation intensity after 3 hours (C) of shear stress but significantly decreases after 24 hours (D). The same is seen for translocation of phosphorylation, which increases after 3 (E) but decreases after 24 hours (F) of shear stress shown in *figure 39*.

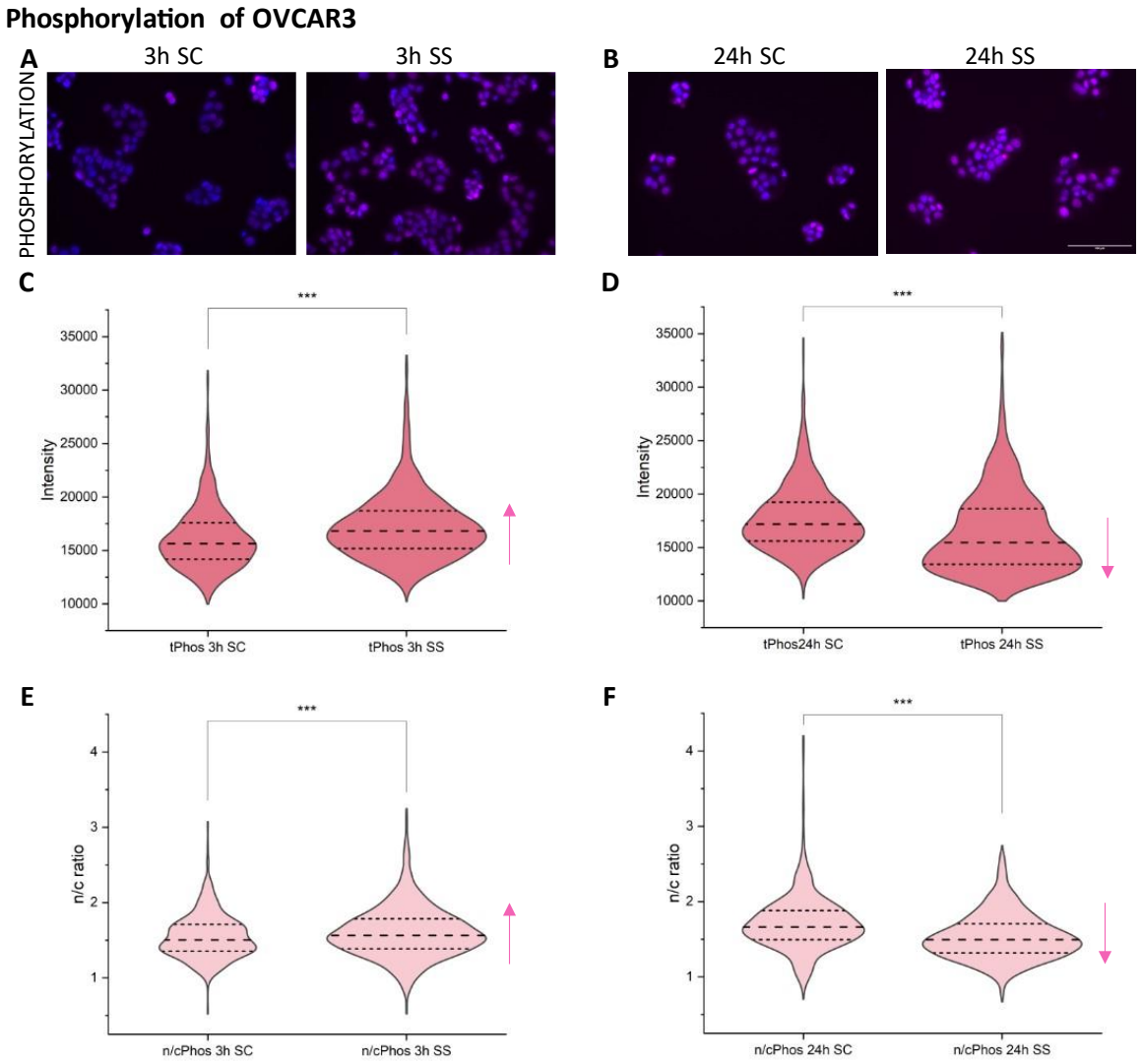

Figure 39: Microscopy: Phosphorylation of static control and shear stress (OVCAR3)

Displayed are images and violin plot with quartiles of OVCAR3 cell line after n = 3 biological experiments. SC = static control, SS = shear stress, tPhos = total Phosphorylation, n/c = nucleus to cytoplasm. A+C+E = 3 hours static and shear, B+D+F = 24 hours static and shear.
*Significant difference with *p<0,05, **p<0,01, ***p<0,001 (t-Test).*
A+B: Images are acquired with Lionheart FX automated microscope, 20x magnification, nuclei in blue and phosphorylation in pink, scale bar 100 µm.

4 Discussion

Ovarian cancer cells are surrounded by a variety of physical stressors in the peritoneal cavity and especially fluid shear stress increases with the ascitic build-up in many women. The impact of shear stress stimuli *in vitro* has been previously described by Bileck et al., 2021 via proteomic and structure analysis. In this work, it was described how differently SKOV3 and OVCAR3 cell lines react to external stressors and how this reflects on cells morphology and in changes in phosphoproteome signature that could already be observed after 3 hours of shear stress [94]. Already the very first experiment regarding proliferation rates (*figure 11*) demonstrates that both cell lines decrease proliferation after short term exposure to mechanical cues (3 hours of shear stress), revealing a high sensitivity to physical stimulation. Even though significances between static control and the corresponding shear stress samples are not strong, a trend can be seen. Especially when looking at the percentual growth of the cell lines, shear stress decreases growth. However, when looking at the kinetic of the events, between 24-72 hours an increased cell growth could be observed. Previous research has shown reduced cell viability and cellular adaptations to shear stress [102] but also the impact of different matrix stiffness on the behavior of ovarian cancer cell lines was reported [103]. Additionally, it was proven that cells can retain a memory of their previous environment, e.g. past matrix stiffness or mechanical cues even after they have been removed from that environment. This cellular memory can influence cell behavior and function when cells are subsequently placed in a different environment [104, 105]. Cells cultured at different seeding densities can exhibit distinct responses to their surrounding environment and the cell-cell contact might change cell signaling as has been shown for the Hippo pathway [106].

Cisplatin is the most efficient and most frequently used platinum-based drug in ovarian cancer treatment [107]. But as treatment frequency rises, resistance to cisplatin emerges and both cell lines show some baseline resistance [89, 91]. However, the specific effects of shear stress on the efficiency of cisplatin or other platinum-based drugs on ovarian cancer cell lines have not been extensively studied. The impact of mechanical stimulation on chemoresistance especially against cisplatin depends on the substrate stiffness [103] as well as on shear stress [87, 108, 109], which is consistent with our findings but effects further depend on the specific characteristics of the cancer cells. Treatment efficiency for SKOV3 cells with cisplatin resulted in a complex response profile. However, treatment efficiency for SKOV3 cell line follows a more dose-dependent response where treatment with 20 µM cisplatin was observed with the

lowest cell mass after 3 hours (*figure 13*). After 24 hours the response appeared to be U-shaped with the highest treatment efficiency at 1 µM cisplatin (*figure 14*). An incubation time of 48 hours seems to be more efficient in cells that underwent mechanical stimulation protocol for treatment with 0,5-5 µM cisplatin changing to a decreased sensitivity for treatment with higher concentrations of 5-20 µM similar for 3 and 24 hours of shear stress (*figure 13 and 14, panel A*). The equal effect is seen for 24 hours of cisplatin incubation after 24 hours of shear stress (*figure 14, panel B*), but compared to the same layout after 3 hours of shear stress, where all concentration except for 20 µM the static control seems to be more sensitive to the treatment (*figure 13, panel B*). A very low response to cisplatin treatment was observed in the third layout with treatment after 24 hours of recovery time for the cells. For SKOV3 cell line, Hassan et al., 2022 found a decreased sensitivity towards 0,05 mM cisplatin treatment through the activation of PI3K/Akt signaling pathway induced by shear stress [108]. Moreover, in spheroid formation shear stress leads to a greater chemoresistance in SKOV3 for 25 mM cisplatin [87] supporting the results achieved for higher cisplatin concentration in our experiments. The results of cisplatin treatment on the OVCAR3 cell line did not show any significant differences between static and shear and an overall linear treatment response was observed (*figure 15 and 16*). Even though slight differences might be seen, shifts and changes in active signaling pathways and cell cycle phase progression could play a role in treatment efficiency. Nath et al., 2020 showed a carboplatin resistance of the OVCAR5 cell line through increased ERK-activation induced by shear stress [109]. Notably, the lowest effect of cisplatin was observed in the third layout with 24 hours of recovery time regardless of static or sheared. Overall, the data might lead to the conclusion that SKOV3 and OVCAR3 cell lines have different drug responses. However further studies are in progress to elucidate molecular mechanisms underpinning these data.

Ovarian cancer cells are sensitive to physical stimulation and therefore structural changes in nuclei area, elongation and the formation of stress fibers can occur [94]. This was seen in nuclear area observing a significant increase in size, indicating stress sensation and cellular adaptations through shear stress in SKOV3 and OVCAR3. Furthermore, both cell lines show an initial decrease in actin intensity after shear stress, which is comparingly more pronounced in OVCAR3. Previous research has shown that stress fiber formation occurs in the OVCAR3 cell line due to physical movement [94, 110], which was visually seen with the microscope. However, actin intensity decreases significantly after shear stress compared to the static

control (*figure 21*). This was not expected since stress fibers would typically increase signal intensity, hence these results need to be interpreted with caution and additional quantification strategies are currently in progress to verify these results. For SKOV3 cell line the cytoskeleton seems to contract lightly after 3 hours of shear stress but spreads again as shear stress continues seen as an increase in actin intensity (*figure 19*). This points to various adaptational strategies of the cell to shear stress.

A very well-known mechanosensor is Caveolin-1 since Cav1 interacts with the actin cytoskeleton and is involved in formation of caveolae at the plasma membrane. 3 hours of shear stress led to a significant increase in Cav1 in the SKOV3 cell line (*figure 22*), but to a decrease in the OVCAR3 cell line (*figure 23*). In literature Cav1 has been reported with different results regarding the cell type, shear stress intensity and duration. For example, increased expression of Cav1 has been observed in breast cancer cells after lower shear stress (2 dyn/cm^2) [111]. In epithelial cells high shear stress (20 dyn/cm^2) lead to an increased Cav1 expression but to a suppression of expression after lower shear stress (4 dyn/cm^2) [112]. Moreover, a prolongation of shear stress led to a gradual decrease in Cav1 in epithelial cells [68], which is also seen in SKOV3, resulting in a less significant expression in Cav1 level after 24 hours of shear stress. The interplay of Cav1 and actin explored by Xiong et al., 2017 is correlated to lower stress fiber formation in breast cancer cells after silencing Cav1 expression [113]. A similar trend was observed also in our experiments with OVCAR3: after 3 hours of shear stress the Cav1, as well as actin intensity, were significantly decreased, but after 24 hours Cav1 was stabilized back to normal (static control level), accompanied by a higher stress fiber formation.

Further, we evaluated the expression of Piezo1, as a mechanosensitive ion channel impacting downstream signaling pathways through the transduction of mechanical stimuli into cellular responses [38]. Piezo1 was influenced by shear stress with a decrease in intensity observed in both cell lines. In the SKOV3 cell line a significant decrease in Piezo1 intensity occurred after 24 hours (*figure 26*), but much faster adaptations were seen for the OVCAR3 cell line with a shear stress induced decrease already after 3 hours (*figure 27*). Furthermore, opposite results were observed for total YAP and YAP translocation regarding the application of shear stress and YODA treatment, which is an agonist of Piezo1 and chemically activates the ion channel which can be used to mimic the effects of shear stress [100]. In the SKOV3 cell line shear stress

led to no translocation of YAP (*figure 28*), but after 3 hours of YODA treatment translocation was observed (*figure 29*). The results for OVCAR3 cell lines showed a shear stress induced translocation (*figure 30*) which was not seen after the treatment with YODA (*figure 31*). The effects could be linked to the changes in cell morphology and formation of stress fibers [114] which stiffens the cytoskeleton of the OVCAR3 cell line and enables YAP to translocate, unlike in SKOV3 where stress fibers are absent. Lee et al., 2019 previously correlated the absence of stress fibers in breast cancer cytoskeleton to a lack of YAP activity [115], which might be similar in the SKOV3 cell line after shear stress. As previously described, Ajuba negatively regulates YAP activity [64], which in fact was observed to be reversely correlated. The protein Ajuba was increased in intensity in the SKOV3 cell line after 3 hours of shear stress but decreased after 24 hours in comparison to static control (*figure 24*). On the other hand, in the OVCAR3 cell line shear stress of 3 hours led to a decrease in Ajuba intensity which was stabilized after 24 hours re-equilibrating to normal state of static control (*figure 25*). Downstreaming toward the intracellular compartment, additional transcription factors can contribute to the regulation of mechanotransduction. Among these, transcription factor Nrf2 regulates antioxidant defense of the cell towards different stimuli [55]. Moreover, Nrf2 was shown to be mechanosensitive, in other words, Nrf2 translocates to the nucleus upon mechanical stimulation [116]. Nrf2 activity might amplify the different responses in chemoresistance seen with cisplatin treatment. In the SKOV3 cell line total Nrf2 is significantly decreased after 3 hours of shear stress but increases after 24 hours (*figure 32*), as well as translocation to the nucleus is increased, which suggests Nrf2 transcriptional activity. Contrary to SKOV3 cell line, OVCAR3 cells showed a decrease in Nrf2 signal after 24 hours of shear stress (*figure 33*). Overall, Nrf2 is known to be an important player in cellular defense and the activation of its downstream targets strongly depends on several different mechanisms and their crosstalk. In this regard, the effects on drug response are dependent on the duration and regulation of Nrf2 activity in each tumor [117].

Shear stress can trigger various post-translational modifications, including phosphorylation, acetylation, and farnesylation, which in turn regulate protein function and cellular responses to mechanical forces. These modifications seem to work very specifically in their contribution to cellular mechanotransduction pathways [118]. In this regard, farnesylation can influence protein-protein signaling at the plasma membrane through interaction with other membrane-associated proteins or anchor signaling complexes. These interactions are essential for the

proper functioning of various cellular processes, including signal transduction, vesicular trafficking, and cytoskeletal organization [119]. Our results show a decrease in farnesylation (*figure 35*), acetylation (*figure 37*) and phosphorylation (*figure 39*) in the OVCAR3 cell line which might be linked to stress fiber formation, with significant decrease in all three PTMs correlated to prolongation of shear stress. In contrast, for the SKOV3 cell line farnesylation (*figure 34*) and acetylation (*figure 36*) are increased after shear stress in a time-dependent manner, but phosphorylation (*figure 38*) is significantly decreased. This might suggest similar pathways involved in phosphorylation between both cell lines.

In conclusion, physical forces are inseparable part of tissue and tumor microenvironment and can not be omitted as factor impacting cellular behavior in both healthy and pathologic states. Our results show considerable heterogeneity between ovarian cancer cell lines with respect to cellular response to mechanical stimulation. This could further lead to differential response to treatment. The acquired chemoresistance of ovarian cancer cells is a major obstacle in successful therapy and understanding of the molecular mechanisms potentially sustaining these phenomena is essential to support alternative approaches and science-based intervention. The presented results offer some initial perspectives for a deeper understanding of these pathomechanisms with a special focus on cancer mechanotransduction.

References

[1] U.A. Matulonis, A.K. Sood, L. Fallowfield, B.E. Howitt, J. Sehouli, B.Y. Karlan, Ovarian cancer, Nat Rev Dis Primers, 2 (2016) 16061.
[2] https://gco.iarc.fr/today/data/factsheets/populations/908-europe-fact-sheets.pdf, Cancer: Europe Fact Sheet Accessed: 17.01.2023.
[3] https://www.efpia.eu/publications/cancer-comparator-report/cancer-types/ovarian-cancer/, Cancer EFPIA, Accessed: 16.01.2023.
[4] https://gco.iarc.fr/today/data/factsheets/cancers/25-Ovary-fact-sheet.pdf, Ovary: Fact Sheet, Accessed: 17.01.2023.
[5] https://seer.cancer.gov/statfacts/html/ovary.html, Cancer Stat Facts: Ovarian Cancer, Accessed: 17.01.2023.
[6] https://www.esmo.org/newsroom/press-releases/death-rates-from-ovarian-cancer-will-fall-in-the-eu-and-uk-in-2022#:~:text=The%20researchers%20predict%20that%2026%2C500,and%20UK%20respectively%20%5B2%5D., Death rates from Ovarian Cancer will fall in the EU and UK in 2022, Accessed: 16.01.2023.
[7] K.A. Michels, R.M. Pfeiffer, L.A. Brinton, B. Trabert, Modification of the Associations Between Duration of Oral Contraceptive Use and Ovarian, Endometrial, Breast, and Colorectal Cancers, JAMA Oncol, 4 (2018) 516-521.
[8] V. Sopik, J. Iqbal, B. Rosen, S.A. Narod, Why have ovarian cancer mortality rates declined? Part II. Case-fatality, Gynecol Oncol, 138 (2015) 750-756.
[9] P.T. Kroeger, Jr., R. Drapkin, Pathogenesis and heterogeneity of ovarian cancer, Curr Opin Obstet Gynecol, 29 (2017) 26-34.
[10] M. Kossaï, A. Leary, J.Y. Scoazec, C. Genestie, Ovarian Cancer: A Heterogeneous Disease, Pathobiology, 85 (2018) 41-49.
[11] M.A. Lisio, L. Fu, A. Goyeneche, Z.H. Gao, C. Telleria, High-Grade Serous Ovarian Cancer: Basic Sciences, Clinical and Therapeutic Standpoints, Int J Mol Sci, 20 (2019).
[12] C. Novak, E. Horst, G. Mehta, Review: Mechanotransduction in ovarian cancer: Shearing into the unknown, APL Bioeng, 2 (2018) 031701.
[13] M. Yousefi, S. Dehghani, R. Nosrati, M. Ghanei, A. Salmaninejad, S. Rajaie, M. Hasanzadeh, A. Pasdar, Current insights into the metastasis of epithelial ovarian cancer - hopes and hurdles, Cell Oncol (Dordr), 43 (2020) 515-538.
[14] K.L. Talia, C. Parra-Herran, W.G. McCluggage, Ovarian mucinous and seromucinous neoplasms: problematic aspects and modern diagnostic approach, Histopathology, 80 (2022) 255-278.
[15] J. Brown, M. Friedlander, F.J. Backes, P. Harter, D.M. O'Connor, T. de la Motte Rouge, D. Lorusso, J. Maenpaa, J.W. Kim, M.E. Tenney, M.J. Seckl, Gynecologic Cancer Intergroup (GCIG) consensus review for ovarian germ cell tumors, Int J Gynecol Cancer, 24 (2014) S48-54.
[16] A.M. Shaaban, M. Rezvani, K.M. Elsayes, H. Baskin, Jr., A. Mourad, B.R. Foster, E.A. Jarboe, C.O. Menias, Ovarian malignant germ cell tumors: cellular classification and clinical and imaging features, Radiographics, 34 (2014) 777-801.
[17] M. Furuya, Ovarian cancer stroma: pathophysiology and the roles in cancer development, Cancers (Basel), 4 (2012) 701-724.
[18] T.M. Ulbright, Germ cell tumors of the gonads: a selective review emphasizing problems in differential diagnosis, newly appreciated, and controversial issues, Mod Pathol, 18 Suppl 2 (2005) S61-79.
[19] M. McMullen, K. Karakasis, R. Rottapel, A.M. Oza, Advances in ovarian cancer, from biology to treatment, Nat Cancer, 2 (2021) 6-8.
[20] A. Gadducci, V. Guarneri, F.A. Peccatori, G. Ronzino, G. Scandurra, C. Zamagni, P. Zola, V. Salutari, Current strategies for the targeted treatment of high-grade serous epithelial ovarian cancer and relevance of BRCA mutational status, J Ovarian Res, 12 (2019) 9.
[21] M.A. Skowron, C. Oing, F. Bremmer, P. Ströbel, M.J. Murray, N. Coleman, J.F. Amatruda, F. Honecker, C. Bokemeyer, P. Albers, D. Nettersheim, The developmental origin of cancers defines basic principles of cisplatin resistance, Cancer Lett, 519 (2021) 199-210.

[22] S. Ghosh, Cisplatin: The first metal based anticancer drug, Bioorg Chem, 88 (2019) 102925.
[23] C. Zhang, C. Xu, X. Gao, Q. Yao, Platinum-based drugs for cancer therapy and anti-tumor strategies, Theranostics, 12 (2022) 2115-2132.
[24] T. Makovec, Cisplatin and beyond: molecular mechanisms of action and drug resistance development in cancer chemotherapy, Radiol Oncol, 53 (2019) 148-158.
[25] L. Galluzzi, L. Senovilla, I. Vitale, J. Michels, I. Martins, O. Kepp, M. Castedo, G. Kroemer, Molecular mechanisms of cisplatin resistance, Oncogene, 31 (2012) 1869-1883.
[26] M. Song, M. Cui, K. Liu, Therapeutic strategies to overcome cisplatin resistance in ovarian cancer, Eur J Med Chem, 232 (2022) 114205.
[27] A.J. McKenzie, S.R. Hicks, K.V. Svec, H. Naughton, Z.L. Edmunds, A.K. Howe, The mechanical microenvironment regulates ovarian cancer cell morphology, migration, and spheroid disaggregation, Sci Rep, 8 (2018) 7228.
[28] I.P. Uray, K. Uray, Mechanotransduction at the Plasma Membrane-Cytoskeleton Interface, Int J Mol Sci, 22 (2021).
[29] M.B. Goodman, E.S. Haswell, V. Vásquez, Mechanosensitive membrane proteins: Usual and unusual suspects in mediating mechanotransduction, J Gen Physiol, 155 (2023).
[30] G. Del Favero, A. Kraegeloh, Integrating Biophysics in Toxicology, Cells, 9 (2020).
[31] V.G. Macefield, T.P. Knellwolf, Functional properties of human muscle spindles, J Neurophysiol, 120 (2018) 452-467.
[32] T.N. Thrasher, Baroreceptors and the long-term control of blood pressure, Exp Physiol, 89 (2004) 331-335.
[33] P. Jin, L.Y. Jan, Y.N. Jan, Mechanosensitive Ion Channels: Structural Features Relevant to Mechanotransduction Mechanisms, Annu Rev Neurosci, 43 (2020) 207-229.
[34] Y. Gu, C. Gu, Physiological and pathological functions of mechanosensitive ion channels, Mol Neurobiol, 50 (2014) 339-347.
[35] Z. Sun, S.S. Guo, R. Fässler, Integrin-mediated mechanotransduction, J Cell Biol, 215 (2016) 445-456.
[36] A.J. Ehrlicher, F. Nakamura, J.H. Hartwig, D.A. Weitz, T.P. Stossel, Mechanical strain in actin networks regulates FilGAP and integrin binding to filamin A, Nature, 478 (2011) 260-263.
[37] V. Swaminathan, M. Gloerich, Decoding mechanical cues by molecular mechanotransduction, Curr Opin Cell Biol, 72 (2021) 72-80.
[38] A. Lai, C.D. Cox, N. Chandra Sekar, P. Thurgood, A. Jaworowski, K. Peter, S. Baratchi, Mechanosensing by Piezo1 and its implications for physiology and various pathologies, Biol Rev Camb Philos Soc, 97 (2022) 604-614.
[39] M. Bachmann, S. Kukkurainen, V.P. Hytönen, B. Wehrle-Haller, Cell Adhesion by Integrins, Physiol Rev, 99 (2019) 1655-1699.
[40] D. Casares, P.V. Escribá, C.A. Rosselló, Membrane Lipid Composition: Effect on Membrane and Organelle Structure, Function and Compartmentalization and Therapeutic Avenues, Int J Mol Sci, 20 (2019).
[41] A.L. Le Roux, X. Quiroga, N. Walani, M. Arroyo, P. Roca-Cusachs, The plasma membrane as a mechanochemical transducer, Philos Trans R Soc Lond B Biol Sci, 374 (2019) 20180221.
[42] J.M. Kefauver, A.B. Ward, A. Patapoutian, Discoveries in structure and physiology of mechanically activated ion channels, Nature, 587 (2020) 567-576.
[43] X.C. Zhang, Z. Liu, J. Li, From membrane tension to channel gating: A principal energy transfer mechanism for mechanosensitive channels, Protein Sci, 25 (2016) 1954-1964.
[44] W.A. Shihata, D.L. Michell, K.L. Andrews, J.P. Chin-Dusting, Caveolae: A Role in Endothelial Inflammation and Mechanotransduction?, Front Physiol, 7 (2016) 628.
[45] L. Sotodosos-Alonso, M. Pulgarín-Alfaro, M.A. Del Pozo, Caveolae Mechanotransduction at the Interface between Cytoskeleton and Extracellular Matrix, Cells, 12 (2023).
[46] R. Moreno-Vicente, D.M. Pavón, I. Martín-Padura, M. Català-Montoro, A. Díez-Sánchez, A. Quílez-Álvarez, J.A. López, M. Sánchez-Álvarez, J. Vázquez, R. Strippoli, M.A. Del Pozo, Caveolin-1 Modulates

Mechanotransduction Responses to Substrate Stiffness through Actin-Dependent Control of YAP, Cell Rep, 25 (2018) 1622-1635.e1626.
[47] S.E. Murthy, A.E. Dubin, A. Patapoutian, Piezos thrive under pressure: mechanically activated ion channels in health and disease, Nat Rev Mol Cell Biol, 18 (2017) 771-783.
[48] S. Wang, R. Chennupati, H. Kaur, A. Iring, N. Wettschureck, S. Offermanns, Endothelial cation channel PIEZO1 controls blood pressure by mediating flow-induced ATP release, J Clin Invest, 126 (2016) 4527-4536.
[49] C.D. Cox, C. Bae, L. Ziegler, S. Hartley, V. Nikolova-Krstevski, P.R. Rohde, C.A. Ng, F. Sachs, P.A. Gottlieb, B. Martinac, Removal of the mechanoprotective influence of the cytoskeleton reveals PIEZO1 is gated by bilayer tension, Nat Commun, 7 (2016) 10366.
[50] P.A. Gottlieb, C. Bae, F. Sachs, Gating the mechanical channel Piezo1: a comparison between whole-cell and patch recording, Channels (Austin), 6 (2012) 282-289.
[51] F.N. Lolo, V. Jiménez-Jiménez, M. Sánchez-Álvarez, M. Del Pozo, Tumor-stroma biomechanical crosstalk: a perspective on the role of caveolin-1 in tumor progression, Cancer Metastasis Rev, 39 (2020) 485-503.
[52] R. Strippoli, P. Sandoval, R. Moreno-Vicente, L. Rossi, C. Battistelli, M. Terri, L. Pascual-Antón, M. Loureiro, F. Matteini, E. Calvo, J.A. Jiménez-Heffernan, M.J. Gómez, V. Jiménez-Jiménez, F. Sánchez-Cabo, J. Vázquez, M. Tripodi, M. López-Cabrera, M. Del Pozo, Caveolin1 and YAP drive mechanically induced mesothelial to mesenchymal transition and fibrosis, Cell Death Dis, 11 (2020) 647.
[53] D.A. Fletcher, R.D. Mullins, Cell mechanics and the cytoskeleton, Nature, 463 (2010) 485-492.
[54] S. Seetharaman, S. Etienne-Manneville, Integrin diversity brings specificity in mechanotransduction, Biol Cell, 110 (2018) 49-64.
[55] F. He, X. Ru, T. Wen, NRF2, a Transcription Factor for Stress Response and Beyond, Int J Mol Sci, 21 (2020).
[56] A. Totaro, T. Panciera, S. Piccolo, YAP/TAZ upstream signals and downstream responses, Nat Cell Biol, 20 (2018) 888-899.
[57] S. Piccolo, S. Dupont, M. Cordenonsi, The biology of YAP/TAZ: hippo signaling and beyond, Physiol Rev, 94 (2014) 1287-1312.
[58] A. Pocaterra, P. Romani, S. Dupont, YAP/TAZ functions and their regulation at a glance, J Cell Sci, 133 (2020).
[59] F. Zanconato, M. Cordenonsi, S. Piccolo, YAP/TAZ at the Roots of Cancer, Cancer Cell, 29 (2016) 783-803.
[60] T. Panciera, L. Azzolin, M. Cordenonsi, S. Piccolo, Mechanobiology of YAP and TAZ in physiology and disease, Nat Rev Mol Cell Biol, 18 (2017) 758-770.
[61] S. Ma, Z. Meng, R. Chen, K.L. Guan, The Hippo Pathway: Biology and Pathophysiology, Annu Rev Biochem, 88 (2019) 577-604.
[62] Y. Zheng, D. Pan, The Hippo Signaling Pathway in Development and Disease, Dev Cell, 50 (2019) 264-282.
[63] I.M. Moya, G. Halder, Hippo-YAP/TAZ signalling in organ regeneration and regenerative medicine, Nat Rev Mol Cell Biol, 20 (2019) 211-226.
[64] I. Tanaka, H. Osada, M. Fujii, A. Fukatsu, T. Hida, Y. Horio, Y. Kondo, A. Sato, Y. Hasegawa, T. Tsujimura, Y. Sekido, LIM-domain protein AJUBA suppresses malignant mesothelioma cell proliferation via Hippo signaling cascade, Oncogene, 34 (2015) 73-83.
[65] E. Kirichenko, K.D. Irvine, AJUBA and WTIP can compete with LIMD1 for junctional localization and LATS regulation, MicroPubl Biol, 2022 (2022).
[66] H. Li, L. Fu, B. Liu, X. Lin, Q. Dong, E. Wang, Ajuba overexpression regulates mitochondrial potential and glucose uptake through YAP/Bcl-xL/GLUT1 in human gastric cancer, Gene, 693 (2019) 16-24.
[67] Q. Wang, X. Peng, Y. Chen, X. Tang, Y. Qin, M. He, W. Chen, H. Chen, Piezo1 alleviates acetaminophen-induced acute liver injury by activating Nrf2 and reducing mitochondrial reactive oxygen species, Biochem Biophys Res Commun, 652 (2023) 88-94.

[68] L. Wang, B. Wang, L. Jia, H. Yu, Z. Wang, F. Wei, A. Jiang, Shear stress leads to the dysfunction of endothelial cells through the Cav-1-mediated KLF2/eNOS/ERK signaling pathway under physiological conditions, Open Life Sci, 18 (2023) 20220587.
[69] A. Fragoulis, M. Tohidnezhad, Y. Kubo, C.J. Wruck, R.B. Craveiro, A. Bock, M. Wolf, T. Pufe, H. Jahr, F. Suhr, The Contribution of the Nrf2/ARE System to Mechanotransduction in Musculoskeletal and Periodontal Tissues, Int J Mol Sci, 24 (2023).
[70] S.R. McSweeney, E. Warabi, R.C. Siow, Nrf2 as an Endothelial Mechanosensitive Transcription Factor: Going With the Flow, Hypertension, 67 (2016) 20-29.
[71] I. Bellezza, I. Giambanco, A. Minelli, R. Donato, Nrf2-Keap1 signaling in oxidative and reductive stress, Biochim Biophys Acta Mol Cell Res, 1865 (2018) 721-733.
[72] C. Tonelli, I.I.C. Chio, D.A. Tuveson, Transcriptional Regulation by Nrf2, Antioxid Redox Signal, 29 (2018) 1727-1745.
[73] T. Suzuki, M. Yamamoto, Stress-sensing mechanisms and the physiological roles of the Keap1-Nrf2 system during cellular stress, J Biol Chem, 292 (2017) 16817-16824.
[74] A.O. Ward, G.B. Sala-Newby, S. Ladak, G.D. Angelini, M. Caputo, M.S. Suleiman, P.C. Evans, S.J. George, M. Zakkar, Nrf2-Keap-1 imbalance under acute shear stress induces inflammatory response in venous endothelial cells, Perfusion, 37 (2022) 582-589.
[75] W. Li, F. Li, X. Zhang, H.K. Lin, C. Xu, Insights into the post-translational modification and its emerging role in shaping the tumor microenvironment, Signal Transduct Target Ther, 6 (2021) 422.
[76] T. Bilbrough, E. Piemontese, O. Seitz, Dissecting the role of protein phosphorylation: a chemical biology toolbox, Chem Soc Rev, 51 (2022) 5691-5730.
[77] V. Singh, M. Ram, R. Kumar, R. Prasad, B.K. Roy, K.K. Singh, Phosphorylation: Implications in Cancer, Protein J, 36 (2017) 1-6.
[78] J.D. Jones, C.D. O'Connor, Protein acetylation in prokaryotes, Proteomics, 11 (2011) 3012-3022.
[79] M. Shvedunova, A. Akhtar, Modulation of cellular processes by histone and non-histone protein acetylation, Nat Rev Mol Cell Biol, 23 (2022) 329-349.
[80] A. Marchwicka, D. Kamińska, M. Monirialamdari, K.M. Błażewska, E. Gendaszewska-Darmach, Protein Prenyltransferases and Their Inhibitors: Structural and Functional Characterization, Int J Mol Sci, 23 (2022).
[81] G. Novelli, M.R. D'Apice, Protein farnesylation and disease, J Inherit Metab Dis, 35 (2012) 917-926.
[82] H. Yamaguchi, G.M. Taouk, A Potential Role of YAP/TAZ in the Interplay Between Metastasis and Metabolic Alterations, Front Oncol, 10 (2020) 928.
[83] S.M. Sebti, Protein farnesylation: implications for normal physiology, malignant transformation, and cancer therapy, Cancer Cell, 7 (2005) 297-300.
[84] J.H. Koo, K.-L. Guan, Interplay between YAP/TAZ and Metabolism, Cell Metabolism, 28 (2018) 196-206.
[85] W. Mi, Q. Lin, C. Childress, M. Sudol, J. Robishaw, C.H. Berlot, M. Shabahang, W. Yang, Geranylgeranylation signals to the Hippo pathway for breast cancer cell proliferation and migration, Oncogene, 34 (2015) 3095-3106.
[86] M.E. Bregenzer, E.N. Horst, P. Mehta, C.M. Novak, T. Repetto, G. Mehta, The Role of Cancer Stem Cells and Mechanical Forces in Ovarian Cancer Metastasis, Cancers (Basel), 11 (2019).
[87] C.K. Ip, S.S. Li, M.Y. Tang, S.K. Sy, Y. Ren, H.C. Shum, A.S. Wong, Stemness and chemoresistance in epithelial ovarian carcinoma cells under shear stress, Sci Rep, 6 (2016) 26788.
[88] K.L. Clark, J.W. George, E. Przygrodzka, M.R. Plewes, G. Hua, C. Wang, J.S. Davis, Hippo Signaling in the Ovary: Emerging Roles in Development, Fertility, and Disease, Endocr Rev, 43 (2022) 1074-1096.
[89] https://www.atcc.org/products/htb-77, SK-OV-3 [SKOV-3; SKOV3], Accessed: 07.03.2023.
[90] B.M. Barnes, L. Nelson, A. Tighe, G.J. Burghel, I.H. Lin, S. Desai, J.C. McGrail, R.D. Morgan, S.S. Taylor, Distinct transcriptional programs stratify ovarian cancer cell lines into the five major histological subtypes, Genome Med, 13 (2021) 140.
[91] https://www.atcc.org/products/htb-161, NIH:OVCAR-3 [OVCAR3], Accesses: 07.03.2023.

[92] A. Bradbury, R. O'Donnell, Y. Drew, N.J. Curtin, S. Sharma Saha, Characterisation of Ovarian Cancer Cell Line NIH-OVCAR3 and Implications of Genomic, Transcriptomic, Proteomic and Functional DNA Damage Response Biomarkers for Therapeutic Targeting, Cancers (Basel), 12 (2020).
[93] C.M. Warboys, M. Ghim, P.D. Weinberg, Understanding mechanobiology in cultured endothelium: A review of the orbital shaker method, Atherosclerosis, 285 (2019) 170-177.
[94] A. Bileck, P. Bortel, M. Kriz, L. Janker, E. Kiss, C. Gerner, G. Del Favero, Inward Outward Signaling in Ovarian Cancer: Morpho-Phospho-Proteomic Profiling Upon Application of Hypoxia and Shear Stress Characterizes the Adaptive Plasticity of OVCAR-3 and SKOV-3 Cells, Front Oncol, 11 (2021) 746411.
[95] G. Del Favero, L. Woelflingseder, D. Braun, H. Puntscher, M.L. Kütt, L. Dellafiora, B. Warth, G. Pahlke, C. Dall'Asta, G. Adam, D. Marko, Response of intestinal HT-29 cells to the trichothecene mycotoxin deoxynivalenol and its sulfated conjugates, Toxicol Lett, 295 (2018) 424-437.
[96] https://www.abcam.com/wst-1-assay-reagent-cell-proliferation-ready-to-use-ab155902.html, WST-1, Accessed: 20.04.2023.
[97] G. Del Favero, M. Zeugswetter, E. Kiss, D. Marko, Endoplasmic Reticulum Adaptation and Autophagic Competence Shape Response to Fluid Shear Stress in T24 Bladder Cancer Cells, Front Pharmacol, 12 (2021) 647350.
[98] https://www.abcam.com/products/assay-kits/crystal-violet-assay-kit-cell-viability-ab232855.html, CV, Accessed: 20.04.2023.
[99] G. Del Favero, R.M. Mayer, L. Dellafiora, L. Janker, L. Niederstaetter, C. Dall'Asta, C. Gerner, D. Marko, Structural Similarity with Cholesterol Reveals Crucial Insights into Mechanisms Sustaining the Immunomodulatory Activity of the Mycotoxin Alternariol, Cells, 9 (2020).
[100] M. Jobst, E. Kiss, C. Gerner, D. Marko, G. Del Favero, Activation of autophagy triggers mitochondrial loss and changes acetylation profile relevant for mechanotransduction in bladder cancer cells, Arch Toxicol, 97 (2023) 217-233.
[101] J. Bergen, M. Karasova, A. Bileck, M. Pignitter, D. Marko, C. Gerner, G. Del Favero, Exposure to dietary fatty acids oleic and palmitic acid alters structure and mechanotransduction of intestinal cells in vitro, Arch Toxicol, 97 (2023) 1659-1675.
[102] A.R. Hyler, N.C. Baudoin, M.S. Brown, M.A. Stremler, D. Cimini, R.V. Davalos, E.M. Schmelz, Fluid shear stress impacts ovarian cancer cell viability, subcellular organization, and promotes genomic instability, PLoS One, 13 (2018) e0194170.
[103] Y. Fan, Q. Sun, X. Li, J. Feng, Z. Ao, X. Li, J. Wang, Substrate Stiffness Modulates the Growth, Phenotype, and Chemoresistance of Ovarian Cancer Cells, Frontiers in Cell and Developmental Biology, 9 (2021).
[104] S. Nasrollahi, C. Walter, A.J. Loza, G.V. Schimizzi, G.D. Longmore, A. Pathak, Past matrix stiffness primes epithelial cells and regulates their future collective migration through a mechanical memory, Biomaterials, 146 (2017) 146-155.
[105] J. Li, Y. Fang, D. Wu, Mechanical forces and metabolic changes cooperate to drive cellular memory and endothelial phenotypes, Curr Top Membr, 87 (2021) 199-253.
[106] T. Sun, J.T. Chi, Regulation of ferroptosis in cancer cells by YAP/TAZ and Hippo pathways: The therapeutic implications, Genes Dis, 8 (2021) 241-249.
[107] A. Zoń, I. Bednarek, Cisplatin in Ovarian Cancer Treatment-Known Limitations in Therapy Force New Solutions, Int J Mol Sci, 24 (2023).
[108] A.A. Hassan, M. Artemenko, M.K.S. Tang, Z. Shi, L.Y. Chen, H.C. Lai, Z. Yang, H.C. Shum, A.S.T. Wong, Ascitic fluid shear stress in concert with hepatocyte growth factor drive stemness and chemoresistance of ovarian cancer cells via the c-Met-PI3K/Akt-miR-199a-3p signaling pathway, Cell Death Dis, 13 (2022) 537.
[109] S. Nath, M. Pigula, A.P. Khan, W. Hanna, M.K. Ruhi, F.M. Dehkordy, K. Pushpavanam, K. Rege, K. Moore, Y. Tsujita, C. Conrad, F. Inci, M.G.D. Carmen, W. Franco, J.P. Celli, U. Demirci, T. Hasan, H.C. Huang, I. Rizvi, Flow-induced Shear Stress Confers Resistance to Carboplatin in an Adherent Three-Dimensional Model for Ovarian Cancer: A Role for EGFR-Targeted Photoimmunotherapy Informed by Physical Stress, J Clin Med, 9 (2020).

[110] L. Avraham-Chakim, D. Elad, U. Zaretsky, Y. Kloog, A. Jaffa, D. Grisaru, Fluid-flow induced wall shear stress and epithelial ovarian cancer peritoneal spreading, PLoS One, 8 (2013) e60965.
[111] X. Chen, Q. Xia, N. Sun, H. Zhou, Z. Xu, X. Yang, R. Yan, P. Li, T. Li, X. Qin, H. Yang, C. Wu, F. You, X. Liao, S. Li, Y. Liu, Shear stress enhances anoikis resistance of cancer cells through ROS and NO suppressed degeneration of Caveolin-1, Free Radic Biol Med, 193 (2022) 95-107.
[112] L. Jia, L. Wang, F. Wei, C. Li, Z. Wang, H. Yu, H. Chen, B. Wang, A. Jiang, Effects of Caveolin-1-ERK1/2 pathway on endothelial cells and smooth muscle cells under shear stress, Exp Biol Med (Maywood), 245 (2020) 21-33.
[113] N. Xiong, S. Li, K. Tang, H. Bai, Y. Peng, H. Yang, C. Wu, Y. Liu, Involvement of caveolin-1 in low shear stress-induced breast cancer cell motility and adhesion: Roles of FAK/Src and ROCK/p-MLC pathways, Biochim Biophys Acta Mol Cell Res, 1864 (2017) 12-22.
[114] K. Wada, K. Itoga, T. Okano, S. Yonemura, H. Sasaki, Hippo pathway regulation by cell morphology and stress fibers, Development, 138 (2011) 3907-3914.
[115] J.Y. Lee, J.K. Chang, A.A. Dominguez, H.P. Lee, S. Nam, J. Chang, S. Varma, L.S. Qi, R.B. West, O. Chaudhuri, YAP-independent mechanotransduction drives breast cancer progression, Nat Commun, 10 (2019) 1848.
[116] G. Del Favero, R. Zaharescu, D. Marko, Functional impairment triggered by altertoxin II (ATXII) in intestinal cells in vitro: cross-talk between cytotoxicity and mechanotransduction, Arch Toxicol, 92 (2018) 3535-3547.
[117] C.J. Schmidlin, A. Shakya, M. Dodson, E. Chapman, D.D. Zhang, The intricacies of NRF2 regulation in cancer, Semin Cancer Biol, 76 (2021) 110-119.
[118] S. Chien, Mechanotransduction and endothelial cell homeostasis: the wisdom of the cell, Am J Physiol Heart Circ Physiol, 292 (2007) H1209-1224.
[119] O. Gutman, M. Ehrlich, Y.I. Henis, Ras Diffusion and Interactions with the Plasma Membrane Measured by FRAP Variations, Methods Mol Biol, 2262 (2021) 185-197.